DM

Nitrile based PAMAM dendrimers functionalized with $[RuCp(PPh_3)_2]^+$ moiety for anticancer applications

MASTER DISSERTATION

Nádia Sofia Henriques Nunes
MASTER IN APPLIED BIOCHEMISTRY

UNIVERSIDADE da MADEIRA
A Nossa Universidade
www.uma.pt

June | 2017

Nitrile based PAMAM dendrimers functionalized with $[RuCp(PPh_3)_2]^+$ moiety for anticancer applications

MASTER DISSERTATION

Nádia Sofia Henriques Nunes
MASTER IN APPLIED BIOCHEMISTRY

SUPERVISOR
João Manuel Cunha Rodrigues

CO-SUPERVISOR
Helena Maria Pires Gaspar Tomás

ACKNOWLEDGMENTS

I would like to express my sincere gratitude to my supervisor, Professor João Rodrigues for all the support, patience, understanding, supervision, willingness, and share of knowledge and the review of this master thesis. I would like to extend my thanks to my co-supervisor Professor Helena Tomás for the encouragement and kindness. The given encouragement, ideas, useful critiques, and constructive suggestions helped me to keep improving my work. In addition, I would like to acknowledge for the opportunity to work in cancer research and nanotechnology, a dream that I had for a while, namely through my valued internship, poster and oral communications.

I am particularly grateful for all the precious assistance, share of knowledge, motivation and friendship of my lab colleagues of Molecular Materials Research Group (MMRG), Dr.ª Cláudia Camacho, Dr.ª Dina Maciel, Dr.ª Nilsa Oliveira, Dr.ª Carla Alves, Dr.ª Mara Gonçalves and Dr.ª Rita Castro.

To my lab colleague and friend Dr.ª Ana Olival for all the appreciated support and share of ideas in the NMR characterization which helped me to improve the quality of my work.

To the laboratory technicians from Chemistry Department, Paula Andrade and Paula Vieira for all the kindness and readiness in providing some lab materials and reagents that I needed for this project.

I would also like to acknowledge the Madeira Chemistry Research Centre (CQM), Chemistry Department and University of Madeira (UMa) for disclosing the facilities to carry out this work.

I would like to extend my thanks to the Fundação para a Ciência e a Tecnologia (FCT) because this work would not have been possible without the partial support of this agency through the CQM Strategic Project PEst-OE/QUI/UI0674/2015-2016, and the NMR and MS Portuguese Networks (PTNMR-2015-2016, RNEM-2015-2016). The partial support of ARDITI – Agência Regional para o Desenvolvimento da Investigação Tecnologia e Inovação – through the project M1420-01-0145-FEDER-000005 – Centro de Química da Madeira – CQM^+ (Madeira 14-20), was highly appreciated.

To my dearest friends, Ana Morna, Sofia Ferreira, Carolina Cardoso, André Delgado, Liliana Rodrigues, Jackie Ferreira, Daniel Huang, João Leça and Jorge Gonçalves for all the relentless and caring support, companionship, understanding, enthusiasm and cherished

moments that helped me to overcome all the encountered obstacles and to celebrate the achievements in the progress of this work and life.

I am everlastingly thankful for all the love, care and believe that my grandparents, Maria Isabel Henriques and Martinho Henriques, and my aunt, Fátima Célia Henriques, and cousin, Cassandra Gomes, deposited on me through all my life and work.

Finally, but not less important at all, I would like to express my sincere gratitude to my mum, Zita Henriques, for all the endless love, comprehension, inspiration, care and for always believing in my potential, not only professionally but also emotionally, which helped me to always move forward. I find it hard to express by words all my sincere appreciation and love. Thank you!!

LIST OF PUBLICATIONS

Part of the results and findings of this work were presented in the following:

Oral communications:

- Maciel D., Camacho C., Nunes N., Muñoz-Fernández Mª.A., Tomás H., Rodrigues J.; Metallodendrimers as anticancer and antiviral drug candidates; The 10th International Dendrimer Symposium (IDS10), August 5-9, Weihai, China, 2017 (invited talk).
- Nunes N., Rodrigues J., Tomás H.; Generation 0 and 1 of new PAMAM dendrimers with different terminal groups. Synthesis and characterization; 3rd CQM Annual Meeting, April 01-02, Funchal, Madeira Island-Portugal, 2016.
- Nunes N., Camacho C., Rodrigues J.; Synthesis and functionalization of PAMAM dendrimers with different surface groups; 2nd CQM Annual Meeting, January 30-31, Funchal, Madeira Island-Portugal, 2015.

Poster communications:

- Nunes N., Rodrigues J., Tomás H.; PAMAM dendrimers as a platform for the preparation of low-generation of ruthenium metallodendrimers; MAD-Nano16: Madeira International Conference on Emerging Trends and Future of Nanomaterials for Human Health, November 17-20, Funchal, Madeira Island-Portugal, 2016.
- Olival A., Nunes N., Rodrigues J.; Low generation dendrimers with different surface groups. Characterization by nuclear magnetic resonance; 1st Joint French-Portuguese NMR congress, April 19-23, Lisbon, 2016.
- Nunes N., Camacho C., Rodrigues J.; Synthesis and functionalization of PAMAM dendrimers with different surface groups; INCB: Indo-Portuguese Workshop on Emerging Trends of Nanotechnology in Chemistry and Biology, February 12-13, New Delhi, India, 2016.

RESUMO

Os dendrímeros são moléculas hiperramificadas que se apresentam com diferentes grupos terminais na sua estrutura e que, por exemplo, podem ser conjugados com complexos de metais de transição. Esta estratégia conduz à preparação de metalodendrímeros com propriedades de interesse e diversas aplicações, incluindo as terapêuticas. Os complexos de Ruténio (II) são potenciais fármacos anticancerígenos que poderão vir a substituir os fármacos derivados da *cisplatina* por serem dotados de uma variedade de propriedades mais vantajosas, como por exemplo: uma cinética de permuta dos ligandos biocompatível, múltiplos estados de oxidação acessíveis, a capacidade de interagir com o DNA e/ou com proteínas e baixa toxicidade.

O objetivo principal desta dissertação de mestrado consistiu na preparação e caracterização de novos tipos de metalodendrímeros tendo como base os dendrímeros PAMAM: G0/G1-CN, G0/G1-(CNRu(η^5-C_5H_5)(PPh_3)$_2$)$_x$(CF_3SO_3)$_x$, G0/G1-$CO_2{}^t$Bu e G0/G1-OH. Os polinitrilos – G0-$(CN)_4$ e G1-$(CN)_8$ – sintetizados a partir de G0/G1-PAMAM foram utilizados na preparação de nitrilo-metalodendrímeros de ruténio G0-(CNRu(η^5-C_5H_5)(PPh_3)$_2$)$_4$(CF_3SO_3)$_4$ e G1-(CNRu(η^5-C_5H_5)(PPh_3)$_2$)$_8$(CF_3SO_3)$_8$, respetivamente. A estratégia de síntese aplicada foi adaptada a partir da metodologia previamente desenvolvida pelo Grupo de Materiais Moleculares do CQM e as técnicas de caracterização utilizadas para cada um dos dendrímeros e metalodendrímeros foram as técnicas de RMN (^{1}H, ^{13}C, ^{31}P, HSQC) e de IV (com transformada de Fourier). G0/G1-PAMAM foram caracterizados adicionalmente por espetroscopia de massa. Todos os compostos foram sintetizados com sucesso, com bons rendimentos (77% – 94%), e os resultados obtidos confirmaram a sua estrutura. Os hidroxilo-dendrímeros – G0-$(OH)_8$ and G1-$(OH)_{16}$ – foram sintetizados a partir dos ésteres G0-$(CO_2{}^t Bu)_8$ e G1-$(CO_2{}^t Bu)_{16}$, respetivamente, segundo a adaptação da metodologia de N. Jayaraman *et al.* (1, 2). A sua caracterização foi realizada por espetroscopia de RMN (^{1}H, ^{13}C, COSY e HSQC) e de IV (com transformada de Fourier). Apenas os dendrímeros G0-$(OH)_8$ e G0-$(CO_2{}^t Bu)_8$ foram caracterizados por espetroscopia de massa. Os resultados adquiridos validaram a estrutura de todos os dendrímeros sintetizados que foram obtidos com rendimentos elevados (83% – 93%). Uma das principais linhas de trabalho futuro será a análise da atividade anticancerígena destes novos nitrilo-metalodendrímeros e a comparação destes resultados com a *cisplatina*.

Palavras-chave: Dendrímeros, Ruténio (II), Metalodendrímeros, RMN, MS.

ABSTRACT

Dendrimers are hyperbranched molecules having different terminal groups that can be conjugated with, for example, transition-metal complexes leading to new and interesting compounds with a variety of interesting therapeutic applications. In the last decade, Ruthenium (II) complexes revealed to be potential alternatives to the clinically used antitumor Platinum-based drugs due to several characteristics, *e.g.* biocompatible ligand exchange rates, redox-accessible oxidation states, covalent binding with DNA and/or proteins and low toxicity.

The main goal of this master thesis was to prepare and characterize new PAMAM dendrimers based: G0/G1-CN, G0/G1-$(CNRu(\eta^5\text{-}C_5H_5)(PPh_3)_2)_x(CF_3SO_3)_x$, G0/G1-$CO_2{}^tBu$ and G0/G1-OH. The polynitrile dendrimers – G0-$(CN)_4$ and G1-$(CN)_8$ – synthesized from the G0/G1-PAMAM, were used in the preparation of the nitrile ruthenium-based metallodendrimers G0-$(CNRu(\eta^5\text{-}C_5H_5)(PPh_3)_2)_4(CF_3SO_3)_4$ and G1-$(CNRu(\eta^5\text{-}C_5H_5)(PPh_3)_2)_8(CF_3SO_3)_8$, respectively. The applied synthetic strategy was adapted from the reported methodology previously developed by the Molecular Materials Research Group of CQM (Madeira Chemistry Research Centre) and the structural characterization techniques used for each dendrimer/metallodendrimer were the NMR (^1H, ^{13}C, ^{31}P, HSQC) and FTIR. G0/G1-PAMAM were also characterized by MS. All the compounds were successfully synthesized, with good yields (77% – 94%), and the characterization data have confirmed their adequate structure.

The hydroxyl moieties – G0-$(OH)_8$ and G1-$(OH)_{16}$ – were synthesized from the ester compounds – G0-$(CO_2{}^tBu)_8$ and G1-$(CO_2{}^tBu)_{16}$ – respectively, through the adaptation of the reported methodology of N. Jayaraman *et al* (1, 2). These compounds were characterized by NMR (^1H, ^{13}C, COSY and HSQC) and FTIR spectroscopy and only the G0-$(OH)_8$ and G0-$(CO_2{}^tBu)_8$ were characterized by MS. The obtained results have showed that all the dendrimers were properly synthesized with very good yields (83% – 93%). The main future goal is to analyse the anticancer activity of these new metallodendrimers G0/G1-$(CNRu(\eta^5\text{-}C_5H_5)(PPh_3)_2)_x(CF_3SO_3)_x$ and to compare it with *cisplatin*.

Keywords: Dendrimers, Ruthenium (II), Metallodendrimers, NMR, MS.

Table of Contents

List of Tables

List of Figures

List of Schemes

List of Acronyms

ACN – Acrylonitrile

$AgCF_3SO_3$ – Silver trifluoromethanesulfonate

AgCl – Silver chloride

ASR – Age-standardized cancer incidence and mortality rates

CAS No. – Chemical Abstracts Service number

$CDCl_3$ – Deuterated chloroform

$CHCl_3$ – Chloroform

COSY – Correlation spectroscopy

Cp – Cyclopentadiene

DCM – Dichloromethane

DMSO – Dimethyl sulfoxide

D_2O – Deuterated water

EtOH – Ethanol

Et_2O – Diethyl ether

FDA – Food and Drug Administration

FTIR – Fourier Transform Infrared Spectroscopy

G0 – Generation 0

G1 – Generation 1

G0/G1-CN – Nitrile dendrimers from generations 0 and 1

G0/G1-CNRuCp$(PPh_3)_2)x(CF_3SO_3)x$ – Nitrile Ruthenium metallodendrimers with cyclopentadienyl and diphenylphosphine ligands from generation 0 and 1

G0/G1-$CO_2{}^t$Bu – *tert*-Butyl ester dendrimers from generations 0 and 1

G0/G1-OH – Hydroxyl dendrimers from generation 0 and 1

HSQC – Heteronuclear single-quantum correlation

ICR – Imidazole-containing complex

IR – Infrared

KBr – Potassium bromide

KP46 – *tris*(8-quinolinolate)gallium(III)

LC-ESI-MS/MS – Liquid Chromatography-Electrospray Ionization-Mass Spectrometry

$LiAlH_4$ – Lithium Aluminium hydride

L-L – Liquid-liquid

MeOH – Methanol

MS – Mass Spectrometry

Me_4Si or TMS – Tetramethylsilane

m/z – Mass-to-charge ratio

m – Multiplet

NaCl – Sodium chloride

NaH – Sodium hydride

NaOH – Sodium hydroxide

NMR – Nuclear Magnetic Resonance

N_2 – Nitrogen

n.d. – not defined

PAMAM – Polyamidoamine

PPh_3 – Triphenylphosphine

ppm – Parts per million

q – Quartet

RDC – Ruthenium derived compounds

$RuCl_3.xH_2O$ – Ruthenium (III) chloride hydrate

$[RuCp(\eta^5\text{-}C_5H_5)]$ – cyclopentadienyl ruthenium (II) complex with a piano stool structure

s – Singlet

t – Triplet

THF – Tetrahydrofuran

$TlPF_6$ – Thalium (I) hexafluorophosphate

1D – One-dimensional

^{1}H-NMR – Proton Nuclear Magnetic Resonance

^{13}C-NMR – Carbon-13 Nuclear Magnetic Resonance

2D – Two-dimensional

^{31}P-NMR – Phosphorous-31 Nuclear Magnetic Resonance

+MS – Total fragmentation

+MS2 – Second fragmentation

+MS3 – Third fragmentation

PART I - INTRODUCTION

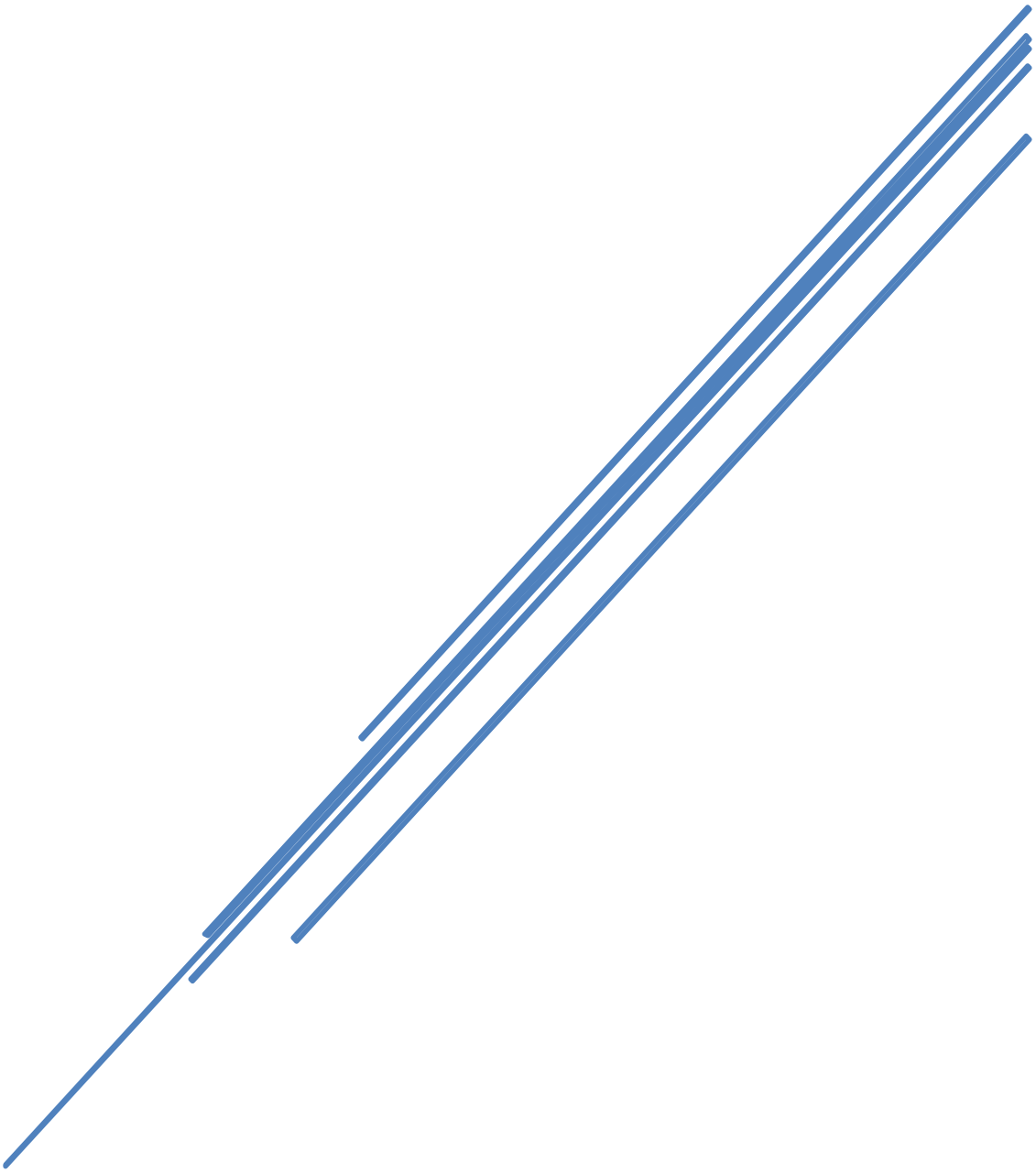

1. METAL-BASED ANTICANCER DRUGS

Metals, specifically transition metals, have a list of properties that offer several advantages in comparison with the more common organic-based drugs, which lead to the design of numerous therapeutic agents: a) a wide range of coordination numbers and geometries, b) "tune-ability" of the thermodynamics and kinetics of ligand substitution, c) accessible redox states and d) a wide structural diversity. These properties of metals or more appropriately of the metal complexes can be exploited for oncology treatment (3-5).

Cancer is a leading cause of death worldwide and was responsible for 8.8 million deaths in 2015. Nearly 1 in 6 deaths is due to cancer and the three deathliest types of cancer are: lung (1.69 million deaths), liver (788 000 deaths) and colorectal (774 000 deaths) (6). In a study from the World Health Organization published in 2014 (7), breast cancer was the most predominant among women while among men, the lung and prostate cancer had the highest incidences (fig. 1).

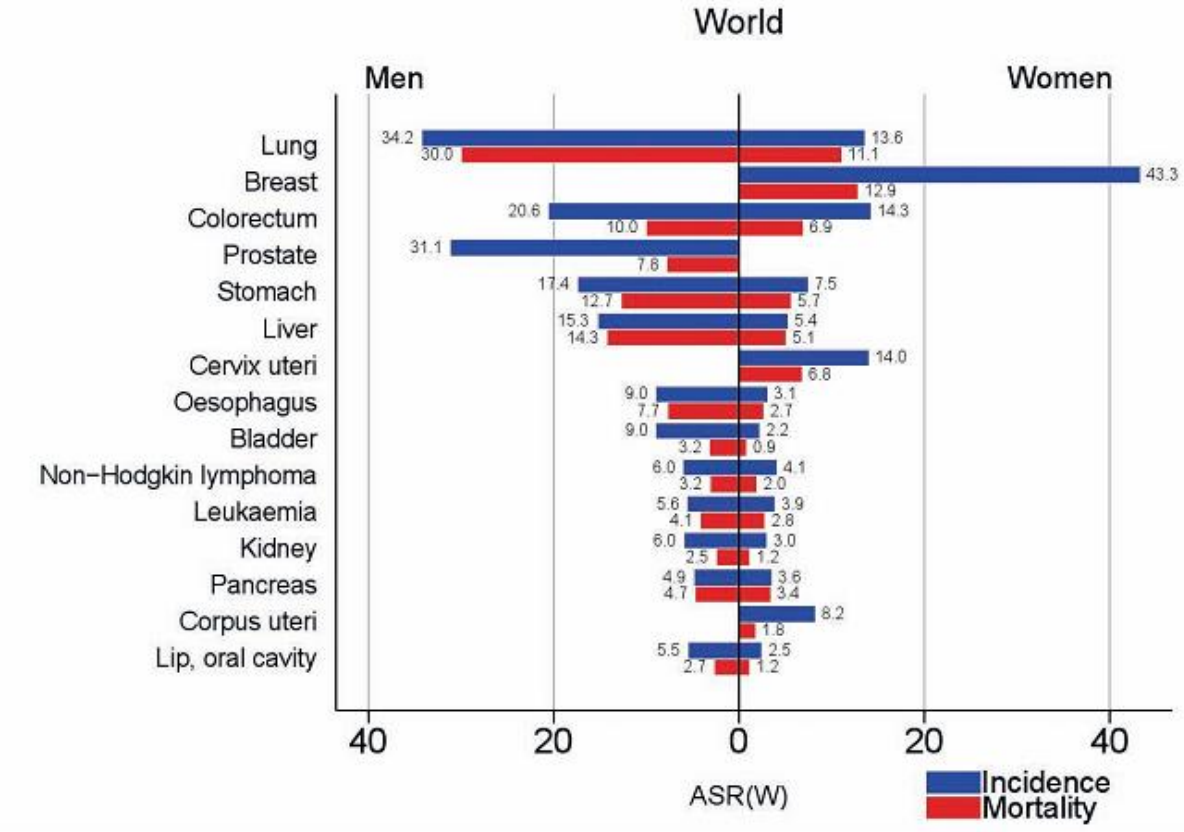

Figure 1 – Estimated world age-standardized cancer incidence and mortality rates (ASR), from the year of 2012, per 100 000, in men and women (7).

Due to the progresses that were made in cancer therapy and diagnosis in the last 27 years, 23% of the cancer death rate has dropped since 1991 but, despite this progress, for the pancreatic, liver and uterine corpus types of cancer, death rates are increasing (8, 9). In the next two decades, about 20 million cancer cases are expected to occur, which leads to the quest for new and improved anticancer agents (10).

Medicinal inorganic chemistry is a prosperous area for cancer research and, just about 50-40 years ago, its potential for designing new anticancer agents has only been elucidated and explored after *a)* the pioneering work of Köpf H. and Köpf-Maier P. (11) (in the late 1970´s) that have tested transition metal cyclopentadienyl complexes for antitumor activity, and *b)* the discovery of the biological activity of *cisplatin* (cis-diamminedichloroplatinum (II), fig. 2) (12, 13).

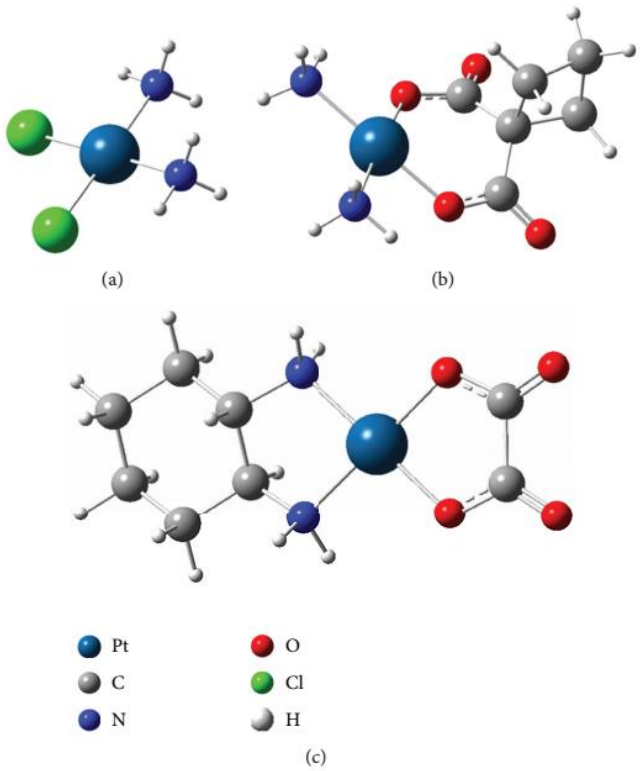

Figure 2 – Chemical structure (with optimised geometries) of three recognised platinum anticancer drugs: a) *cisplatin*; b) *carboplatin* and c) *oxaliplatin* (10).

This metallic coordination compound was firstly synthesized by Peyrone M., in 1844, and Werner A., in 1893, have discovered its chemical structure (14). Nevertheless, just in the mid 1960´s, the findings of Rosenberg B. *et al.* (15) initiated several preclinical and clinical studies that have revealed its cytotoxic effects and its safety and therapeutic profile. Thus, in 1978,

cisplatin was approved by FDA (US Food and Drug Administration) to treat patients with testicular and bladder cancer types. Since then, the treatment was extended to head, neck, lung, colorectal and ovarian cancers (16, 17). In the early 1980´s, two additional platinum derivatives were discovered – *cis*-diamine(cyclobutene-1,1-dicarboxylate-O,O')platinum (II) (carboplatin) and [(1*R*,2*R*)-cyclohexane-1,2-diamine](ethanedioato-O,O')platinum (II) (oxaliplatin) (both structures are represented in fig. 2) – and nowadays are also approved by FDA for cancer therapy (18, 19). However, the use of *cisplatin* (the most used anticancer metallodrug) has been associated with several toxic side effects as neurotoxic, cardiotoxic, nephrotoxic (20), ototoxic and hepatoxic (21, 22). Additionally, the resistance to this drug revealed to be the major drawback (23, 24). During the last 40 years, an investigational effort was done to overcome this problem, including the use of *cisplatin* in combination with targeted anticancer agents but, truly, most of these solutions failed to improve the therapeutic profile of *cisplatin* in the clinical trials (25-27). Approximately ten other platinum compounds are currently in clinical trials (4) and more recently, it was published some studies that suggests the potential of novel platinum (II) complexes that were tested for anticancer activity *in vitro* (28) and *in vivo* (29) but there´s still a long way to go. For this reason, besides the platinum compounds, the development of other inorganic anticancer agents has increased, encompassing a large variety of metal ions and ligands that have been tailored according to the specific biological target.

The main classes of metal-based anticancer drugs include: platinum (II and IV), gold (I and III), palladium (II), ruthenium (II and III), copper (II), bismuth (III), gallium (III), rhenium (I) and tin (IV) derivatives. It has been showed that, some of them, have higher *in vitro* anticancer activity when compared with *cisplatin*. Their therapeutic effect in malignant formations is, specially, based in their ability to interact with the DNA (30-36) (examples in fig. 3), leading to its damage and cell death (10, 37). Though, they can exhibit additional interactions with proteins and enzymes (38-43) (fig. 4) and even suffer a transformation in vivo that activate and/or improve their physiochemical, biopharmaceutical and pharmacokinetic properties (prodrug strategy (44-49); examples of these compounds in fig. 5) (4).

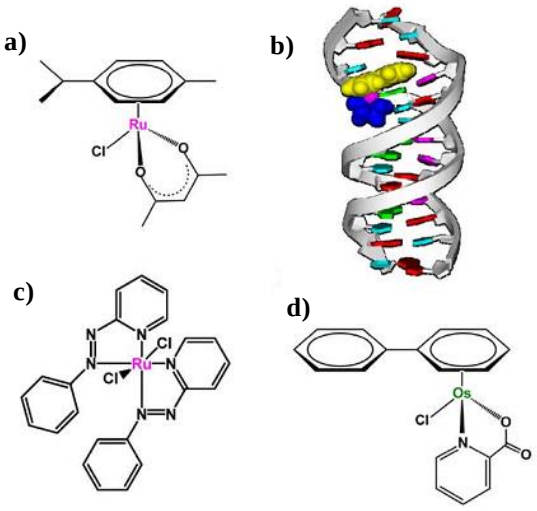

Figure 3 - Examples of metal-based compounds that target DNA: a) Cytotoxic Ru (II) arene complex (36); b) Intercalation of a Ru (II) complex into DNA (34); c) [γ-Ru(azpy)$_2$Cl$_2$] (31); d) A cytotoxic Os (II) arene complex (30) (adapted from ref. (4)).

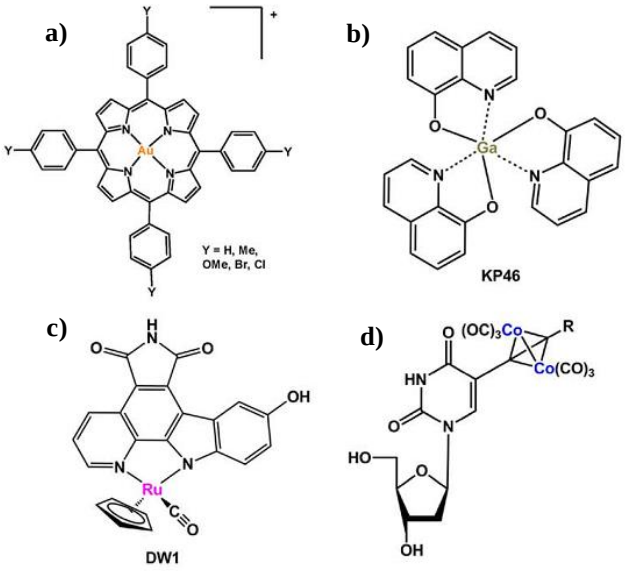

Figure 4 - Examples of metal-based anticancer drugs that target proteins and enzymes: a) Gold(III) meso-tetraarylporphyrins complex (43); b) *tris*(8-quinolinolate)gallium(III) (KP46) (40); c) DW1 – a ruthenium staurosporin bioconjugate (41); d) Hexacarbonyl dicobalt complex containing a nucleoside ligand (39) (adapted from ref. (4)).

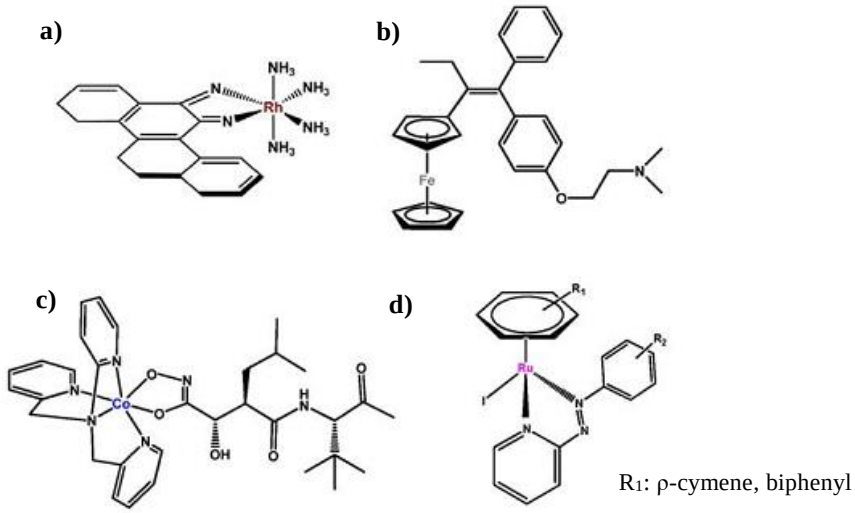

Figure 5 – Examples of metal-based anticancer prodrugs: a) Rh (III) complex photoactivatable (48); b) Ferrocifen (49); c) Cobalt–marimastat bioconjugate (47); d) Ru (II) arene complex with iodo and a phenylplazopyridine ligand (46) (adapted from ref. (4)).

1.1. Ruthenium complexes

The search for new compounds to treat cancer diseases have been relentless and ruthenium complexes are a potential target because of their unique properties: *a)* their expanded set of octahedral coordination geometry provides them the possibility to occupy a high number of spatial positions (with approximately 30 stereo isomers) which offers them unique possibilities to interact with DNA *b)* their ability of exist in the biological fluids in different oxidation states from II to IV and *d)* the facility to exchange with oxygen and nitrogen donor molecules in a similar way to platinum compounds (41, 50, 51). The idea of studying these compounds as anticancer agents started in 1975 with the observation that they, preferentially, localize in tumour tissue. The findings of this pioneering work begun with the hypothesis proposed by Clarke M.J. *et al* (52-55) that emphasized the mechanism of "activation by reduction" with the *fac*-$[RuCl_3(NH_3)_3]$ (fig. 6): Ru (III) (low reactive prodrug) is reduced in Ru (II) in a way that only the tumour cells get this activated or toxic form of the drug: the low oxygen content in the solid tumour masses creates a reducing environment and the lowering of the pH in the surrounding tissues, as a result of the lactic acid production from glycolysis (51, 56, 57).

Som P. *et al* (58) studied the transportation of this metal to the cancer cells by transferrin, a molecule present in plasma and other fluids that have specific receptors overexpressed in the

tumour cells, presumably because of the higher need of iron of these rapidly dividing cells (59). Its strong affinity to transferrin launch the hypotheses that Ru (III) substitute Fe (III), leading the cancer cells to cellular damage and induced apoptosis. Ruthenium not only have the ability to bind to transferrin but also to albumin (54). Brabec V. (60, 61) discovered the ability of ruthenium to interact with DNA through a different mechanism than *cisplatin*. This fact is extremely important to overcome the challenging resistance of tumour cells to platinum compounds (55, 62, 63). With the knowledge of this basic but imperative properties of ruthenium, the work of Keppler B. K. *et al* (64) and Sava G. *et al* (65, 66) press forward the progress for the ruthenium anticancer drugs. Firstly, a lead structure was found in the imidazole-containing complex (ICR) named KP418 (fig. 6) – imidazolium *trans*-[tetrachloridobis(1H-imidazole)ruthenate(III)] – that have showed *in vivo* anticancer activity against autochthonous colorectal cancer (67). This study lead to the discovery of several analogues of the KP418 compound. The first to show promising results was the KP1019 (indazolium *trans*-[tetrachloridobis(1*H*-indazole)ruthenate(III)], fig. 6) that have showed to be more active against the studied *in vivo* model of colon cancer and even more than 5-fluorouacil (5-FU), the standard anticancer drug for the colorectal cancer (68). Thus, this compound was selected for (pre)clinical evaluations and clinical phase I (69-71). In the other hand, Sava G. *et al* (65, 66) have synthesized DMSO-containing ruthenium complexes that was also inspired by the KP418 compound: the imidazolium *trans*-[tetrachlorido(1*H*-imidazole)(*S*-dimethyl sulfoxide)ruthenate(III)] or NAMI-A ((72), fig. 6). It was not only active against primary tumours but also against metastases and the process of metastasising. Both compounds, KP1019 and NAMI-A (42, 73, 74) have been clinically developed. In fact, NAMI-A was the first ruthenium compound to enter clinical trials and has completed the phase I study for dose finding, toxicity evaluation and PK determination (51). Another compound, the NKP-1339 (sodium *trans*-[tetrachloridobis(1*H*-indazole)ruthenate(III)], fig. 6), that is the sodium salt equivalent of KP1019, due to its higher solubility in water, has been selected as a lead candidate for clinical trials. It should be noted that both NAMI-A and NKP-1339 are currently under clinical evaluation (75-79).

Besides this promising ruthenium complexes, in the last two decades, it was published a large number of papers that reported the preparation of novel compounds with biological activity against cancer cells *in vitro* and *in vivo*. Complexes such as RM175 (fig. 7a)) represented a breakthrough in the ruthenium mechanism of action since they are based of Ru

(II) that is already an active molecule and don´t need to be reduced. The expectations for this type of compounds are high because of the type of interactions with DNA that are conferred by

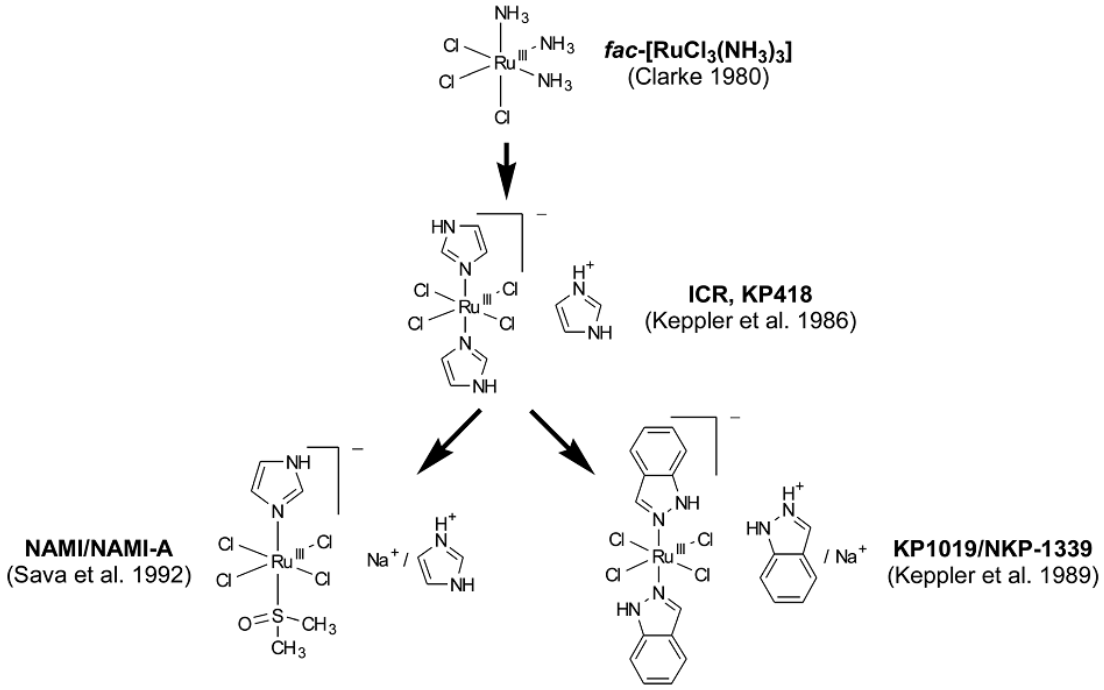

Figure 6 – Genealogy of antitumour ruthenium complexes. The represented references refer to the first published studies that have suggested their therapeutic activity in an in vivo tumor model (75).

the "piano-stool" shape which could overcome the mechanism of resistance. In the RM175, the "piano-stool" structure is given by an arene (η^6-C_6H_5) and the amine ligands represent the "legs" with one chloride as leaving group (80, 81). Nevertheless, a series of different ligands could be incorporated, such as in the complexes of the RAPTA family (fig. 7b)). In this case, the ligand is a PTA (1,3,5-triaza-7-phosphoadamantane) molecule that enable this complexes to be selectively activated in the hypoxic environment of solid tumours showing antimetastatic (82, 83), antiangiogenic (84, 85) and anticancer (86) properties *in vivo* (51, 87). Recently it was reported several studies with O,O- and O,N- chelating ligands linked to the arene-Ru (II), showing a potent *in vitro* cytotoxic activity (88-90). RDC11 (fig. 7c)) (RDC: ruthenium derived compounds) is a complex that showed excellent preclinical data and represents a good candidate for clinical trials. This compound does not cause severe side effects to the liver, neuronal sensory system, kidneys, or blood cells and are free of resistance in several cancer cell lines (91).

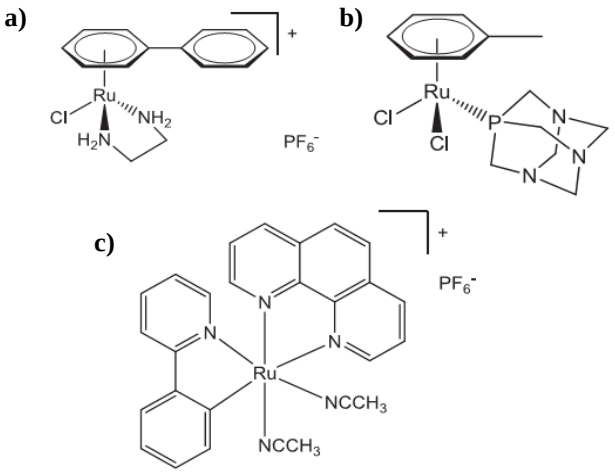

Figure 7 – Chemical structures of three ruthenium drug candidates: a) RM175 ([(η^6-$C_6H_5C_6H_5$)RuCl($H_2NCH_2CH_2NH_2$-N,N′)]PF_6); b) RAPTA-T (Ru(η^6-C_6H_5Me)(PTA)Cl_2) and c) RDC11 ([Ru(phenanthroline)(κ-*C*,*N*-(2-phenyl-pyridine)$(NCMe)_2$]PF_6 (adapted from ref. (51)).

1.1.1. Cyclopentadienyl Ru (II) complexes

The cyclopentadienyl ruthenium (II) complexes (with the general formula [(η^5-C_5H_5)Ru(P-P)L]$^+$) (e.g. P-P: 1,2-bis(diphenylphosphine)ethane (dppe) or triphenylphosphine (PPh_3); L: monodentate or bidentate nitrogen donors) have a piano-stool structure and were being prepared with different type of ligands in the past years. However, the anticancer activity of these compounds has been insufficiently studied, fact that is emphasized with the few number of papers that have been published. Nevertheless, promising results were observed (92, 93). Along this point, some examples of them will be mentioned.

One of the explored aspects were the preparation of ruthenium compounds with the aim to mimic the activity of staurosporine, a biomolecule that has a high affinity to the ATP binding site of the protein kinases, thus inhibiting their biological activity(94-96). This approach is very promising, since kinases are important molecular targets for the cancer treatment (their mutation or deregulation of their activity can induce cancer) (97). Additionally, the syntheses of such biomolecules, as the staurosporin, are often quite difficult because of their complex three-dimensional structure and the need to maintain a specific conformation and special orientation (98). In the other hand, the organometallic moieties are relatively easy to synthesize in a specific spatial conformation and their specificity to target kinases, in some cases, is even higher than staurosporin (99, 100). An example of this type of ruthenium complexes is represented in fig.

3c) and other more have showed auspicious results. Some examples are the prepared compounds in the studies of Atilla-Gokcumen G.E. *et al* (101), Pagano N. *et al* (102), Smalley K.S. *et al* (103) and Bregmann H., Meggers E. (104).

Ruthenium (II) cyclopentadienyl complexes with the general formula of $[(\eta^5\text{-}C_5H_5)Ru(P\text{-}P)L]^+$ (P-P: 1,2-bis(diphenylphosphine)ethane (dppe) or triphenylphosphine (PPh_3); L: monodentate or bidentate nitrogen donors) has been prepared and studied for anticancer applications by the group of Professor Helena Garcia at Lisbon University (ULisboa) during for, at least, 16 years (105-112). They exhibit anticancer activity against several cancer lines in the nanomolar range with better results when compared with *cisplatin* (105-107, 111). Among one of the most effective is the TM34 ($[(\eta^5\text{-}C_5H_5)Ru(2,2'\text{- bipy})(PPh_3)][CF_3SO_3]$, fig. 8a)) (92). Not only its anticancer activity was studied but also its mechanism of action. More recently, they have prepared quite a few carbohydrate Ru(II) complexes with the same general formula (the ligand is a carbohydrate-derived molecule) (109, 110, 112), which some of them have showed leading cytotoxic results (one of the most promising is presented in fig. 8b)) against the colorectal cancer when compared with the oxaliplatin, the chemotherapeutic metallo-drug used in the treatment of this type of cancer (112).

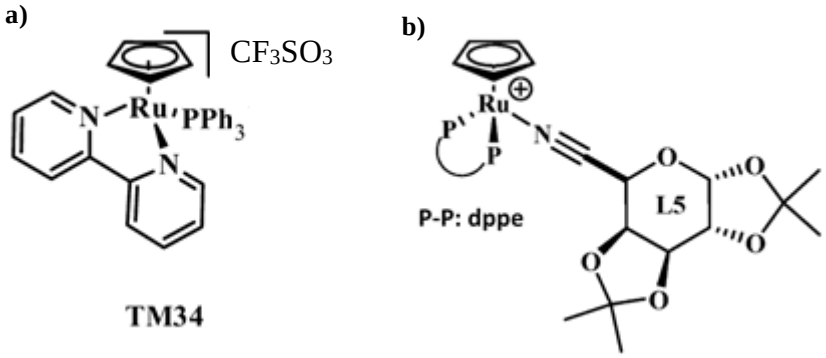

Figure 8 – Molecular structures of two ruthenium complexes with the general formula $[(\eta^5\text{-}C_5H_5)Ru(P\text{-}P)L]^+$ (P-P: 1,2-bis(diphenylphosphine)ethane (dppe) or triphenylphosphine (PPh_3); L: monodentate or bidentate nitrogen donors): a) TM34 ($[(\eta^5\text{-}C_5H_5)Ru(2,2'\text{- bipy})(PPh_3)][CF_3SO_3]$) and b) a Ru (II) cyclopentadienyl complex with a carbohydrate-derived ligand (adapted from ref. (112)).

2. METALLODENDRIMERS AS ANTICANCER DRUGS

Metal-based drugs, as it was already mentioned in the previous section, have a high number of attractive properties for anticancer treatment but there are also some limitations: dose-limiting water solubility, lack of cell specificity, toxicity and the primary structure of the metallocomplexes is affected which may alter its biological activity (3). A promising drug delivery strategy, the use of nanocarriers, can potentially overcome a great part of these limitations. In the past decades, nanotechnology had a great progress in chemotherapy (113-116) and different types of nanocarriers, such as dendrimers, have been designed to enhance the pharmacokinetic properties and increase the water solubility of the metal-based drugs. These molecules are created in a specific way in order to transport the drug(s) safely to the target, protecting them from the elimination mechanisms and *in vivo* degradation and, at the same time, minimizing the toxic effects to the healthy cells (3).

The metal-based anticancer drugs and the concept of multinuclearity is a growing area of research. Combining more than one metal in the same molecule can result in enhanced therapeutic activity (117-121). Furthermore, one way of introducing this concept is by conjugating these therapeutic agents onto dendrimers (122-126).

2.1. Dendrimers in drug delivery applications

Dendrimers are the result of the advances and innovations carried out in the 20th century in the field of polymer science. These molecules were, for the first time, studied during 1970–1990 mainly by two different groups: Vögtle F. *et al*. (127) and Tomalia D.A. *et al*. (128). Since then, numerous papers related to the synthesis of different families of dendrimers have been published. The expression "dendrimer" was built up from two Greek words "dendrons**"** meaning "tree" or "branch" and "meros" meaning "part" and, although having a well-defined finite molecular structure, they should be considered a sub-group of hyperbranched polymers (fig. 9) (129, 130). These synthetic polymeric macromolecules are characterized by having high branching points, three dimensional globular shape (131, 132), narrow polydispersity index (133) and a precisely controlled nanoarchitecture with a large number of tailor-made terminal groups which could be finely tuned. There are three distinct domains in a dendrimer´s architecture: *a)* a core composed by an atom or a molecule (with, at least, two identical chemical

functions), at the center; *b)* branches that arise from the core, represented by repeat units with, at least, one branch junction that are organized in a geometrical progression to originate radially concentric layers called "generations" (represented by the letter "G"); and *c)* many terminal functional groups (or end groups), generally located at the surface, that are vital in determining the properties of dendrimers (fig. 10) (130).

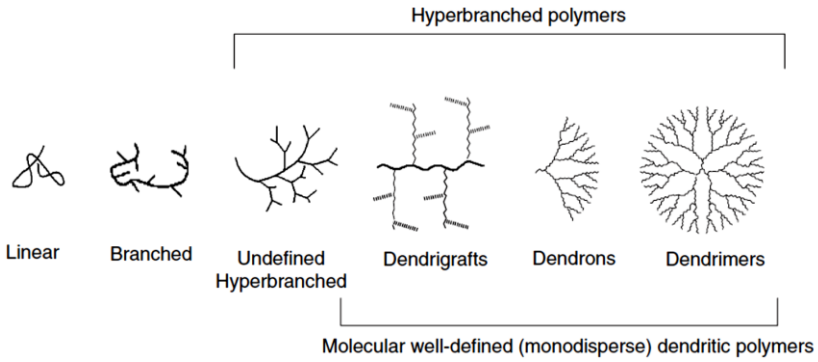

Figure 9 - Evolution of polymers towards dendritic structures (130).

.

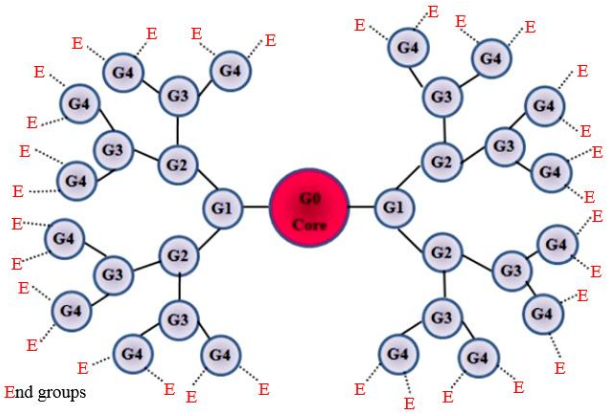

Figure 10 - Schematic representation of the general structure of a dendrimer. G0, G1, G2, G3, and G4 are the generation number (adapted from ref. (130)).

Dendritic architecture is, most frequently, synthetized either by divergent or convergent approaches (fig. 11). In the divergent method (firstly introduced by Tomalia D.A. *et al* (134)), dendrimer is grown away from a central focal point (i.e.: core extending radially to the periphery); whereas in the convergent method (discovered by Frechet J.M. *et al* (135)), synthesis starts from the surface and proceeds towards the interior prior to the attachment of pre-synthetized dendrons to the core (136).

Low-generation dendrimers (G1 to G4 dendrimers), when compared with high-generation dendrimers (G5 to G10) have significant advantages: *a)* are easy to synthesize, purify and characterize using well-known techniques; *b)* their yield is substantially better; *c)*

demonstrate a low level of branching defects but still high degree of functionalities; *d)* show absence or reduced backfolding; *e)* may play an important role in controlling steric effects, the degree of electrophile/nucleophile interaction process and solubility; *f)* exhibit shorter blood

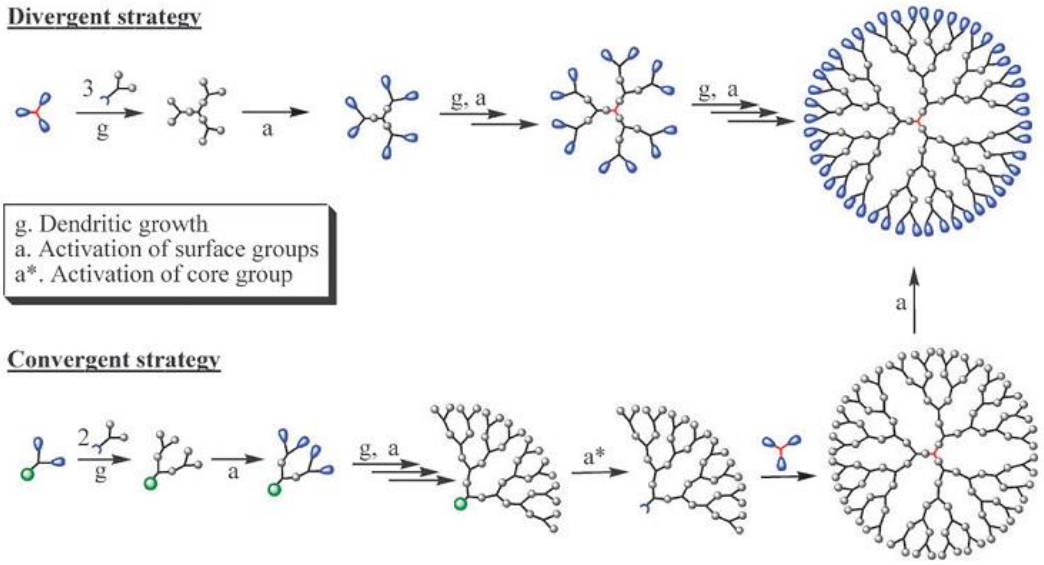

Figure 11 - The two most commonly used methods for dendrimers synthesis: divergent and convergent strategies (130).

circulation time; *g)* show an enhanced permeability and retention (EPR) effect – they accumulate at higher concentrations in the tumor *vs.* normal tissues; *h)* suffer easily cell endocytosis and renal excretion (137).

Dendrimers, specifically as nanocarriers, have a number of peculiar properties that make them apposite for that end: *a)* the capability to transport higher loads of drug with the encapsulation of them in their internal cavities or with their conjugation at the "surface" (138, 139); *b)* the possibilility of designing the complex with a specific number of monomers, polymeric branches and functional groups (138) and *c)* their multifunctional surface that enhances the selectivity of the drug (122, 140, 141).

The mechanism of drug delivery is based on two different strategies. The enhanced permeability and retention (EPR) effect (fig. 12) justifies the accumulation of dendrimers preferably in the cancer cells due to their high vascularization and poor lymphatic drainage, which increase the bioavailability of the transported drug and reduce the side effects. However, the degree of vascularization in different tumours is not homogeneous which creates an important limitation for this strategy (142-145). In contrast, the dendritic complex (dendrimer + drug) could be synthesized with specific moieties at the surface that will interact specifically

with overexpressed cancer cells receptors. This approach will lead to the internalization of the complex, being more effective (146).

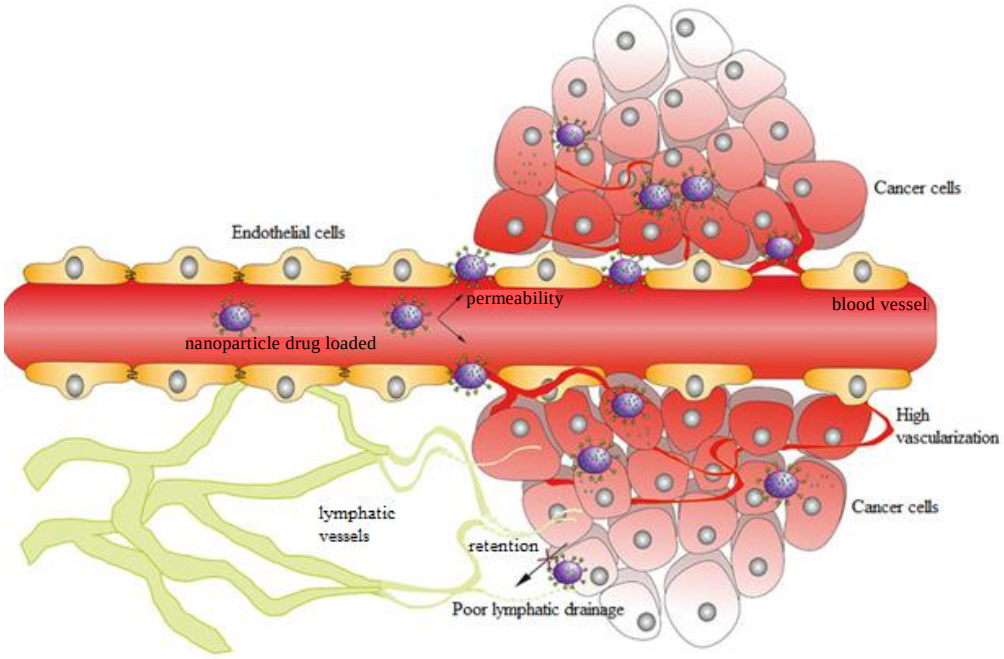

Figure 12 – Schematic representation of the EPR effect in drug delivery (adapted from ref. (145)).

2.1.1. PAMAM dendrimers

There are many types of dendrimers having different functionalities that were synthetized in the last decades. Some of these include the PAMAM (Polyamidoamine) (147), PPI (PolyPropylene Imine) (148), liquid crystalline (LC) (149), core-shell (tecto) (150), chiral (151), peptide (152), hybrid (153), glycodendrimers (154), metallodendrimers (122, 155) (or metal-containing dendrimers), triazine based (156) and dendritics polyesters (157), polyglycerols (158), phosphorous dendrimers (159-161) and hybrid families of dendrimers.

PAMAM dendrimers were firstly synthetized by Tomalia and co-workers (128) in the mid-1980s and were the first dendritic structures that have been exhaustively investigated and have received widespread attention. These dendrimers have polyamide branches with tertiary amines as branching points and their synthesis is possible by using the divergent method with ethylenediamine or ammonia as initiator core reagents. They can be obtained having surface amino groups or carboxylic acid groups, being commercially available, usually as methanol solutions, up to generation 10 (129, 130).

2.2. Metallodendrimers

As it was introduced in point 2., the concept of multinuclearity can be applied to improve the effectiveness of the anticancer drugs. Dendrimers can be used as organic scaffolds for the incorporation of metal-based drugs, hence metallodendrimers. Thus, the attractive properties of dendrimers as nanocarriers and the anticancer activity of some metal-based drugs came together to develop an emerging area of interest. These interesting molecules could be prepared with different frameworks (fig. 13): *a)* the metal could be on the periphery of the metallodendrimer; *b)* scattered all over the framework or *c)* encapsulated in the internal cavities of the dendrimer (117).

Since the metallodendrimers field is still in expansion (when compared to the other classes of dendrimers for biomedical applications), there are only a few examples of them reported in the literature. The first compounds to show promising cytotoxicity in some resistant and sensitive cancer cell lines was prepared through the combination of an anionic G3.5-PAMAM dendrimer with cisplatin (162, 163).

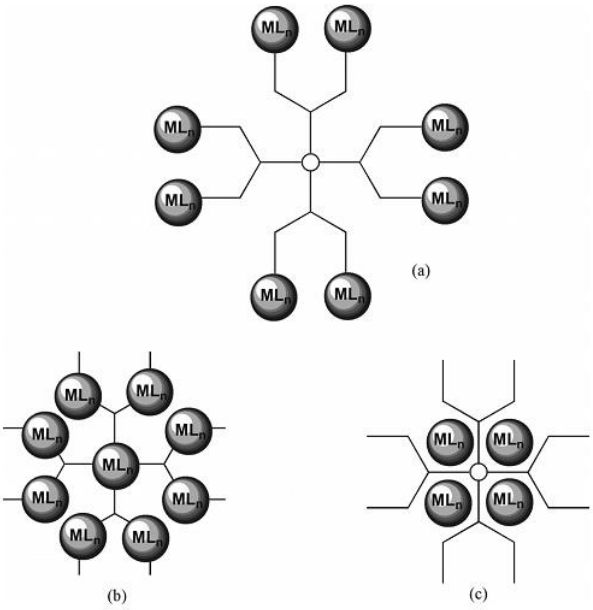

Figure 13 – Schematic representation of the metallodendrimers with the metallic moieties in several positions: a) on the periphery; b) scattered throughout the framework and c) encapsulated between the structure of the dendrimer (111).

Meanwhile, Zhao C. *et al* (141) have modified the G1-PAMAM dendrimer to prepare a multinuclear copper complex that also have showed good in vitro results against several cancer cell lines (fig. 14a)). Other two examples of prepared metallodendrimers are the multinuclear Pt (II) and Pd (II) G2-polyamide metallodendrimers (164) (fig. 14b)) and the G1-dinuclear gold(I) metallodendrimers prepared from alkyne-terminated precursors (165) (fig. 14c)).

2.2.1. Polynitriles compounds as core ligands for the preparation of metallodendrimers

Nitriles compounds are an important family of molecules due to several reasons, for example: they can be the substrates of the nitrile biocatalysis reaction for industrial production of carboxylic acids, waste treatment and surface modification (166, 167) and represent an essential starting material in organic and inorganic processes (168, 169) with applications on the field of materials (170) and other polymers (171, 172) among others. In fact, they are able to form addition compounds both with nucleophilic and electrophilic reagents. This important property derives from the electronic structure of the triple carbon-nitrogen bond. In terms of nucleophilic addition, they have the ability to stabilize a wide variety of transition metals in different oxidation states (173) in order to form new stable complexes with different properties, namely magnetic (174) and second- and third order non-linear optical properties (169, 170, 175, 176). Thus, they act as ligands strongly activated in the presence of metal ions or electron withdrawing R moieties, as the CF_3 (in contrast to their inertness in the free form), which enhances the rate of reaction in the $10^6 – 10^{10}$ range (177). Their coordination with low-valent and electron rich metal centres, also improve their reactivity towards electrophilic attack. They are also good σ-donors and isoelectronic with other unsaturated ligands – acetylide anions, carbon monoxide, dinitrogen, and isocyanides – which allow them to be involved in substitution or ligand conversion processes (137, 168, 178). In fact, the coordination of nitriles with transition metals, in respect to the metal centre, is described not only in terms of acceptor and electron donor, but also with a contribution of electrostatic interactions (179, 180). These interesting properties of nitriles make them, currently, a target of interest (137, 168).

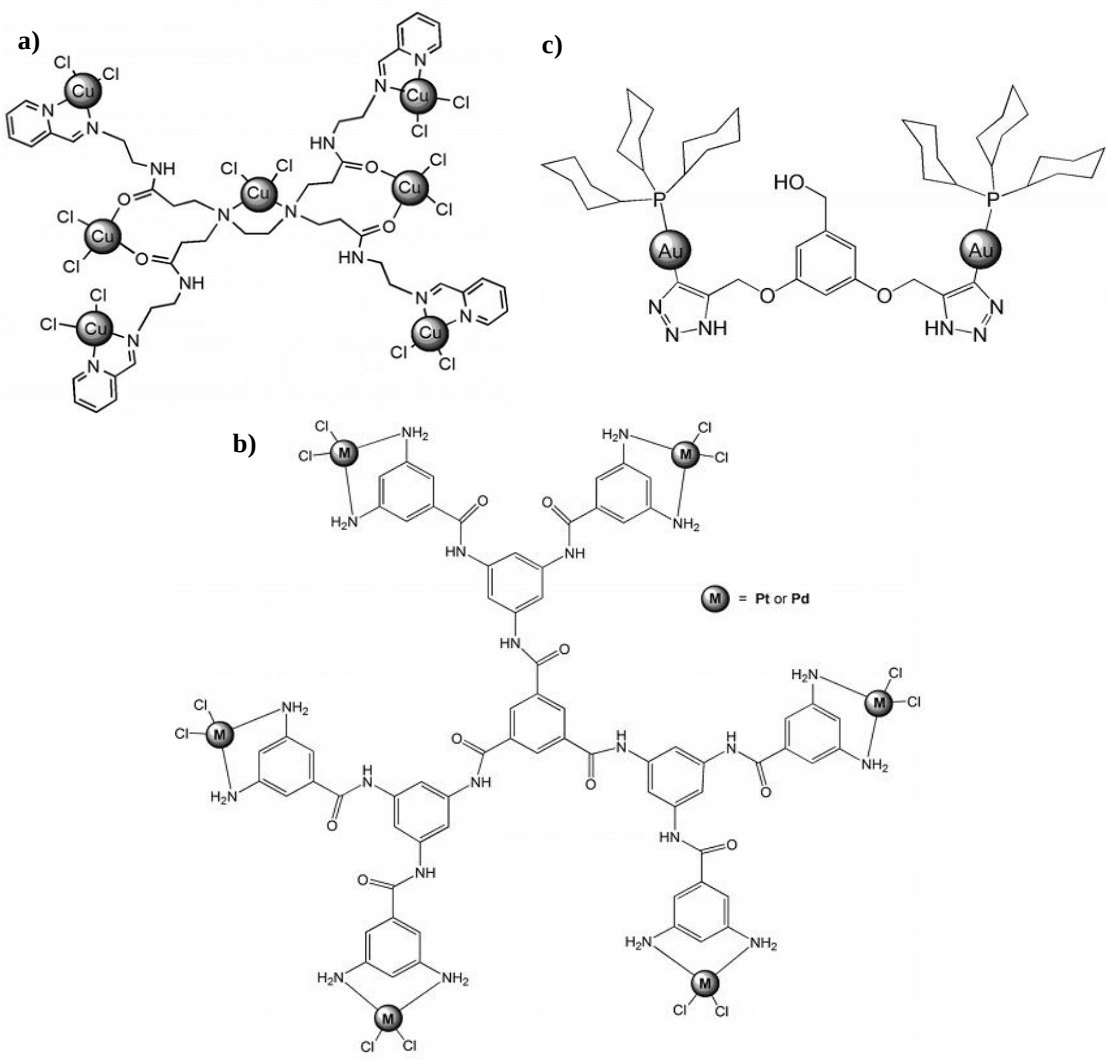

Figure 14 – Molecular structures of three different metallodendrimers: a) multinuclear copper-functionalized, b) a multinuclear Pt (II) and Pd (II) G2-polyamide, and c) G1-dinuclear gold(I) (adapted from ref. (111)).

2.2.2. Ruthenium metallodendrimers

Regarding the ruthenium metallodendrimers as potential anticancer agents there are still few reports available. Some examples are the compounds that were prepared and studied by Govender P. *et al* (122, 140, 181). The first to be prepared was the multinuclear arene ruthenium complexes coordinated to dendritic polypyridyl scaffolds (fig. 15). These compounds have demonstrated a moderate anticancer activity when compared with *cisplatin*, against ovarian cancer cell lines. Additionally, they have discovered a correlation between the size of the complex and the obtained cytotoxicity: the octa-coordinated metallodendrimers have showed the best results, when compared with the tetra-coordinated (140).

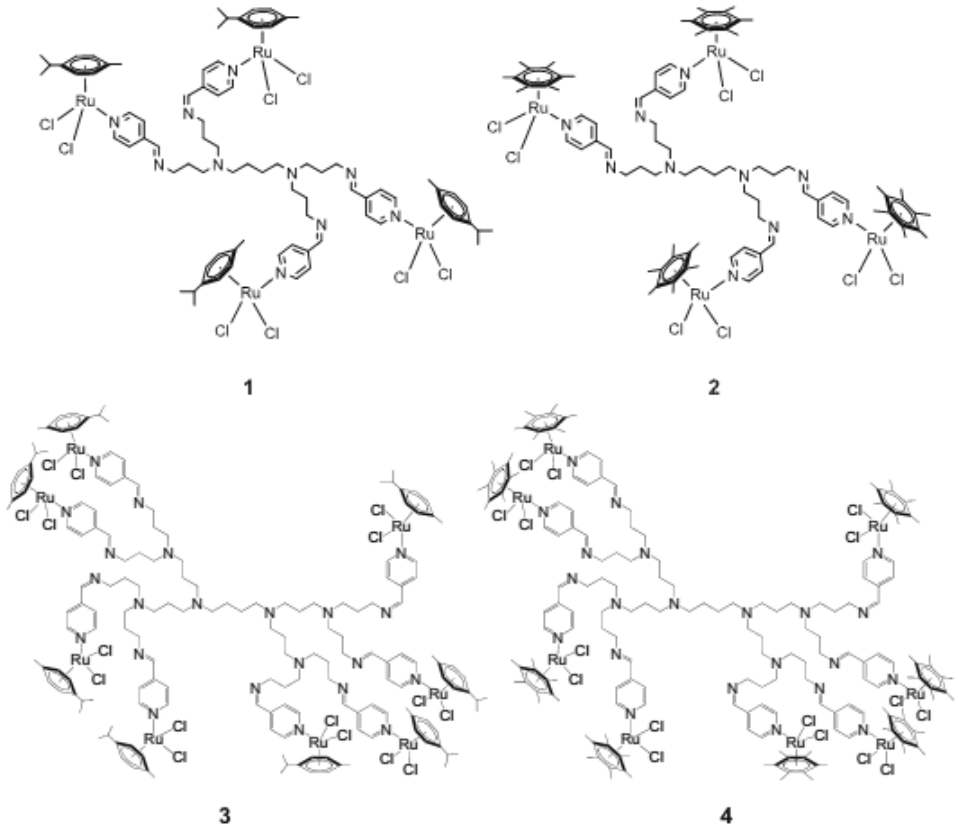

Figure 15 - Tetra- and octanuclear arene ruthenium complexes coordinated to dendritic polypyridyl scaffolds (134).

Two years later, they have also prepared a family of chelating, neutral, and cationic first and second generation ruthenium(II) arene complexes based on poly(propyleneimine) dendrimer scaffolds (fig. 16). The *in vitro* results were similar to their previous studies corroborating the achieved conclusion. They also performed DNA-binding experiments and have found that the observed increased anticancer activity was correlated with their increase of DNA binding activity (181).

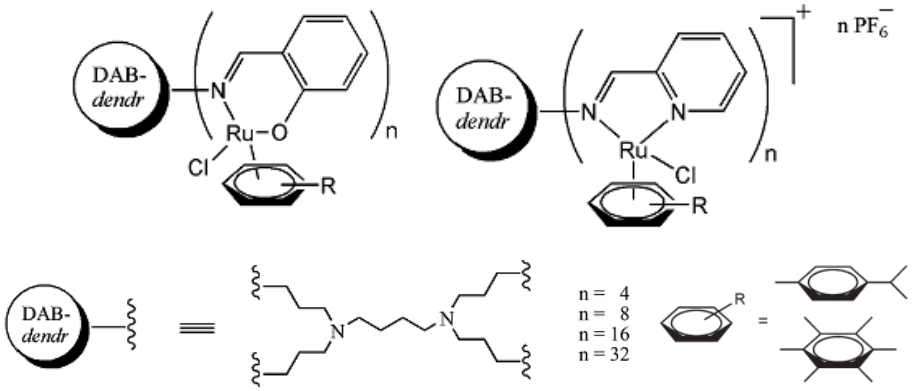

Figure 16 - Chelating *N*,*O*- and *N*,*N*-ruthenium(II) arene metallodendrimers with poly(propyleneimine) dendrimer as scaffolds. They are coordinated with 4, 8, 16 or 32 n groups (adapted from ref. (181)).

The last family of the prepared ruthenium metallodendrimers was a series of neutral, chelating N,O-ruthenium(II)-arene and cationic, chelating N,O-ruthenium(II)-arene-PTA salicylaldimine metallodendrimers (fig. 17). A similar study was performed and the metallodendrimers with 32 end groups have shown the best proliferative activity (122, 182).

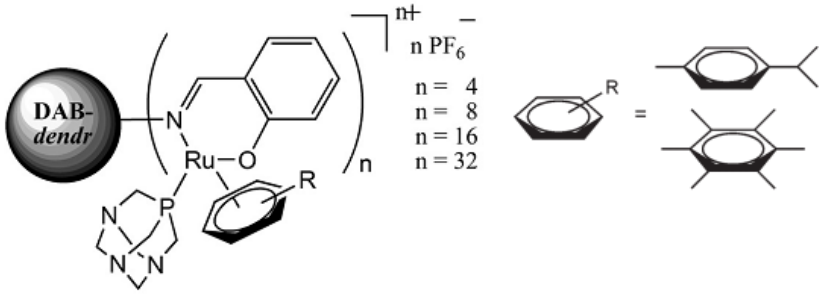

Figure 17 – Cationic, chelating N,O-ruthenium(II)-arene-PTA salicylaldimine metallodendrimers (adapted from ref. (181)).

As it was already demonstrated, metallodendrimers represents an exciting family of compounds with promising anticancer applications when compared with *cisplatin*. However, there are several crucial properties that must be extensively studied, such as the pharmacokinetics, biocompatibility, and stability under physiological conditions, toxicity and biodistribution. Thus, *in vivo* studies are urgent in other to a better understanding of the mechanism of action of these promising therapeutic molecules. Consequently, it is predicted for the next years a continuous increase of interest of the metallodendrimers in the field of anticancer therapy (117).

3. SCOPE AND OBJECTIVES

The theme of this work was inspired in the attractive and promising anticancer properties of the ruthenium complexes combined with the application of dendrimers as nanocarriers. Additionally, the versatility of dendrimers as building blocks for the preparation of other dendrimers with surface groups of interest, including poly-nitrile groups that will act as core ligands for the preparation of ruthenium metallodendrimers was also considered. Previous studies of our group (Molecular Materials Research Group of CQM – Madeira Chemistry Research Centre) (137, 183-185) as explored the ability of the nitrile groups from functionalized poly(alkylidenamine) dendrimers to coordinate and bridge with a ruthenium cyclopentadienyl

complex [Ru(η^5-C_5H_5(PPh$_3$)$_2$Cl] for the preparation of different cationic metallodendrimers. Their findings were crucial for the development of this work and, in this way, the main goal was to optimize a synthetic strategy to functionalize nitrile-based PAMAM dendrimers, from generations 0 and 1, with the organometallic moiety [Ru(η^5-C_5H_5)(PPh$_3$)$_2$Cl]. Other goal was to fully characterize them with 1D/2D-NMR (one-dimensional/two-dimensional-Nuclear Magnetic Resonance), FTIR (Fourier Transform Infrared Spectroscopy) and MS (Mass Spectrometry) in order to evaluate their structure and determine the exact mass.

PART II – DEVELOPED METHODOLOGY

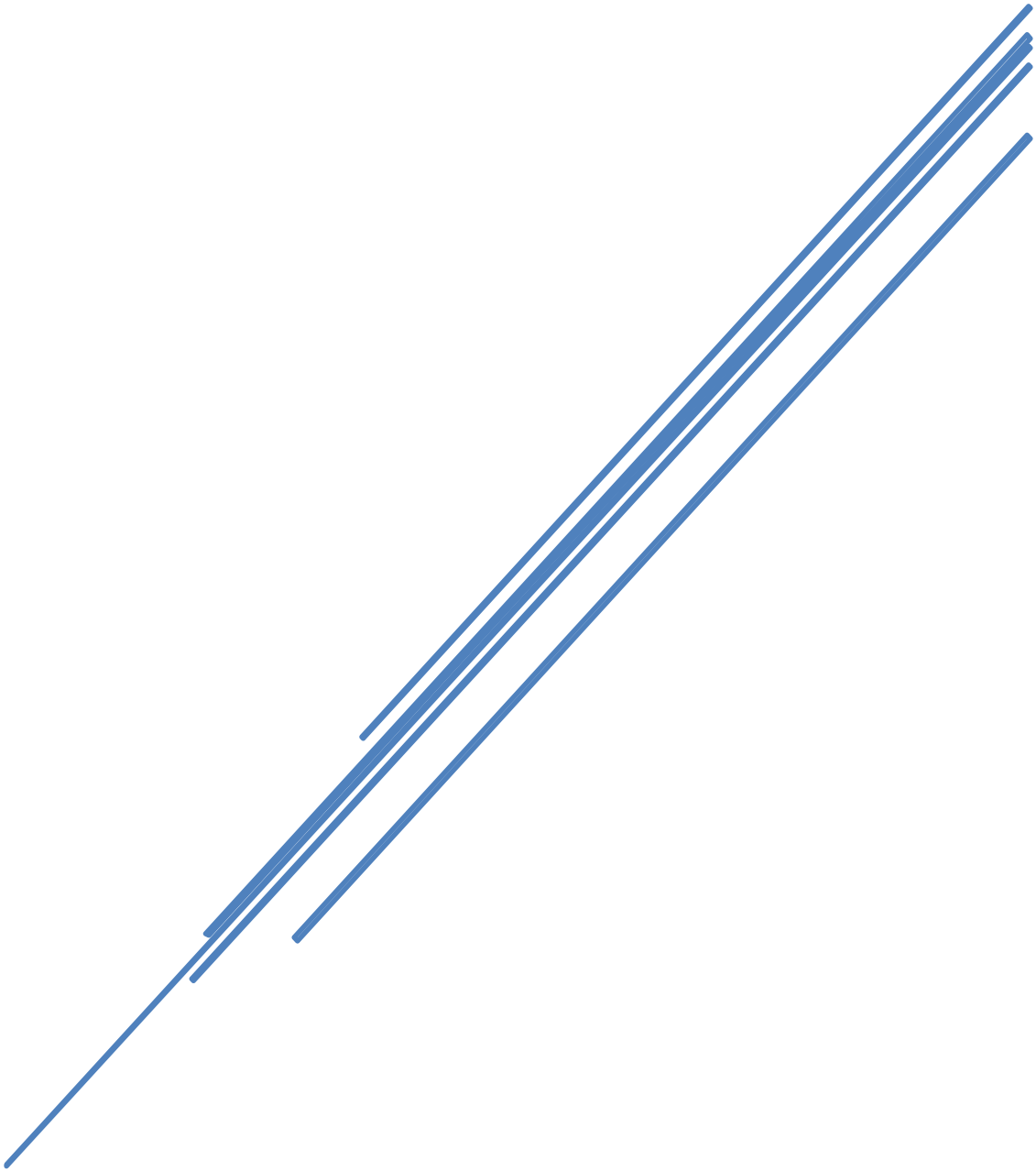

4. ORGANOMETALIC COMPOUNDS

In this section, the developed methodology for the preparation of the nitrile ruthenium-based metallodendrimers G0-(CNRu(η^5-C_5H_5)(PPh_3)$_2$)$_4$(CF_3SO_3)$_4$ and G1-(CNRu(η^5-C_5H_5)(PPh_3)$_2$)$_8$(CF_3SO_3)$_8$ will be presented and discussed.

4.1. Materials and methods

4.1.1. Reagents and solvents

All reactions were carried out under a nitrogen (N_2) atmosphere by using standard Schlenk-tube techniques (186, 187). Et_2O (diethyl ether, $C_4H_{10}O$, ≥ 98%, CAS No. (Chemical Abstracts Service number) 60-29-7, ACROS Organics) and DCM (dichloromethane, CH_2Cl_2, 99.6%, CAS No. 75-09-2, ACROS Organics) were dried by the solvent purification system mBRAUN MB SPS-800 and degassed prior to use. MeOH (methanol, CH_3OH, 99.9%, CAS No. 67-56-1, Fisher Chemical) and EtOH (ethanol absolute, C_2H_6O, ≥ 99.5%, CAS No. 64-17-5, Fisher Chemical) were also degassed. All the other chemicals were used as received: PAMAM dendrimer G(0.0) (surface: NH_2, 54.95 % w/w, solvent: MeOH, Dendritech® Inc.); PAMAM dendrimer G(1.0) (surface: NH_2, 36.25 % w/w, solvent: MeOH, Dendritech® Inc.); MeOH (99.99%, HPLC grade, ACROS Organics); $CDCl_3$ (deuterated chloroform, 99.8 atom %D, CAS No. 865-49-6, Merck); D_2O (deuterated water, 99.8 atom %D, CAS No. 7789-20-0, ACROS Organics); ACN (acrylonitrile, C_3H_3N, 99+%, CAS No. 107-13-1, ACROS Organics); $CHCl_3$ (chloroform, 99.8%, CAS No. 67-66-3, ACROS Organics); $AgCF_3SO_3$ (silver trifluoromethanesulfonate, 99+%, CAS No. 2923-28-6, ACROS Organics); Dicyclopentadiene ($C_{10}H_{12}$, 95%, CAS No. 77-73-6, ACROS Organics); $RuCl_3.xH_2O$ (Ruthenium (III) chloride hydrate, 35 to 40% Ru, CAS No. 14898-67-0, ACROS Organics); and PPh_3 (triphenylphosphine, $C_{18}H_{15}P$, 99%, CAS No. 603-35-0, ACROS Organics).

4.1.2. Samples preparation

The G0/G1-PAMAM dendrimer commercial solutions (in MeOH; 3.46 mL for G0 – 54.95 % w/w) and 5.24 mL for G1 – 36.25 % w/w) were evaporated in the rotatory evaporator and dried under vacuum. It were then dissolved in water and lyophilized.

4.1.3. Synthesis of poly-nitrile dendrimers G0/G1-CN

For the preparation of the G0-nitrile dendrimer (G0-$(CN)_4$), at room temperature and N_2 atmosphere, 1.87 g (3.63 mmol; 1 equivalent (eq.) mol) of G0-PAMAM was dissolved in 100 mL of MeOH and 1.925 mL (1.54 g; 29.03 mmol; 8 eq. mol) of ACN was added dropwise. The reaction mixture was warmed up to 48°C and left stirring. After 3h, the heating was stopped and the mixture was allowed to cool down. The volatiles were removed by the rotatory evaporator and by vacuum to afford a crude product as a light-yellow oil (2.62 g, 3.59 mmol, 99% of yield). The performed ^{1}H (proton) and ^{13}C-NMR (carbon-13 Nuclear Magnetic Resonance) of the crude confirmed the identity of the tetra-nitrile dendrimer but it was needed to purify the compound. It was conducted a liquid-liquid (L-L) extraction with $CHCl_3$-H_2O and the aqueous fraction was freeze-dried to be obtained a purified G0-$(CN)_4$ as a light-yellow oil (2.30 g, 3.15 mmol, 87 % of yield). It was characterized by ^{1}H and ^{13}C-NMR, COSY (correlation spectroscopy), HSQC (heteronuclear single-quantum correlation) and FTIR. ^{1}H-NMR – proton Nuclear Magnetic Resonance – (400 MHz, $CDCl_3$): δ = 7.292 (t (triplet), 3 H), 3.321 (q (quartet), 8 H), 2.918 (t, 7 H), 2.773 (t, 8 H), 2.697 (t, 8 H), 2.524 (t, 8 H), 2.463 (s (singlet), 3 H), 2.343 (t, 8 H), 1.243 (s) ppm. ^{13}C-NMR (100 MHz, $CDCl_3$): δ = 174.69 (–HN*C*=O), 119.20 (N*C*CH_2–), 51.54, 50.53, 48.30, 44.74, 39.18, 34.38, 19.04 ppm. COSY (400 MHz, $CDCl_3$): four signals. HSQC (100 e 400 MHz, $CDCl_3$): seven signals. FTIR (NaCl – sodium chloride – cells): $\tilde{\nu}$ = 2248 (ν_{CN}) cm^{-1}.

The preparation of the G1-nitrile dendrimer (G1-$(CN)_8$) was followed as the abovementioned procedure with 1.295 mL of ACN (1.04 g; 19.52 mmol; 16 eq. mol) for 1.74 g (1.22 mmol; 1 eq. mol) of G1-PAMAM to be obtained 2.23 g (1.20 mmol; 99% of yield) of crude G1-$(CN)_8$ as a dark yellow oil. The performed ^{1}H and ^{13}C-NMR of the crude confirmed the identity of the octa-nitrile dendrimer and, subsequently, it was purified by the same method that was applied for the equivalent G0 dendrimer. It was possible to obtain 2.12 g of a purified G1-$(CN)_8$ (1.14 mmol) with an excellent yield of 94 %, with the same consistency than before, a dark yellow oil. It was fully characterized by the same methods that were used for G0-$(CN)_4$. ^{1}H-NMR (400

MHz, $CDCl_3$): δ = 7.651 (t, 4 H), 7.348 (t, 7 H), 3.375 (q, 16 H), 3.234 (q, 8 H), 2.914 (t, 15 H), 2.757 (q, 39 H), 2.529 (t, 28 H), 2.339 (q, 24 H), 2.195 (s) ppm. ^{13}C-NMR (100 MHz, $CDCl_3$): δ = 172.95 (–HNCH$_2$CH$_2$HN*C*=O), 172.74 (–NCH$_2$CH$_2$HN*C*=O), 119.24 (N*C*CH$_2$–), 52.63, 51.54, 50.54, 48.28, 44.76, 39.18, 37.83, 34.33, 19.01 ppm. COSY (400 MHz, $CDCl_3$): six signals. HSQC (100 e 400 MHz, $CDCl_3$): nine signals. FTIR (NaCl cells): $\tilde{\nu}$ = 2247 (ν_{CN}) cm^{-1}.

4.1.4. Synthesis of the organometallic compound $[RuCp(PPh_3)_2Cl]$

Cyclopentadiene (Cp) is one of the starting compounds that are needed for the preparation of the organometallic moiety [RuCp(PPh$_3$)$_2$Cl] through the reported methodology of Bruce M. and Windsor N. (188) and Dias A.R. *et al* (189). It can be easily obtained from the liquid-phase cracking of dicyclopentadiene with gaseous N_2 as the carrier gas. With temperatures of 170 to 177°C (slower reflux of dicyclopentadiene), cyclopentadiene started distilling at 38° and the distillation continued during 7h at 38 – 42°C. It was obtained 15 mL (11.8 g, 178 mmol, 20 % of yield) of it, as a colorless liquid, that was immediately stored at -20°C to prevent dimerization. The subsequently performed ^{1}H-NMR revealed that the compound was ready to use. A solution of $RuCl_3.xH_2O$ (3.92 g, 18.9 mmol, 1 eq. mol) in degassed EtOH (100 mL) was added to a stirred solution of PPh_3 (16.3 g, 62.4 mmol, 3.3 eq. mol) in refluxing EtOH (100 mL), followed immediately afterward by freshly distilled cyclopentadiene (15 mL, 177.6 mmol, 9.4 eq. mol). The mixture was then refluxed with stirring until the colour has changed from black to reddish (during 2h) to be filtered when still warm. The separated orange solid was dried under vacuum to be obtained a crystalline crude product (11.2 g, 15.5 mmol, 82% of yield). The performed ^{1}H and ^{31}P-NMR spectra confirmed the identity of the [RuCp(PPh$_3$)$_2$Cl]. However, it was observed a small amount of a black-coloured solid impurity which confirmed the need to purify it. Thus, it was washed with cold EtOH, H_2O, EtOH and Et_2O (3 x 30 mL of each solvent), and dried under vacuum. 120 mL of DCM was added to dissolve the impurity (the orange powder has precipitated); the obtained black solution was filtered and the separated powder was dried under vacuum. It was obtained 7.4 g (10.2 mmol, 54% of yield) of a purified [RuCp(PPh$_3$)$_2$Cl] as a dark yellow powder, that was characterized by ^{1}H and ^{31}P-NMR. ^{1}H-NMR (400 MHz, $CDCl_3$): δ = 7.425 – 7.141 (three t, 12 H, overlapped by $CDCl_3$, 12 H, PPh_3), 4.136 (s, 5 H, C_5H_5) ppm. ^{31}P-NMR (161 MHz, $CDCl_3$): δ = 38.83 (s, *P*Ph$_3$) ppm.

4.1.5. Synthesis of metallodendrimers G0/G1-$(CNRuCp(PPh_3)_2)_x(CF_3SO_3)_x$

For the preparation of the G0-$(CNRuCp(PPh_3)_2)_4(CF_3SO_3)_4$ metallodendrimer, the previous prepared organometallic moiety $[RuCp(PPh_3)_2Cl]$ (1.64 g, 2.26 mmol, 4.1 eq. mol) was introduced with degassed MeOH (150 mL), under the N_2 atmosphere, into a two-necked round-bottomed flask. To the orange suspension was added the already dissolved (in 20 mL of the same solvent) G0-$(CN)_4$ (0.40 g, 0.55 mmol, 1 eq. mol) and $AgCF_3SO_3$ (0.77 g, 2.26 mmol, 5.4 eq. mol). The total of MeOH added was 220 ml. The mixture was left stirring at room temperature and protected by light, and after 30 min it was observed that the colour of the suspension has changed to yellow, and after 1.5h was already brownish. After 22h of reaction, the performed ^1H and ^{31}P-NMR spectra revealed that the synthesis was completed. Doing so, after 24h, the reaction was stopped, filtered to remove the silver chloride (AgCl) solid produced as a secondary product, and dried under vacuum. The product was quickly extracted with dichloromethane (DCM; 100 mL; dried and previously degassed), washed with diethyl ether (Et_2O; dried and previously degassed; 3 x 30 mL) and dried under vacuum. The performed ^1H and ^{31}P-NMR spectra exposed the need to purify the compound. The solid was dissolved in 15 mL of DCM and precipitated with Et_2O. After being at -20°C overnight, the solution was filtered (bronze colour) and the brown precipitate was dried under vacuum. This procedure was repeated two times. It was obtained 1.5 g (0.4 mmol) of the G0-$(CNRuCp(PPh_3)_2)_4(CF_3SO_3)_4$ as a brown semi crystalline powder with a good yield of 79 %. The final characterization was performed by ^1H, ^{31}P,^{13}C-NMR, COSY and FTIR. ^1H-NMR (400 MHz, $CDCl_3$): δ = 7.362 – 7.071 (n.d. (not defined), 24 H, overlapped by $CDCl_3$, 48 H, PPh_3), 4.451 (n.d., 20 H, C_5H_5), 3.337 (n.d., 8 H), 3.146 (n.d., 8 H), 3.042 (n.d., 7 H), 2.854 (n.d., 8 H), 2.619 (n.d., 12 H), 2.447 (n.d., 8 H) ppm. ^{31}P-NMR (161 MHz, $CDCl_3$): δ = 41.54 (d, *P*Ph_3) ppm. ^{13}C-NMR (100 MHz, $CDCl_3$): δ = 133.37, 130.25, 128.44 (PPh_3), 122.47 (–$CNRuCp(PPh_3)_2$), 83.65 (C_5H_5), 52.68, 52.36, 48.96, 43.65, 42.99, 29.82, 20.65 ppm. HSQC (100 e 400 MHz, $CDCl_3$): eleven signals. FTIR (KBr – potassium bromide): $\tilde{\nu}$ = 3058 ($\nu_{Aryl\text{-}H}$), 2328 (ν_{CN}), 1436 ($\nu_{Aryl\ C=C}$), 1265 (ν_{CF}), 747 (ν_{CS}) cm^{-1}.

Following the same procedure for the synthesis of the G0-$(CNRuCp(PPh_3)_2)_4(CF_3SO_3)_4$ compound, it was prepared the next generation of it – G1-$(CNRuCp(PPh_3)_2)_8(CF_3SO_3)_8$. From 0.52 g (0.28 mmol, 1 eq. mol) of G1-$(CN)_8$, 1.66 g (2.28 mmol, 8.1 eq. mol) of $[RuCp(PPh_3)_2Cl]$ and 0.68 g (2.65 mmol, 9.4 mmol) of $AgCF_3SO_3$, and 24h of reaction at room temperature (r.t.),

it was possible to synthetize the crude G1 metallodendrimer. After being extracted with DCM, washed by Et_2O and precipitated, two times, also by Et_2O after being dissolved in DCM, it was possible to obtain a much purer compound (1.6 g; 0.23 mmol), as a dark-brown microcrystalline powder, with a good yield of 77%. It was fully characterized by the same methods that were used for G0-$(CNRuCp(PPh_3)_2)_4(CF_3SO_3)_4$. ^{1}H-NMR (400 MHz, $CDCl_3$): δ = 7.344 – 7.055 (n.d. (not defined), 48 H, overlapped by $CDCl_3$, 96 H, PPh_3), 4.422 (s, 40 H, C_5H_5), 3.293 (n.d., 8 H), 3.222 (n.d., 17 H), 3.080 (n.d., 17 H), 2.784 (n.d., 41 H), 2.599 (n.d., 37 H), 2.448 (n.d., 16 H) ppm. ^{31}P-NMR (161 MHz, $CDCl_3$): δ = 41.60 (s, *P*Ph_3) ppm. ^{13}C-NMR (100 MHz, $CDCl_3$): δ = 173.48 (–$HNCH_2CH_2HNC$=O), 173.04 (–NCH_2CH_2HNC=O), 133.32, 130.21, 128.44 (PPh_3), 122.45 (–$CNRuCp(PPh_3)_2$), 83.52 (C_5H_5), 53.58, 52.33, 50.44, 48.37, 44.17, 39.70, 38.71, 31.43, 20.83 ppm. HSQC (100 e 400 MHz, $CDCl_3$): thirteen signals. FTIR (KBr): $\tilde{\nu}$ = 3062 ($\nu_{Aryl\text{-}H}$), 2343 (ν_{CN}), 1435 ($\nu_{Aryl\ C=C}$), 1265 (ν_{CF}), 749 (ν_{CS}) cm^{-1}.

4.1.6. Characterization

The commercial G0/G1-PAMAM dendrimer and the two prepared dendrimers were characterized by ^{1}H, ^{13}C-NMR, HSQC, COSY and FTIR. The two metallodendrimers were characterized by ^{31}P-NMR instead of the COSY and the G0-PAMAM was also characterized also by MS. It was not possible to perform the MS spectra in time of all compounds due to a unsolved malfunction of the equipment.

The NMR (^{1}H, ^{13}C, ^{31}P, COSY and HSQC) characterization was performed with ≈ 10 mg of each compound dissolved in 550 μL of solvent: D_2O for G1-PAMAM and $CDCl_3$ for the remaining compounds, including G0. The NMR spectra were recorded with a Bruker Avance II+ 400 at 299 K (probe temperature) spectrometer. All chemical shifts are reported in parts per million (δ, ppm) with reference to Me_4Si (TMS – tetramethylsilane).

FTIR characterization were recorded on a Nicolet Avatar 360 FTIR spectrometer. About 5 to 10 mg of each oily sample were analyzed in NaCl cells (25 x 4 mm). The solid samples were analysed in KBr. The main characteristics bands are reported in cm^{-1} and the type of vibration of each are also showed. Only the significant bands are cited in the text.

The MS characterization were performed with filtered samples of 1 g/L of G0-PAMAM. The used syringe filter was PTFE hydrophilic with 0.22 μm of pore from SPECANALITICA. The analysis was performed with a Bruker Esquire 6000/Dionex LC-ESI-MS/MS (Liquid

Chromatography – Electrospray Ionization – Mass Spectrometry) spectrometer, in 30 minutes of run. Only one of the various obtained spectrums of +MS (total fragmentation), +MS2 (second fragmentation) and +MS3 (third fragmentation) is presented in this work and likewise, only the significant *m/z* (mass-to-charge ratio) values are cited in the text.

4.2. Results and discussion

The characterization of the newly formed dendrimers was possible through routine physical methods of analysis, namely ^{1}H, ^{13}C, ^{31}P-NMR, COSY, HSQC, FTIR and MS.

NMR is the most widely used technique for the characterization of dendrimers, especially during the step by step synthesis (the chemical transformations undergone by the end groups can be analysed) from low to high generations. They afford information about the structure and morphology of these molecules but they have also been used to probe their size. Due to the ubiquity of protons in organic and inorganic compounds, protons are the most receptive common NMR nuclei and can be easily observed. Thus, a basic one-dimensional (1D) proton NMR (^{1}H-NMR) is the most common experiment. Nevertheless, there are several different experiments that can be extremely useful. For organic dendrimers, ^{1}H and ^{13}C-NMR are the most used, and for heteroatom-containing dendrimers, besides these two nuclei, the ^{31}P-NMR can afford valuable information because this experiment is very sensitive to small changes in the environment. In some cases, the two-dimensional (2D) experiments, such as homonuclear ^{1}H-^{1}H COSY and heteronuclear ^{1}H-^{13}C HSQC, can be extremely useful to aid structural elucidation. In COSY, the coupling patterns and connectivity of spin systems that are coupled can be observed and, in HSQC, the relationships between specific carbon and proton resonances that are bonded by one or two multiple bonds are proton detected, so they produce useful data in a shorter period (190, 191).

The IR (infrared) spectral changes are helpful during the synthetic sequence of dendrimers because they can assess the presence or disappearance of the functional groups at their pheriphery, since the synthetic sequence is typically characterized by changes in one or several functional end groups of atoms (192).

The MS spectra (plots of intensity *vs. m/z*) allow the assessment of the exact mass of the dendrimer by the identification of the molecular ion (the one with the greatest *m/z* value and represented by $M^{+}\cdot$) or the diverse fragments (with lower *m/z* values) obtained by different

fragmentation patterns from the molecular ion. The nature of the fragments often provides a clue to the molecular structure of the compound (192). Thus, it is essential a detailed analysis of the obtained spectra of characterization to confirm if the synthesis reaction has worked and produced the desired compound (with or without impurities or sub-products of the reaction).

The first step of this work was to characterize the starting dendrimers completely – G0/G1-PAMAM (colourless and golden oil, respectively; molecular structures in schemes 1 and 2) – to check their purity. Theirs ^{1}H, ^{13}C-NMR (in $CDCl_3$ and D_2O), COSY, HSQC, FTIR and MS obtained spectra and data are represented, for G0: in figs. 18a), b) and table 1; 1Aa), b) (section 7.1.1. in attachment); 19; 20; 2A (section 7.1.1.) and table 2; and 21, respectively; and for G1: in figs. 22a), b) and table 3; 23; 24 and 2A, respectively. Table 2 organize the data from the FTIR spectra of both generations. At the ^{1}H-NMR (fig. 18a)), the singlet with 7.260 ppm correspond to the signal of the solvent $CDCl_3$ and the other broad peak observed at *ca*. 1.7 ppm possibly belongs to the protons of H_2O that was adsorbed by this solvent. Also, it was detected the characteristic signal for the $–CH_3$ group of MeOH (3.455 ppm) which revealed that this solvent was not entirely removed by the evaporation and freeze-drying procedures. These ppm values were confirmed by the results presented in G. R. Fulmer *et al.*(193). Nevertheless, the presence of MeOH in the oily G0-PAMAM is not a problem for the next step – the synthesis reaction of G0-$(CO_2{}^{t}Bu)_8$ – because the solvent for this reaction is also MeOH. The obtained NMR data from both spectra of G0-PAMAM (fig. 18a) and b); table 1) was confirmed by the results acquired by the same molecule in W. Hung *et al*. (194) and A.P. Davis, *et al*. (195). In relation to the signal with 7.467 ppm it belongs, probably, to the –NH of the amide group ("e" signal). This conclusion is reasoned by the results obtained in H. Vahedi *et al*. (196). By the analysis of the COSY and HSQC spectra (figs. 18 and 19, respectively), the molecular structure of the dendrimer is confirmed. In the COSY spectrum, each spot represents the group of protons that are neighbours and separated by one single carbon bond and in the HSQC spectrum represents the group of protons that are directly linked to each carbon of the molecule (except for the quaternary carbons, of course). The analysis of the FTIR spectrum (fig. 2A in section 7.1.1. in attachment) confirmed the presence of the main functional groups of the molecule: the amide group (3077 cm^{-1}; see table 2), the aliphatic –CN (1115 cm^{-1}) of the core and the primary amine (3336 and 3287 cm^{-1}) of the periphery of the dendrimer. These results are confirmed by the consultation of the table of characteristics IR vibrations frequencies for single bonds to heteroatoms existent on J. B. Lambert *et al*. (197).

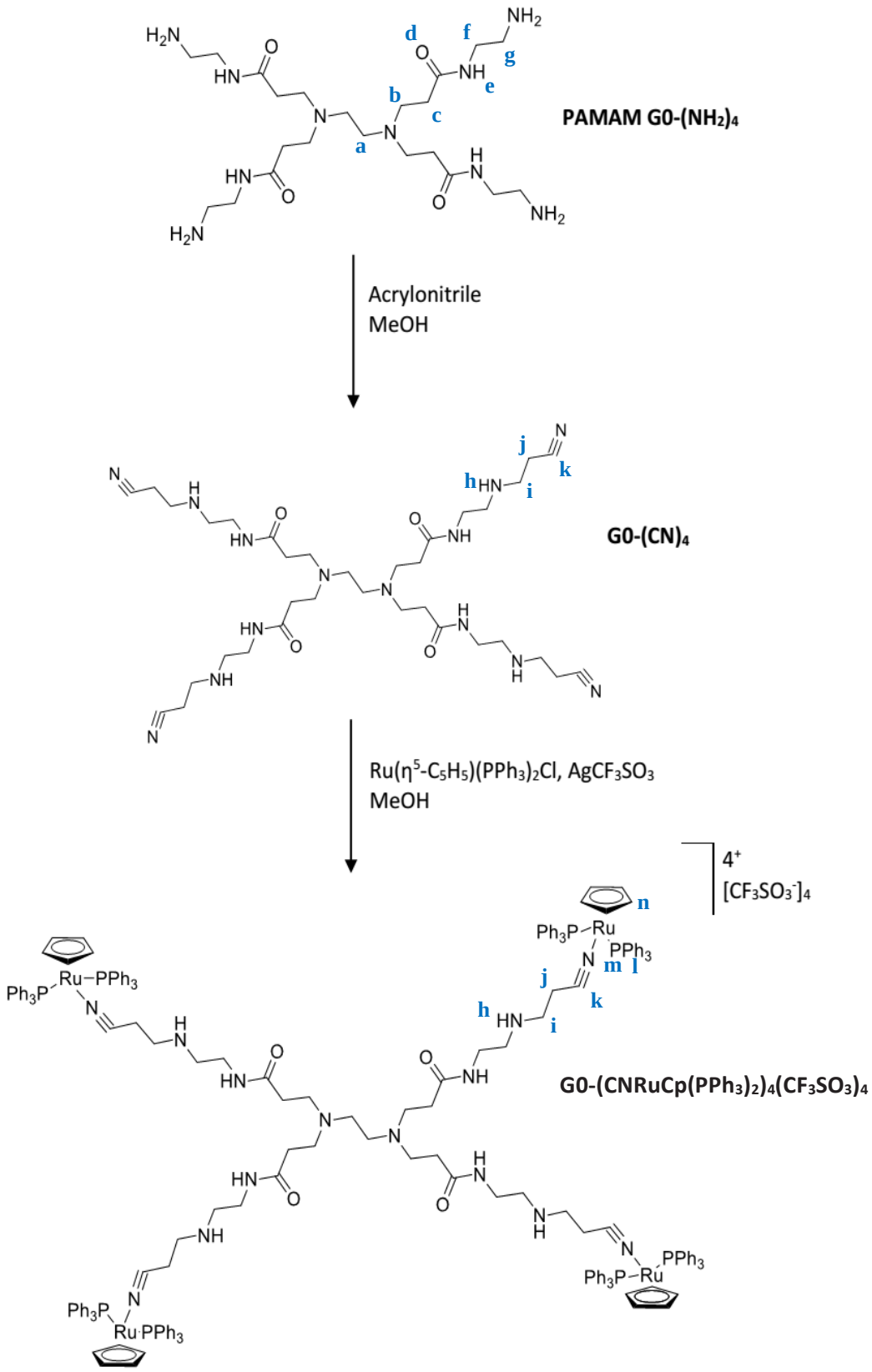

Scheme 1 - Synthetic routes for the synthesis of the metallodendrimer G0-$(CNRuCp(PPh_3)_2)_4(CF_3SO_3)_4$.

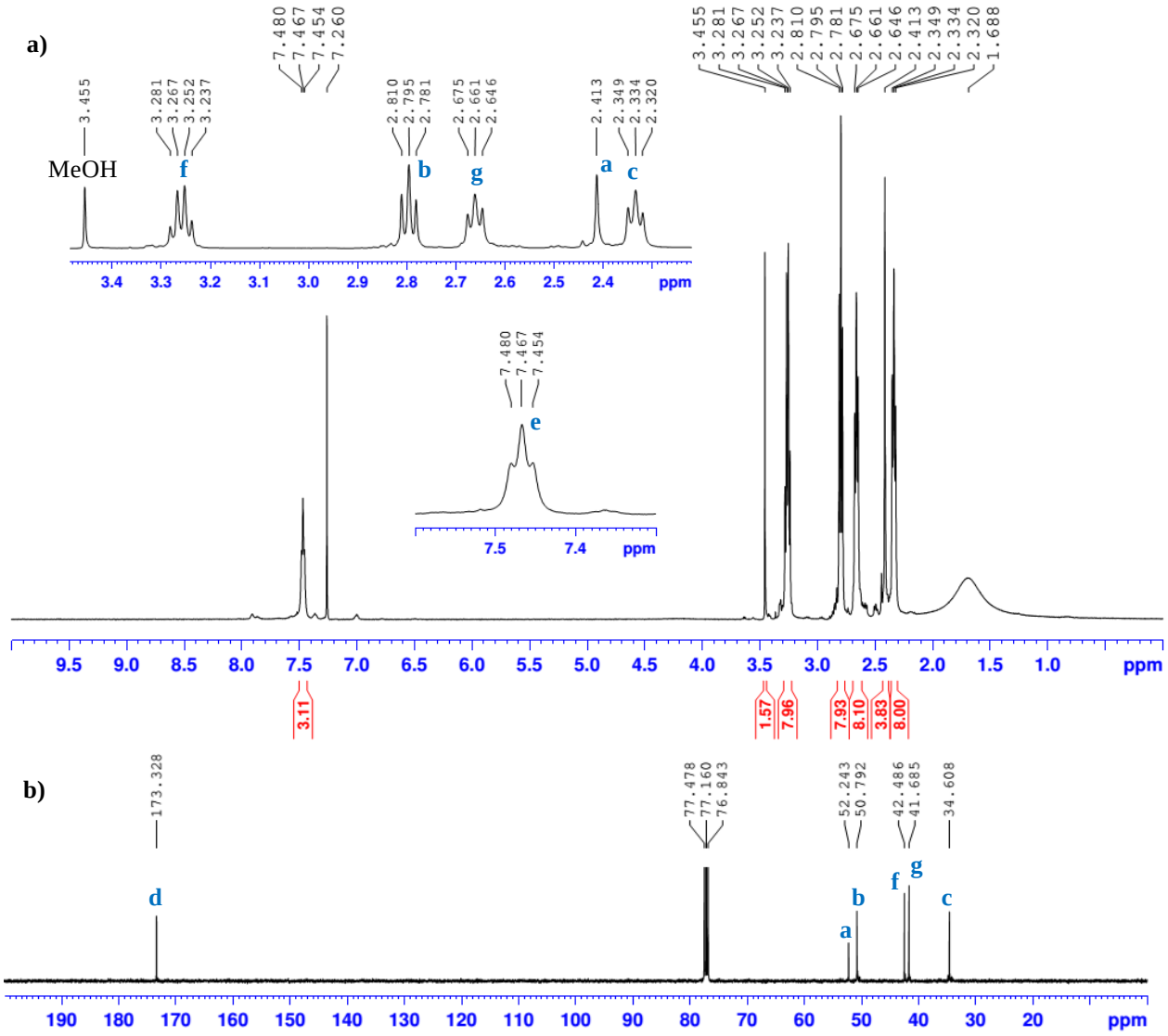

Figure 19 - a) ^{1}H-NMR and b) ^{13}C-NMR spectra of G0-PAMAM, in $CDCl_3$. Each signal is marked with the different type of carbons and protons that are represented with a unique letter – see scheme 1).

Table 1 - ^{1}H and ^{13}C-NMR data, of the corresponding spectra represented in fig. 18a) and b) for G0-PAMAM. $CDCl_3$ was the NMR solvent. The ^{1}H chemical shifts values are averages.

C atom	*^{1}H chemical shift (ppm)*	*Multiplicity*	*Integral*		*^{13}C chemical shift (ppm)*
			Expected	*Obtained*	
a	2.413	1	4	4	52.24
b	2.795	3	8	8	50.79
c	2.334	3	8	8	34.61
d	-	-	-	-	173.3
e	7.467	3	4	3	-
f	3.259	4	8	8	42.49
g	2.661	-	8	8	41.68

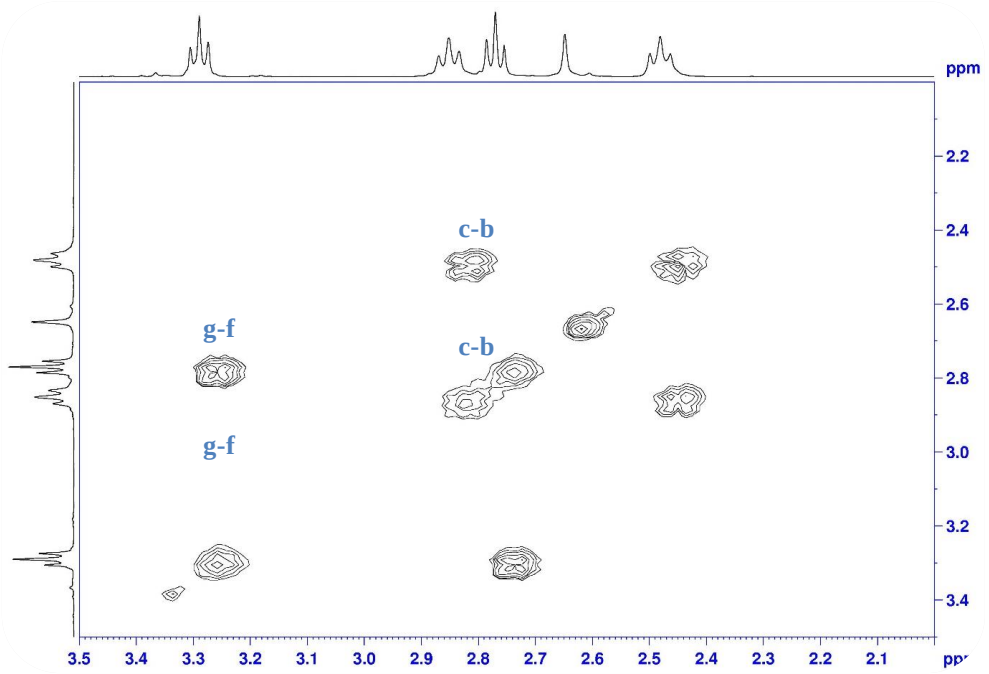

Figure 19 - COSY spectrum of G0-PAMAM, in D_2O. Each signal is marked with the respective group of protons that are neighbours and linked to each other by a carbon bond. Each type of protons is represented with a unique letter (see scheme 1).

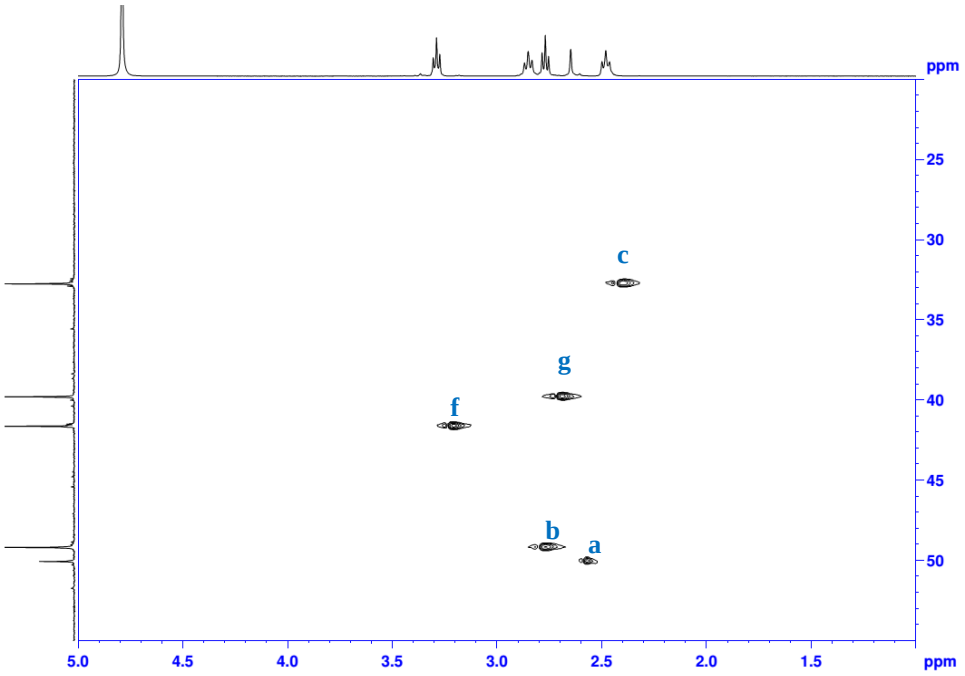

Figure 20 - HSQC spectrum of G0-PAMAM, in D_2O. Each signal is marked with the respective type of protons and type of carbon they are directly linked with. Each type is represented with a unique letter (see scheme 1).

Table 2 - Main characteristic bands (cm^{-1}), obtained by FTIR, for each functional group of G0/G1-PAMAM. The type of vibration is also showed.

Functional group	***band (cm^{-1})***		***Type of vibration****
	G0	**G1**	
C(=O)N–H	3077	3077	str
	1463	1464	bend
C=O of the amide	1644	1651	str
C–N	1115	1130	str
–CH_2 (acyclic)	2937	2939	asym str
	2868	2868	sym str
N–H of the primary amine	3336	3339	str
	3287	3288	
	1557	1557	bend

*str: stretch; asym str: asymmetric stretch; sym str: symmetric stretch

Regarding the MS, from the +MS2 spectrum (fig. 21) it was possible to identify the base peak – 403.2 *m/z* – that corresponds to the most intense ion detected in the spectrum which came from the fragmentation of the molecular ion – 517.7 *m/z*. The obtained *m/z* values are very similar to the expected: 516.4 and 401.3 *m/z*. Both results achieved from the FTIR and MS agree with the results acquired by W. Hung *et al.* (194) and P. Ilaiyaraja *et al.* (198).

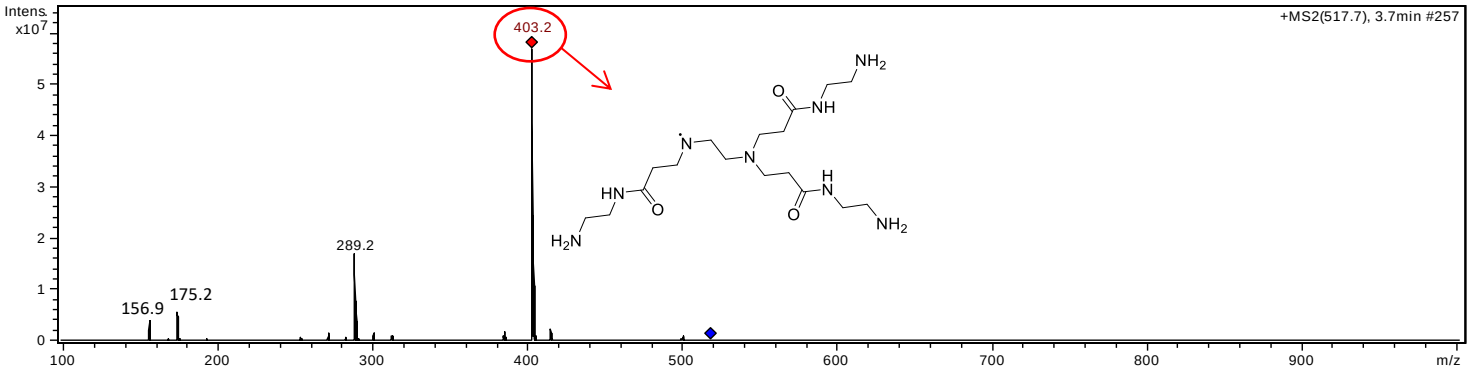

Figure 21 - +MS2 spectrum of G0-PAMAM – fragmentation of the molecular ion (517.7 *m/z*). The molecular structure of the base peak (403.2 *m/z*) is also represented.

Concerning the G1-PAMAM dendrimer (molecular structure in scheme 2), the results obtained for the ^{1}H and ^{13}C-NMR spectra (figs. 22a) and b) and data in table 3) are similar to the spectra obtained for G0-PAMAM, as it was already expected, because of the equivalence of the group of atoms. The main differences, besides the increase of the integration values, is the appearance of four different signals ("**d'**" to "**g'**") from the inner shell of the dendrimer. They have chemical shifts slightly different to the "equivalent" group of protons and carbon of the outer shell – **d** to **g** – because of the change in the electronic environment that surround them. With the increase of the generation number, the "**d'**" to "**g'**" signals stay linked to tertiary amine groups and the others are related to primary amine groups. These obtained NMR data for the both spectra of G1-PAMAM was confirmed by the results acquired by the same molecule in W. Hung *et al*. (194) and P. Ilaiyaraja *et al*. (198). The COSY and HSQC spectra (figs. 23 and 24, respectively) validate this conclusion with the elucidation of the structure of the dendrimer. The data obtained from the FTIR spectroscopy (see table 2 and fig. 2A in section 7.1.1. in attachment) are also in agreement with the data obtained from W. Hung *et al*. (194), being very similar to the results acquired for the G0 dendrimer, as the type of functional groups in their structure are exactly the same.

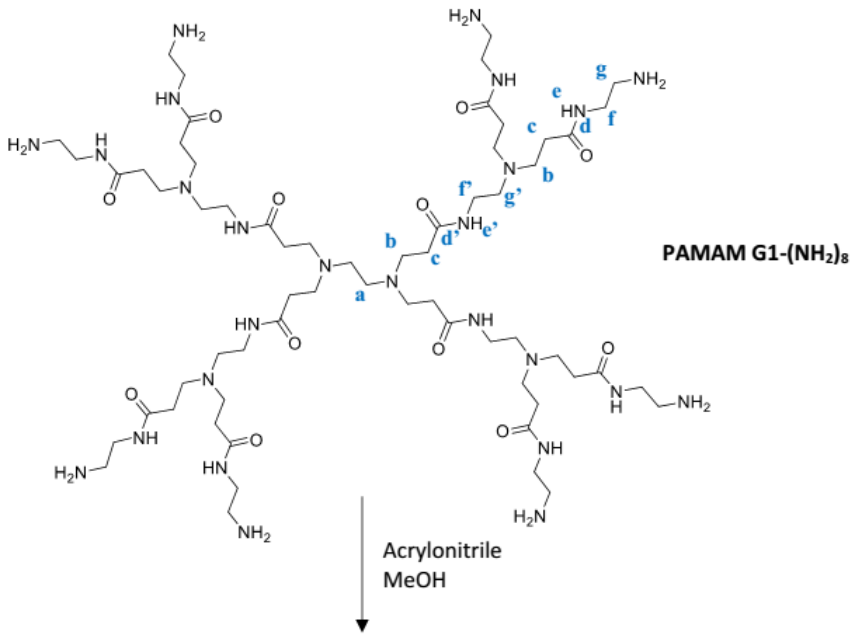

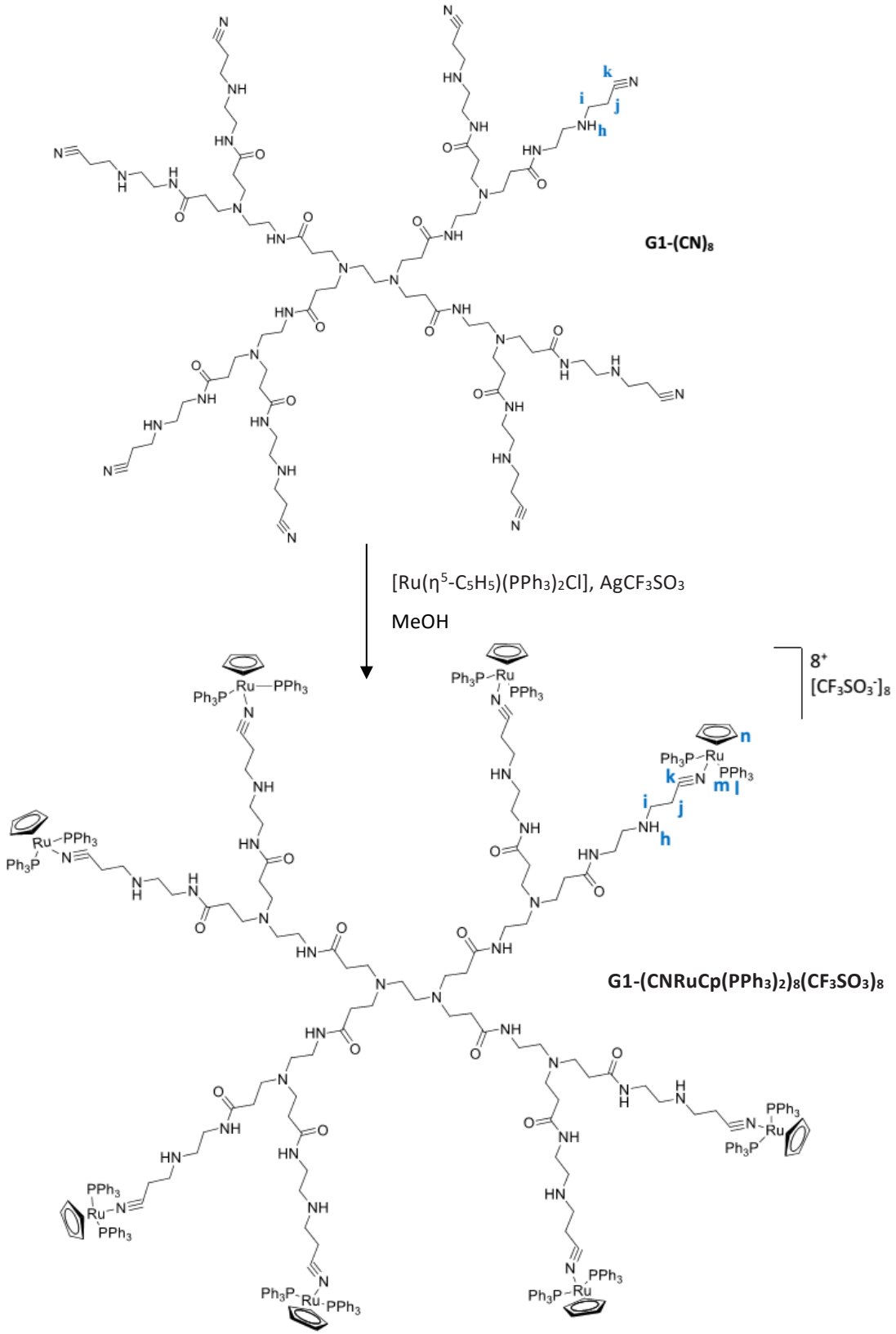

Scheme 2 - Synthetic routes for the synthesis of the metallodendrimer G1-$(CNRuCp(PPh_3)_2)_8(CF_3SO_3)_8$.

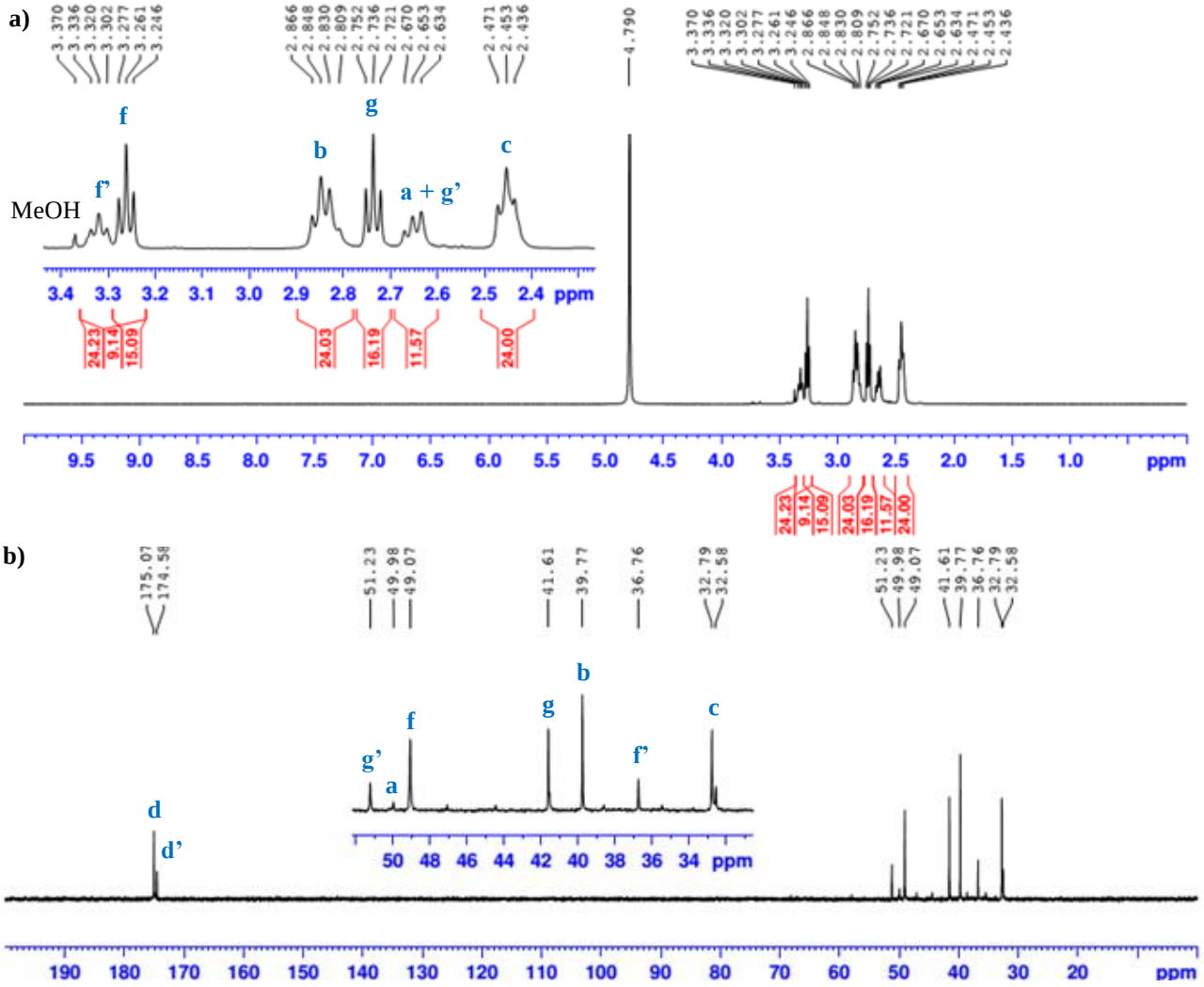

Figure 22 - a) ^{1}H-NMR and b) ^{13}C-NMR spectra of G1-PAMAM, in $CDCl_3$. Each signal is marked with the different type of carbons and protons that are represented with a unique letter – see scheme 2).

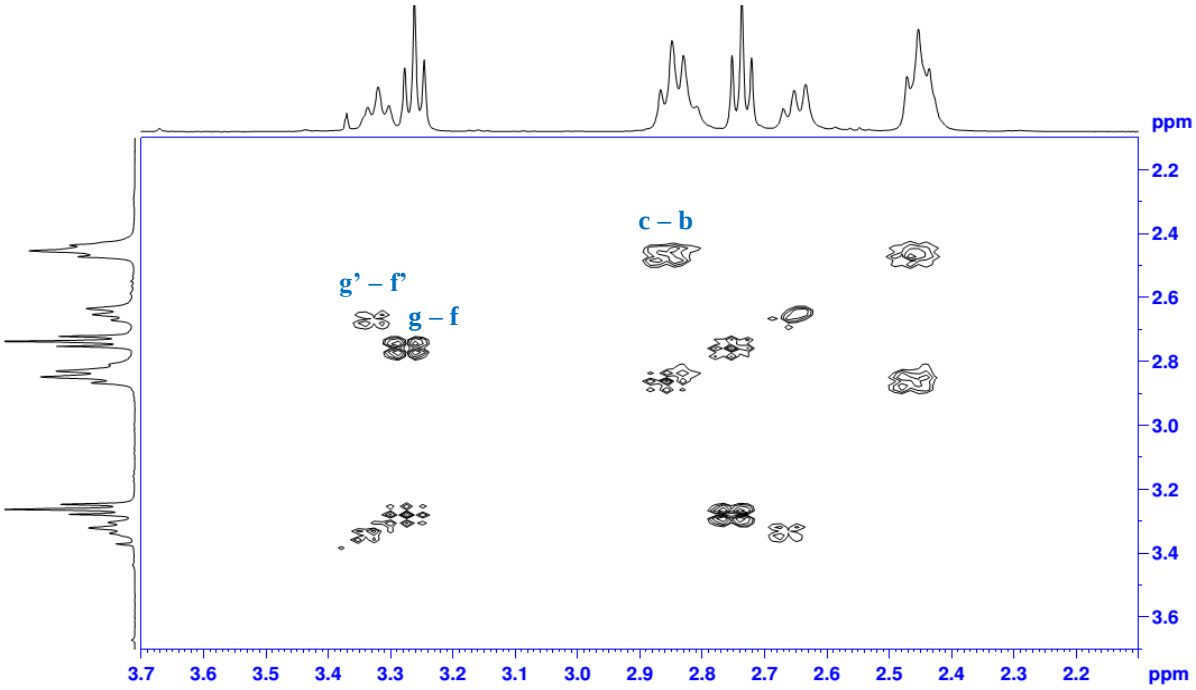

Figure 23 - COSY spectrum of G1-PAMAM, in D_2O. Each signal is marked with the respective group of protons that are neighbours and linked to each other by a carbon bond. Each type of protons is represented with a unique letter (see scheme 2).

Table 3 - ^{1}H and ^{13}C-NMR data, of the corresponding spectra represented in fig. 22a) and b) for G1-PAMAM. $CDCl_3$ was the NMR solvent. The ^{1}H chemical shifts values are averages.

C atom	*^{1}H chemical shift (ppm)*	*Multiplicity*	*Integral*		*^{13}C chemical shift (ppm)*
			Expected	*Obtained*	
a	Overlapped with "***g***""	-	4	*	49.98
b	2.848	3	24	24	39.77
c	2.453	3	24	24	32.79
d	-	-	-	-	175.07
d'	-	-	-	-	174.58
e	Not detectable with D_2O				-
e'					-
f	3.261	3	16	15	49.07
f'	3.320	3	8	9	36.76
g	2.736	3	16	16	41.61
g'	2.653	3	8	*	51.23

*Sum of obtained integrals for "a" and "g"": 12; expected sum: 12

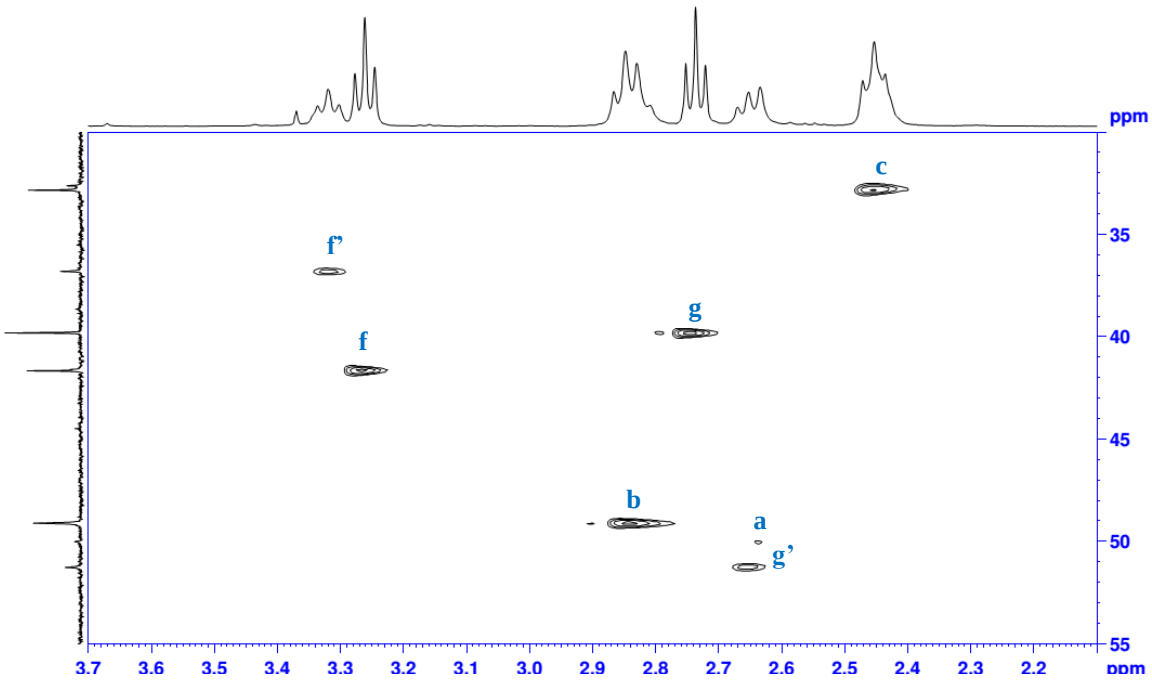

Figure 24 - HSQC spectrum of G1-PAMAM, in D_2O. Each signal is marked with the respective type of protons and type of carbon they are directly linked with. Each type is represented with a unique letter (see scheme 2).

The preparation of the nitrile ruthenium-based metallodendrimers G0/G1-$(CNRuCp(PPh_3)_2)_x(CF_3SO_3)_x$ was accomplished by adapting the reported methodology previously developed by our group (184). Due to the differences in solubility of the PAMAM dendrimers in comparison with the poly(alkylidenamine) dendrimers used by our group in the mentioned published work, it was necessary to optimize some reaction parameters to successfully synthesize the poly-nitrile moieties G0-$(CN)_4$ and G1-$(CN)_8$ by a Michael addition of the primary amines of the PAMAM dendrimers with ACN. It was performed several solubility tests in order to choose the appropriate solvent (table 4); the need of a catalyst was studied; different reaction temperatures were tested, and the effect of the time of reaction and an increasing number of eq. mol of ACN was also verified (table 5). It was concluded that: a) MeOH was the best solvent because it could totally dissolve the G0-PAMAM without reacting with the alkylating agent; b) 48 °C during 3h was enough to promote the reaction without the need of a catalyst and c) 2 eq. mol of ACN per each $–NH_2$ group of the dendrimer was sufficient for the alkylation to occur.

Table 4 - Conditions for the solubility tests performed with G0-PAMAM in several aprotic solvents.

Solvent	***Temperature (°C) and time***	***Result***
1,4-Dioxane	r.t.	Insoluble
Acetone	"	"
Acetonitrile	"	"
DCM	40 (during 30 min)	"
THF	40; 50 and 60 (30 min each)	Suspension
Ethyl acetate	"	Insoluble
DMSO	r.t.	Soluble
10% DMSO: 90% THF	"	Insoluble
20% DMSO: 80% THF	"	Insoluble
30% DMSO: 70% THF	"	Soluble

This first synthesis reaction is a N-alkylation, by Michael addition, of the primary amine groups of the G0/G1-PAMAM with ACN (at 48 °C). The Michael addition refers to the addition of a

nucleophile, designated as Michael donor, to an activated α, β-unsaturated carbonyl-containing compound – the Michael acceptor (199).

Table 5 - Conditions applied for each performed test for the synthesis reaction of G0-$(CN)_4$.

Experiment no.	*Solvent*	*Eq. mol of ACN*	*Time of reaction (h)*	*Temperature (°C)*	*Major Product*
1	MeOH	8 + 8	3 + 3	48 then 80	G0-$(CN)_4$
2	"	16 + 16	"	"	"
3	"	"	6 + 16	"	"
3.1.	-	-	+6	80	"
3.2.	-	-	+18	"	"
3.3.	-	+8	+19	"	"
4	$CHCl_3$	16 + 16	3 + 3	48 then 80	G0-$(NH_2)_3CN$
4.1.	-	-	+17	80	"
4.2.	-	+8	+20	"	"
5	DMSO	8 + 8	6 + 17	48 then 80	G0-$(CN)_4$
5.1.	-	+8	+17	100	"

In the concerned synthesis reaction of G0/G1-CN, the Michael donor is the $–NH_2$ groups of the G0/G1-PAMAM dendrimers and the Michael acceptor is the unsaturated carbons of the ACN molecule (scheme 3). When the Michael donor is a nitrogen group, the Michael addition is often referred as the aza-Michael reaction (200). In this case, there´s no need to add the typical base catalyst for the reaction to occur because amines can act as both nucleophiles and bases. The reaction follows a second-order kinetics based on the concentration of the olefin acceptor and the amine. According to the structure of the ACN, the β-carbon will be more electrophilic than the α-carbon since the nitrile is an electron-withdrawing group. For this reason, the nucleophile adds to the β-carbon of the ACN (201). As follows, 1.87 g (3.63 mmol; 1 eq. mol) of G0-PAMAM reacted with 1.925 mL (1.54 g; 29.03 mmol; 8 eq. mol) of ACN to afford a crude product as a light-yellow oil (2.62 g, 3.59 mmol, 99% of yield).

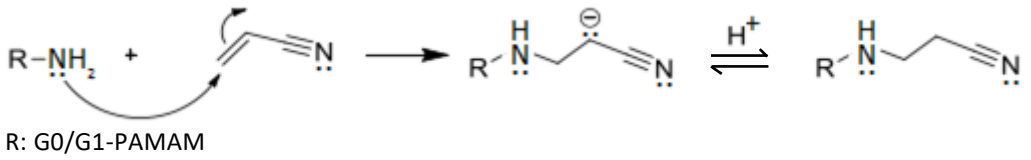

R: G0/G1-PAMAM

Scheme 3 - Mechanism of reaction of the aza-Michael addition for the preparation of the G0/G1-CN dendrimers (adapted from (202)).

The analysis of the ^1H and ^{13}C-NMR spectra (figs. 3A in attachment) of the crude confirmed the identity of the tetra-nitrile dendrimer: the three different signals ("i": 2.5 and 19 ppm, "j": 2.9 and 45 ppm and "k": 119 ppm; see scheme 1) of the incorporated $–CH_2CH_2CN$ were detected with adequate integration values and multiplicity – two triplets with 8 protons each in the ^1H-NMR. These results are in agreement with the obtained data by our group (184) with similar compounds. Even after allowing G0-$(CN)_4$ to be dried by vacuum for several hours and with a 40°C water bath, it was not possible to remove all the solvent (MeOH) from the oily product. Thus, it was needed to purify the compound. It was performed an L-L extraction with $CHCl_3$-H_2O and the aqueous fraction was freeze-dried to be obtained 2.30 g (3.15 mmol) of a purified dendrimer, as a light-yellow oil, with a good yield of 87 %. It was characterized by ^1H and ^{13}C-NMR, COSY, HSQC and FTIR (figs. 25a) and c), 26, 27 and 4A respectively, and corresponding data in table 6 and 7). The analysis of the obtained 1D-NMR spectra revealed that the L-L extraction was appropriate (note that the MeOH peaks are totally absent in figs. 25a) and c) – red stars). The structure of the dendrimer was confirmed by the 2D-NMR and, from the FTIR spectrum, one single typical C≡N stretch band with 2248 cm^{-1} was easily observed which confirms the correct functionalization of the dendrimer with the nitrile groups. The abovementioned synthesis reaction was performed with the objective of synthetizing G0-$(CN)_8$ (fig. 28) but, instead, the obtained product was the half-functionalized molecule G0-$(CN)_4$. In the typical aza-Michael reaction, primary amines react with two equivalents of the olefin acceptor to produce tertiary amines. This happens because secondary amines (the intermediary molecules of the reaction) are more nucleophilic than primary amines and are therefore more reactive. However, if the produced secondary amines are surrounded by an electronic and steric environment, as it happens in the G0-$(CN)_4$ compound (see the structure in scheme 1 and compare with the structure in fig. 27), the abovementioned fact is not valid and consequently, in some cases, the reaction is incomplete with the secondary amine intermediate as final product (203). After performing all the previously described different experiments (table 5) for the synthesis of the tetra-nitrile dendrimer G0-$(CN)_4$, it was possible to conclude that, probably, it is needed a catalyst (NaOH (137) or NaH (204) for the synthesis reaction of the initial compound of interest G0-$(CN)_8$. Unfortunately, due to the presence of amide groups in the structure of the departure dendrimer (G0-PAMAM) it is not possible to use these catalysts because they will hydrolyse the amides in the correspondent carboxylic acids, which will cause the degradation of the dendrimer.

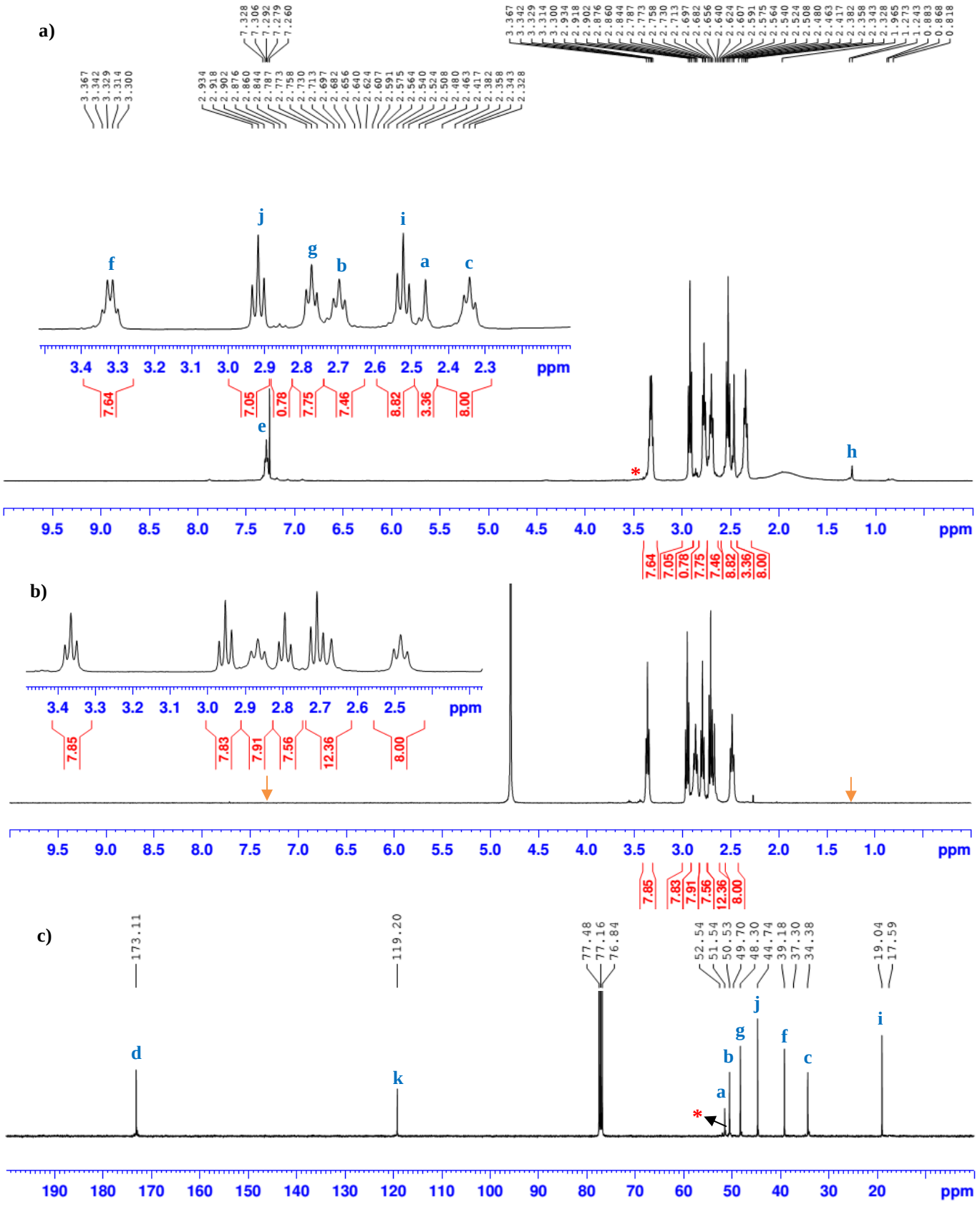

Figure 25 - NMR spectra of purified G0-(CN)$_4$: a) ^{1}H-NMR in $CDCl_3$; b) ^{1}H-NMR in D_2O; c) ^{13}C-NMR in $CDCl_3$. The "e" and "h" signals represents the amide and amine protons, respectively, that are not detected in b) – orange arrows. The red stars represent the absence of MeOH.

Table 6 - ^{1}H and ^{13}C-NMR data, of the corresponding spectra represented in fig. 25a) and c), for the purified G0-$(CN)_4$. $CDCl_3$ was the NMR solvent. The ^{1}H chemical shifts values are averages.

C atom	*^{1}H chemical shift (ppm)*	*Multiplicity*	*Integral*		*^{13}C chemical shift (ppm)*
			Expected	*Obtained*	
a	2.463	1	4	3	51.54
b	2.697	3	8	8	50.53
c	2.343	3	8	8	34.38
d	-	-	-	-	174.69
e	7.292	3	4	3	-
f	3.321	4	8	8	39.18
g	2.773	3	8	8	48.30
h	1.243	1	4	-	-
i	2.524	3	8	9	19.04
j	2.918	3	8	7	44.74
k	-	-	-	-	119.20

The synthesis of related poly-nitrile compounds is available in the reviewed literature (1, 2, 137, 184), which includes the synthetic procedures that were adapted for the applied synthesis of G0-$(CN)_4$ (see scheme 1), but all the departure dendrimers that they have used did not have amide groups. One possibility to successfully synthetize G0-$(CN)_8$ is to protect the amide groups with, for example, *tert*-butyl groups (205) or triphenilmethyl groups (206), then undergo the reaction of the obtained product with ACN and NaOH or NaH as catalysts to produce the octa-nitrile compound and, in the end, unprotect the amide groups. Despite these encountered difficulties, one type of a poly-nitrile compound was successfully synthetized and fully characterized – the G0-$(CN)_4$. The ^{1}H-NMR (fig. 25b)) of it, in D_2O, was another way to justify the half and uniform functionalization properly. Comparing the two ^{1}H-NMR spectra of the product (in figs. 8a) and b)) it is possible to observe that the characteristic signal for the secondary amines of the dendrimer (the "h" signal; see scheme 1), with 1.243 ppm in the ^{1}H-NMR spectrum performed in $CDCl_3$ (fig. 25a)), is absent in the spectrum that was accomplished in D_2O (performed from the same sample and concentration). This happens because of the protons exchange between the secondary amine groups of the dendrimer and D_2O. Obviously, the same behaviour is observed for the signal of the amide groups of the dendrimer (the "e" signal) with 7.292 ppm.

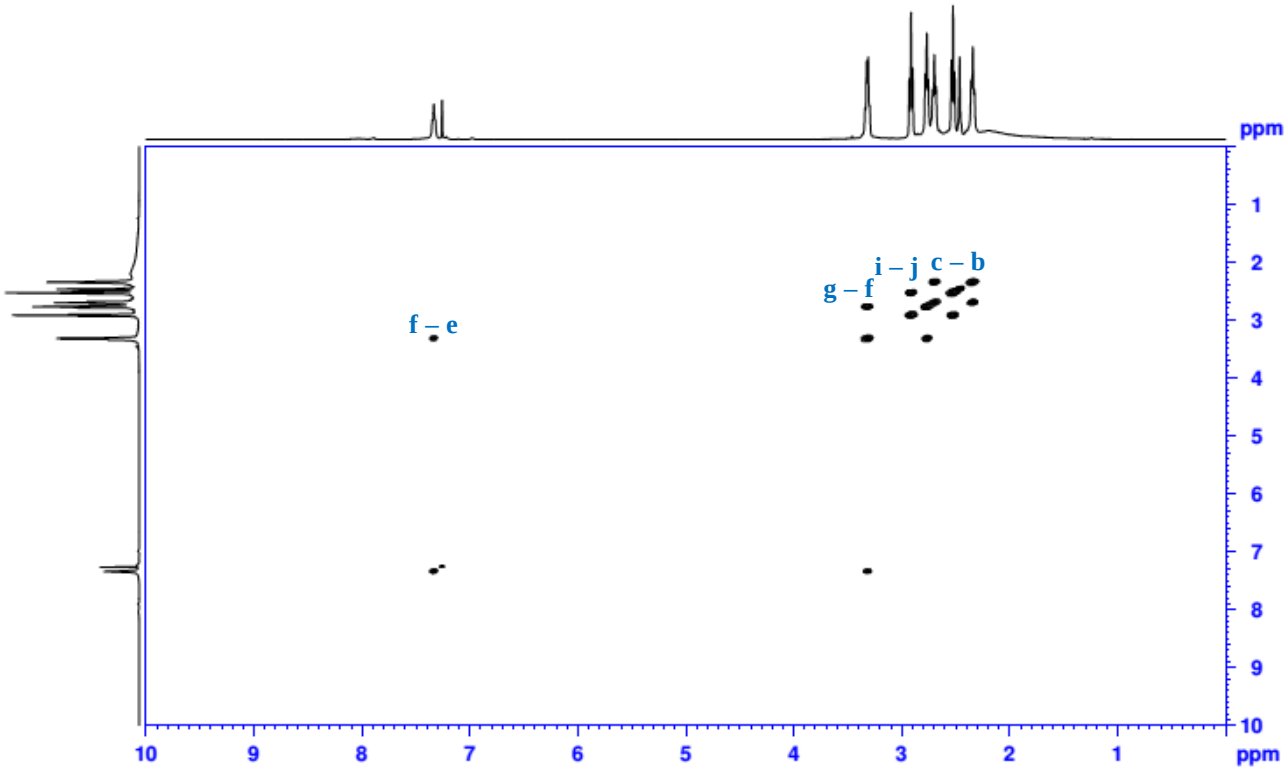

Figure 26 - COSY spectrum of purified G0-$(CN)_4$, in $CDCl_3$. Each signal is marked with the respective group of protons that are neighbours and linked to each other by a carbon bond. Each type of protons is represented with a unique letter (see scheme 1).

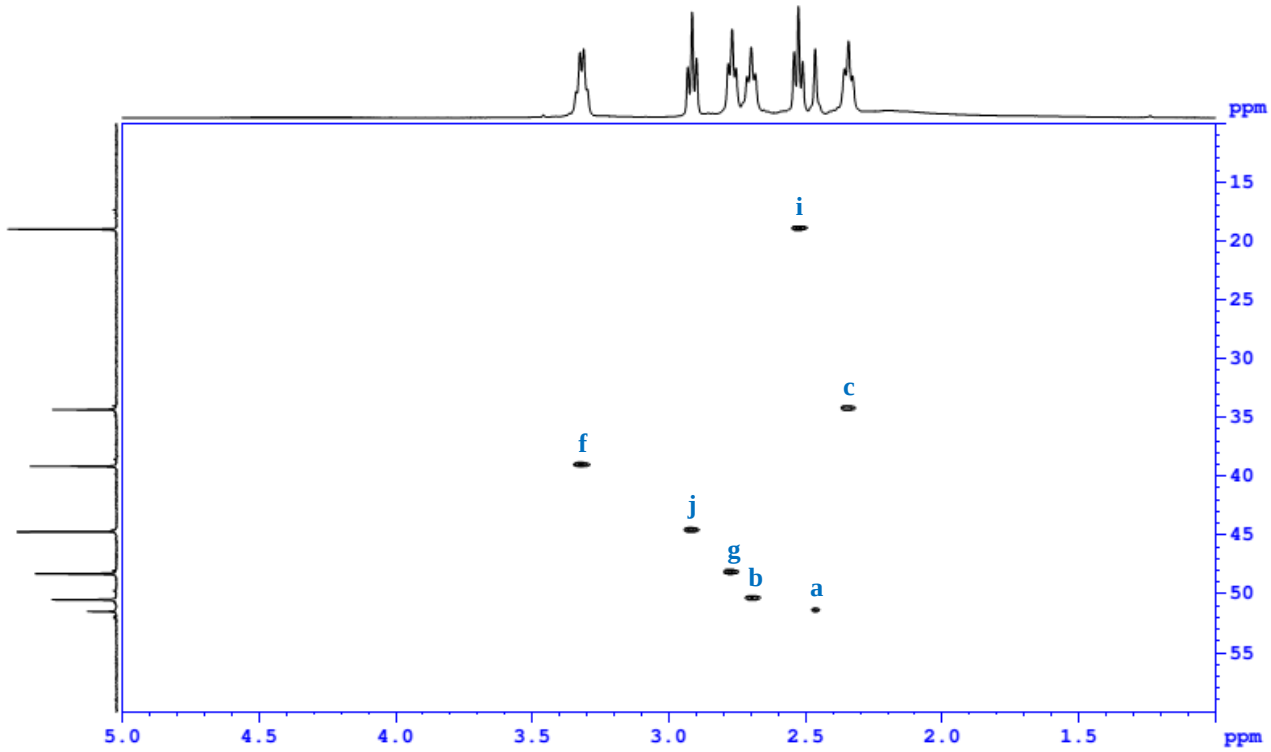

Figure 27 - HSQC spectrum of purified G0-$(CN)_4$, in $CDCl_3$. Each signal is marked with the respective type of protons and type of carbon that are directly linked with. Each type is represented with a unique letter (see scheme 1).

Table 7 - Main characteristic bands (cm^{-1}), obtained by FTIR, for each functional group of the purified G0/G1-CN. The type of vibration is also showed.

Functional group	*band (cm^{-1})*		*Type of vibration**
	G0	**G1**	
C(=O)N–H	3081	3081	str
	1466	1464	bend
C=O of the amide	1651	1645	str
C–N	1129	1131	str
C≡N	**2248**	**2247**	str
–CH$_2$ (acyclic)	2936	2937	asym str
	2841	2838	sym str
N–H of the secondary amine	3288	3288	str
	1555	1552	bend

*str: stretch; asym str: asymmetric stretch; sym str: symmetric stretch

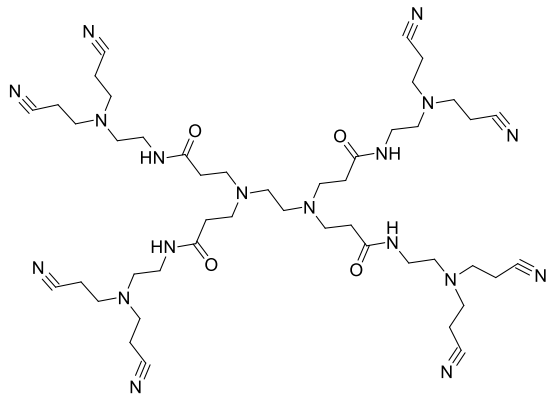

Figure 28 - Molecular structure of G0-(CN)$_8$.

From the liquid-phase cracking of dicyclopentadiene (see scheme 4, ^{1}H-NMR in fig. 29), it was obtained cyclopentadiene (15 mL of a colourless liquid, 11.8 g, 178 mmol) with 20 % of yield (^{1}H-NMR in fig. 30). The obtained yield depends upon the type of method that is used (207, 208). Besides the lower 20% of yield, 15 mL of it was totally enough for the preparation of the [RuCp(PPh$_3$)$_2$Cl]. The cyclopentadiene must be used immediately after distilled or in a period of 24h when properly storage at -20 °C. Thus, in our case, performing another methodology (for example, gas-phase cracking using H_2 as the carrier gas (207) or liquid-phase cracking by reactive distillation (208) would not be beneficial and cost-effective. Furthermore,

the 15 mL that was obtained, as it was already mentioned in section 5.1.4., contributed for the preparation of 11.2 g of [RuCp(PPh$_3$)$_2$Cl] that is useful for several months of work.

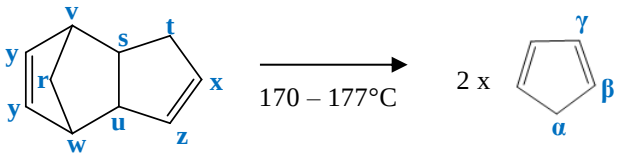

Scheme 4 - Cracking of dicyclopentadiene.

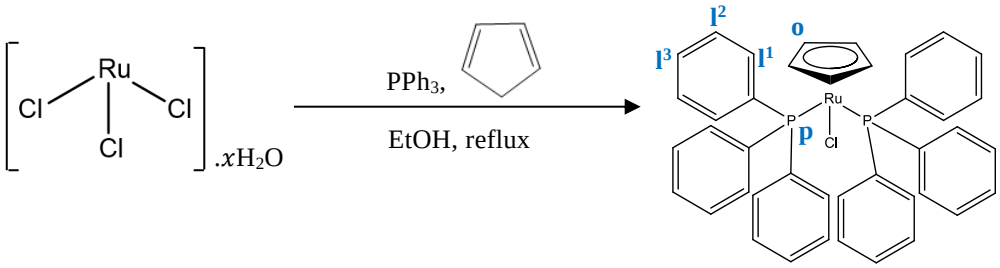

Scheme 5 - Synthesis reaction of [RuCp(PPh$_3$)$_2$Cl].

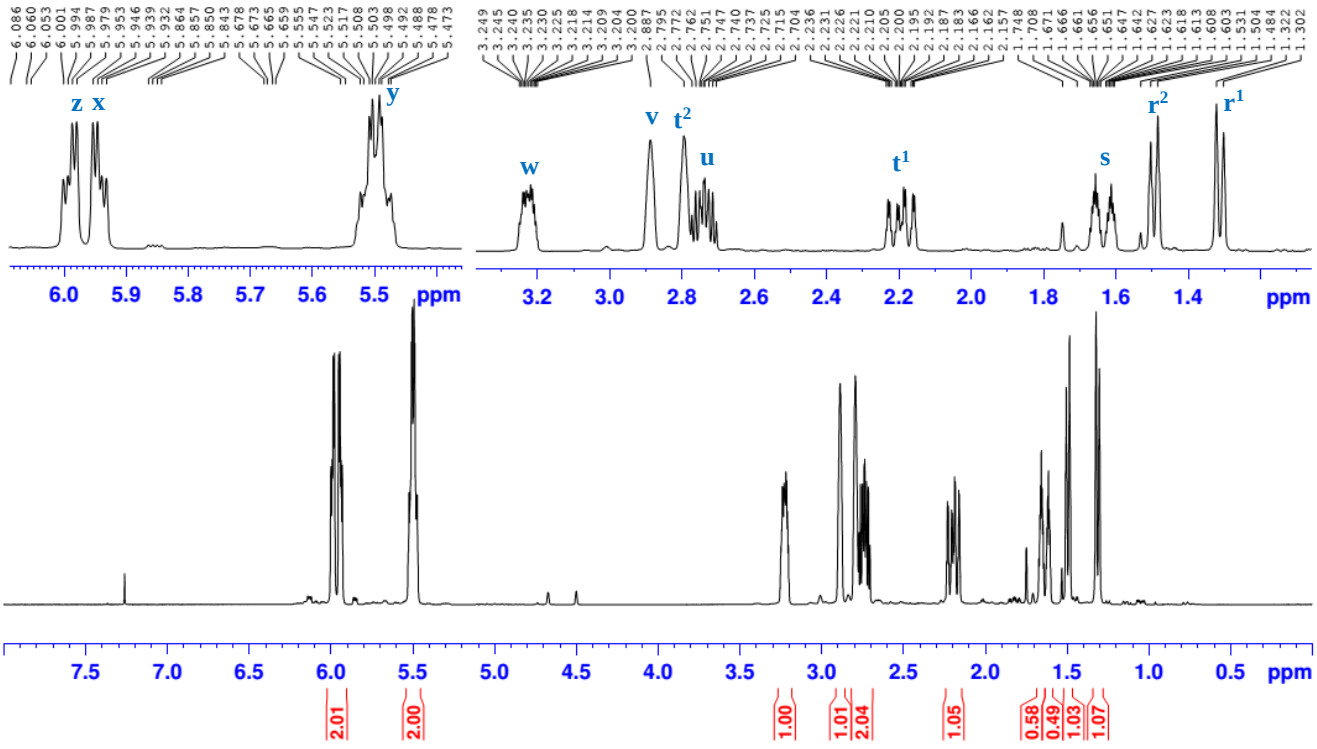

Figure 29 - ^{1}H-NMR spectrum of commercial dicyclopentadiene, in $CDCl_3$. Each signal is marked with the respective type of protons that are represented with a unique letter (see scheme 5).

Adapting the procedures described in M. I. Bruce *et al.* (188) and A. R. Dias *et al.* (189), 3.92 g (18.9 mmol, 1 eq. mol) of $RuCl_3.xH_2O$ in EtOH reacted with 16.3 g (62.4 mmol, 3.3 eq. mol) of PPh_3 in refluxing EtOH and with 15 mL (177.6 mmol, 9.4 eq. mol) of freshly distilled cyclopentadiene to originate 11.2 g (15.5 mmol, 82% of yield) of an orange crystalline crude product of $[RuCp(PPh_3)_2Cl]$ (^1H and ^{31}P-NMR in figs. 31a) and 32a), respectively). The spectra analysis revealed the presence of the three characteristic signals of the organometallic product ("l" from the protons of the -PPh_3 ring, "o" from the protons of the -Cp ring and "p" from the phosphorous; see scheme 4) with adequate integrations on the ^1H-NMR, so it was concluded that the synthesis reaction was successful. However, it was observed a small amount of a solid black-coloured impurity that revealed the need to purify the compound. In this way, and after

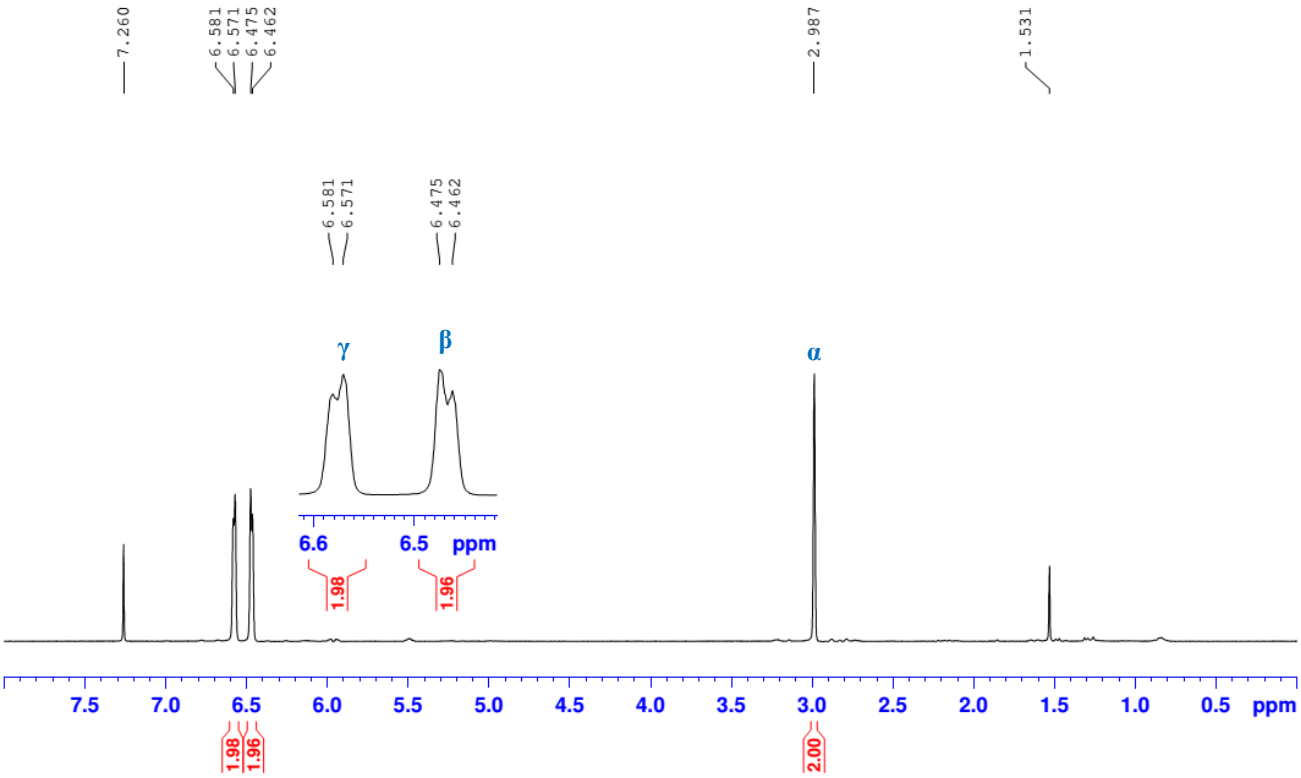

Figure 30 - ^1H-NMR spectrum of distilled cyclopentadiene, in $CDCl_3$. Each signal is marked with the respective type of protons that are represented with a unique letter (see scheme 5).

washing, filtrating, and drying the crude product as it is described in section 4.1.4., it was obtained 7.4 g (10.2 mmol, 54% of yield) of a purified dark yellow powder that was characterized by ^1H and ^{31}P-NMR (figs. 31b) and 32b), respectively). The separated impure fraction, as a brown powder, was also characterized by the same methods (see figs. 31c) and 32c), respectively).

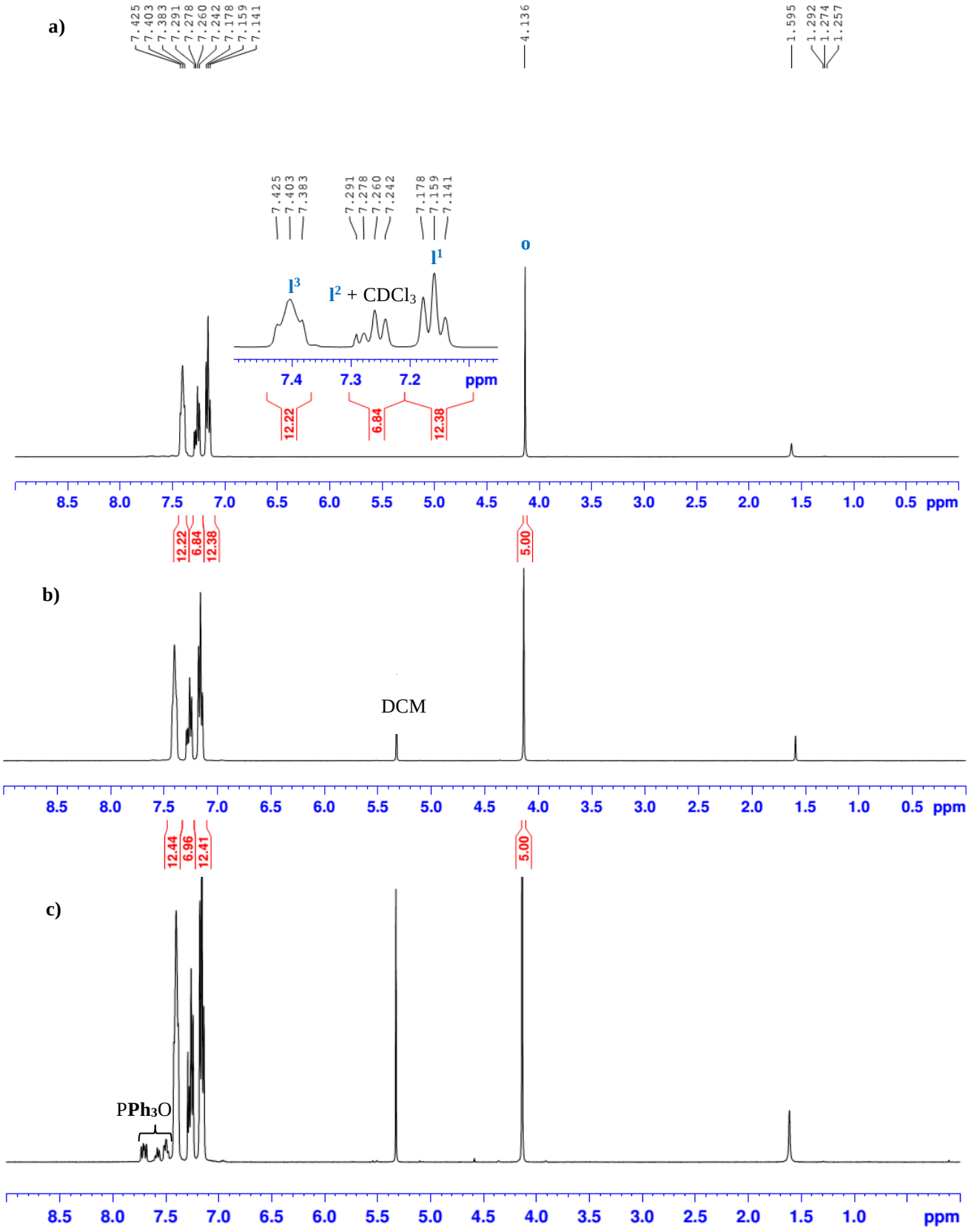

Figure 31 - ^{1}H-NMR spectrums of the obtained $[RuCp(PPh_3)_2Cl]$: a) orange crude crystals; b) purified dark yellow powder and c) impure brown powder, in $CDCl_3$. Each signal is marked with the respective type of protons that are represented with a unique letter (see scheme 4).

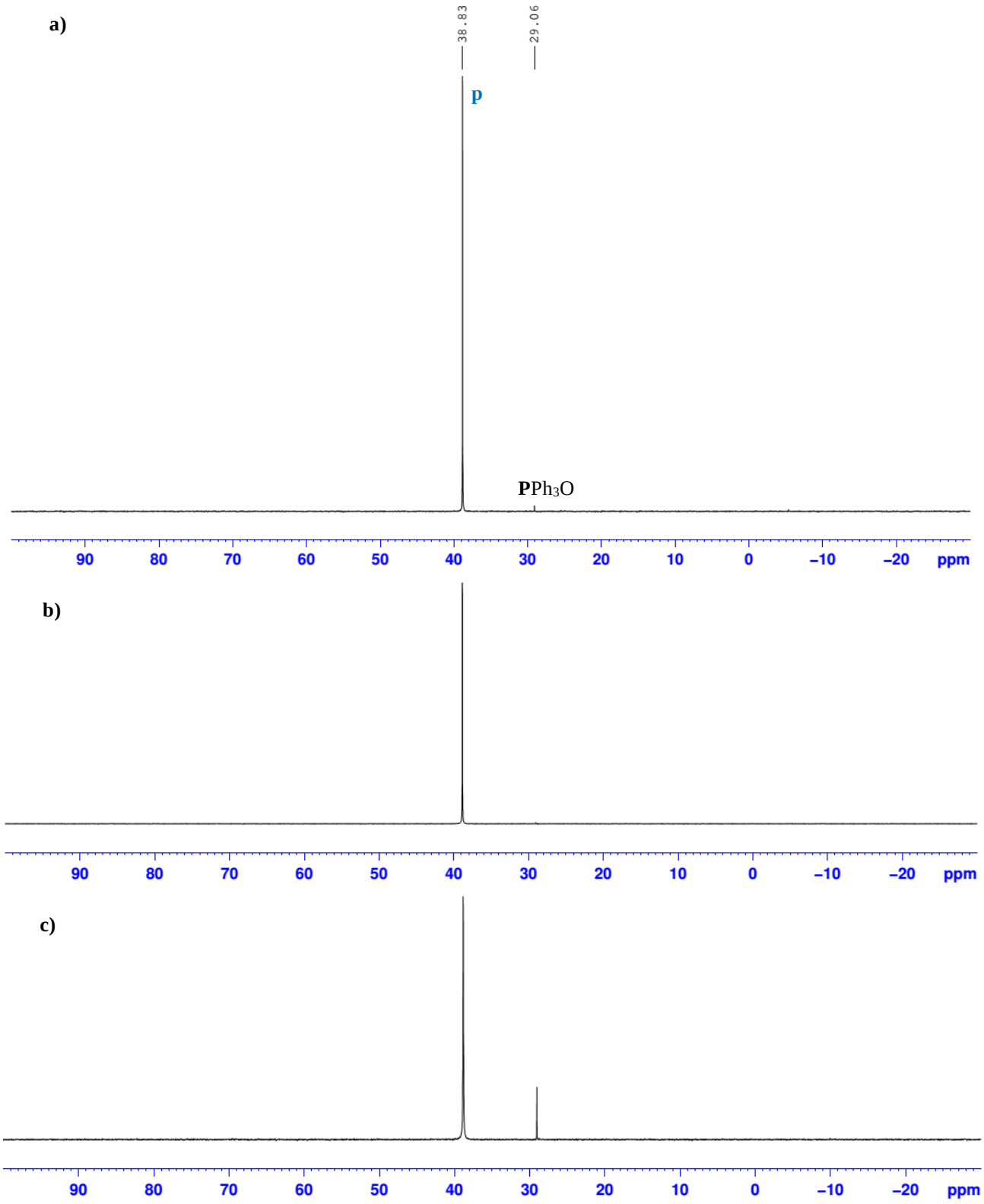

Figure 32 - ^{31}P-NMR spectrums of the corresponding samples from fig. 31; in $CDCl_3$. The "p" signal corresponds to the phosphorus from the $[RuCp(PPh_3)_2Cl]$ (see scheme 4).

The preparation of the G0/G1-$(CNRuCp(PPh_3)_2)_x(CF_3SO_3)_x$ metallodendrimers, as it is described in section 4.1.5., was accomplished using the $AgCF_3SO_3$ instead of using Thalium (I) hexafluorophosphate ($TlPF_6$), as the chloride abstractor used by our group (183, 184), for the preparation of similar compounds. In this work, it was decided to follow this alternative strategy, because of the high probability that the presence of residues of thalium in the purified metallodendrimer could affect the cytotoxic studies, as it is known that thalium is highly toxic (209). Additionally, to successfully synthesize the desired metallodendrimer, it was necessary to optimize some reaction parameters. Thus, some tests were performed and the conditions applied for each one are resumed in table 8.

Table 8 - Conditions applied for each performed test for the synthesis reaction of G0-$(CNRuCp(PPh_3)_2)_4(CF_3SO_3)_4$.

Exp. no.	***Solvent (mL to mg of -RuCp*)***	***Molar eq***		****R. tracking (h)***	***Total and best r. time (h)***	***Colour (sol.)****	***T (°C)***	***Major Product (after purification); η****
		-RuCp	***$AgCF_3SO_3$***					
1	EtOH (60 to 304)	4.1	5.4	72; 96	118; 72	brown	r.t.	G0-$(CNRuCp(PPh_3)_2)_4(CF_3SO_3)_4$ (dark brown powder); 8%
2	MeOH (50 to 350)	5	6.3	22; 44	66; 44	"	r.t.	G0-$(CNRuCp(PPh_3)_2)_4(CF_3SO_3)_4$ (dark brown powder); 7%
3	MeOH (40 to 112)	4.1	5.4 (added in 3 parts)	22; 42; 70	96	light brown	r.t.	Mixture of Ru compounds
4	MeOH (75 to 317)	"	"	5; 23	49	bronze	85 (reflux)	G0-$[(CN)_2(CNRuCp(PPh_3)_2)_2][(CF_3SO_3)_4]$ (brown powder)

*****Exp. no.: experiment number; -RuCp: $[RuCp(PPh_3)_2Cl]$; R.: reaction; colour (sol.): colour of the solution after filtration; η: yield

After performing the first experiment and obtaining a purified G0-$(CNRuCp(PPh_3)_2)_4(CF_3SO_3)_4$ with a low yield of 8%, it was decided to change the solvent from EtOH to MeOH for the second test. The smaller size of MeOH (in comparison with EtOH) will contribute to a less interference during the functionalization of the ruthenium moiety with the tetra-nitrile dendrimer G0-$(CN)_4$ since that, probably, the solvent with a partial negative charge (δ-) will interact with the $[RuCp(PPh_3)_2]^+$ moiety (after the Cl^- removal by the $AgCF_3SO_3$) which could form an aggregate (210, 211). Also, the eq. mol of the -RuCp complex and $AgCF_3SO_3$ was increased to 5 and 6.3,

respectively, and the reaction was monitored at 22 and 44h (sooner than the exp. no. 1.) to be stopped after 66h. It was obtained a crude product with more undesired side-products than before and, consequently, to get a purer G0-$(RuCp(PPh_3)_2)_4$ it was necessary to perform several purification procedures (precipitations with DCM/Et_2O) that lead to a very low 7 % of yield for the purified compound. By this means, it was decided to perform another test (exp. no. 3) with the same conditions than experiment no. 1 (4.1 eq. of -RuCp and 5.4 of $AgCF_3SO_3$), but now maintaining MeOH as solvent, adding the $AgCF_3SO_3$ in 3 parts (with 5 min of interval between each addition) and with the first tracking of the reaction at 22h. At this time, the G0-$(CNRuCp(PPh_3)_2)_4(CF_3SO_3)_4$ could be already synthetized with small quantities of the discussed undesired side-products, but due to the intense signal of the departure -RuCp complex it was decided to leave the reaction ongoing. The tracking of the reaction at 42, 70 and 96h has demonstrated that the G0-$(CNRuCp(PPh_3)_2)_4(CF_3SO_3)_4$ probably became de-functionalized with the increase of the reaction time to originate a mixture of ruthenium compounds. This conclusion was supported by the decrease in the intensity of the -Cp ring signal combined with the change of the multiplicity to a duplet in the ^{1}H-NMR and the same behaviour was observed for -PPh_3 signal in the ^{31}P-NMR, while the signal of the departure -RuCp has remained practically unchanged. For the last experiment – exp. no. 4 – it was decided to apply high temperatures (reflux, at 85°C) while conserving the other conditions. The reaction was monitored at 5 and 22h and stopped after 49h. It was observed that the the high temperatures lead to the formation of several undesired side-products and the preparation of a half functionalized metallodendrimer – G0-$(CN)_2(CNRuCp(PPh_3)_2)_2$. This last observation was justified by the presence of the -Cp ring signal, in the ^{1}H-NMR spectra, with an integration of $\approx$ 10, a half of the value observed for the G0-$(CNRuCp(PPh_3)_2)_4(CF_3SO_3)_4$. Finally, after performing the discussed four experiments it was possible to optimize one set of experimental conditions that was needed to prepare the desired metallodendrimer with success: *a)* 4.1 and 5.4 eq. mol of $[RuCp(PPh_3)_2Cl]$ and $AgCF_3SO_3$, respectively; *b)* MeOH as solvent (at least 60 mL for 304 mg of $[RuCp(PPh_3)_2Cl]$); *c)* approximately 22h of reaction at room temperature; *d)* the colour of the reactional solution has to change from orange to yellow and finally to brownish; *e)* the produced AgCl powder has to settle completely (during at least 60 to 120 min) before filtration; *f)* the best filter paper is the one with 2 – 3 µm in size; *g)* the filtration has to be performed dropwise with a minimum pressure that is conferred, preferentially, only by the gaseous nitrogen current and *h)* the precipitation with DCM/Et_2O has to be accomplished on the

same day to prevent the decomposition of the product. Accordingly, 1.64 g (2.26 mmol, 4.1 eq. mol) of the organometallic moiety $[RuCp(PPh_3)_2Cl]$ reacted with 0.77 g (2.26 mmol, 5.4 eq. mol) of $AgCF_3SO_3$ (protected from light) and 0.40 g (0.55 mmol, 1 eq. mol) of the previously prepared G0-$(CN)_4$ (scheme 1). After 22h of reaction, one fraction of the obtained crude product was analysed by ^1H and ^{31}P-NMR (figs. 33a) and 34a), respectively). The analysis of the spectra revealed that the synthesis was certainly completed due to the absence of the signals from the departure organometallic moiety $[RuCp(PPh_3)_2Cl]$ (with $\delta \approx 4.1$ and 38.9 ppm; see figs. 31a) and 32a), respectively) and the presence of two characteristic signals of the G0-$(CNRuCp(PPh_3)_2)_4(CF_3SO_3)_4$: a singlet with $\delta \approx 4.4$ ppm with an adequate integration of ≈ 20 H^+ (in the ^1H-NMR spectrum) that belongs to the "n" group of protons (see scheme 1) and the "m" signal with $\delta \approx 41.5$ ppm (in the ^{31}P-NMR spectrum). Also, the characteristics "l" protons and all the group of protons of the core are present between $\delta \approx 7.0 – 7.4$ and $2.4 – 3.3$ ppm, respectively. Accordingly, the "n", "m" and "l" signals are all shifted when compared with the corresponding spectra of the free $[RuCp(PPh_3)_2Cl]$ moiety, which also emphasizes the functionalization with the tetra-nitrile dendrimer. Additionally, the "j" signal (-CH_2C≡N-) have a downfield shift when compared to the free G0-$(CN)_4$. These results are in agreement with the obtained by our group (183, 184) with similar metallodendrimers. The only group of protons that were not detected in the ^1H-NMR spectrum was the four protons of the amide ("e" signal) and amine groups ("h" signal) of the molecule. Probably it´s not possible to identify them in this concentration – 0.018 mg/µL – besides being identified in the departure compound G0-$(CN)_4$ with the same concentration, because of the big difference between the number of protons of these two signals (4 protons each) in comparison to the 140 protons from the signals of the functionalized ruthenium moieties of the metallodendrimer. After this confirmation that the reaction was completed, the reaction could be stopped, filtered to remove the AgCl solid produced as a secondary product, and dried under vacuum. It was obtained a brown powder (2.35 g, 0.67 mmol), analysed by ^1H and ^{31}P-NMR (figs. 33b) and 34b), respectively), with a yield higher than 100% certainly due to the presence of several molecules of solvent (MeOH) and impurities and/or by-products (note the orange arrows in the mentioned figs.). This fact revealed the need to purify the obtained product.

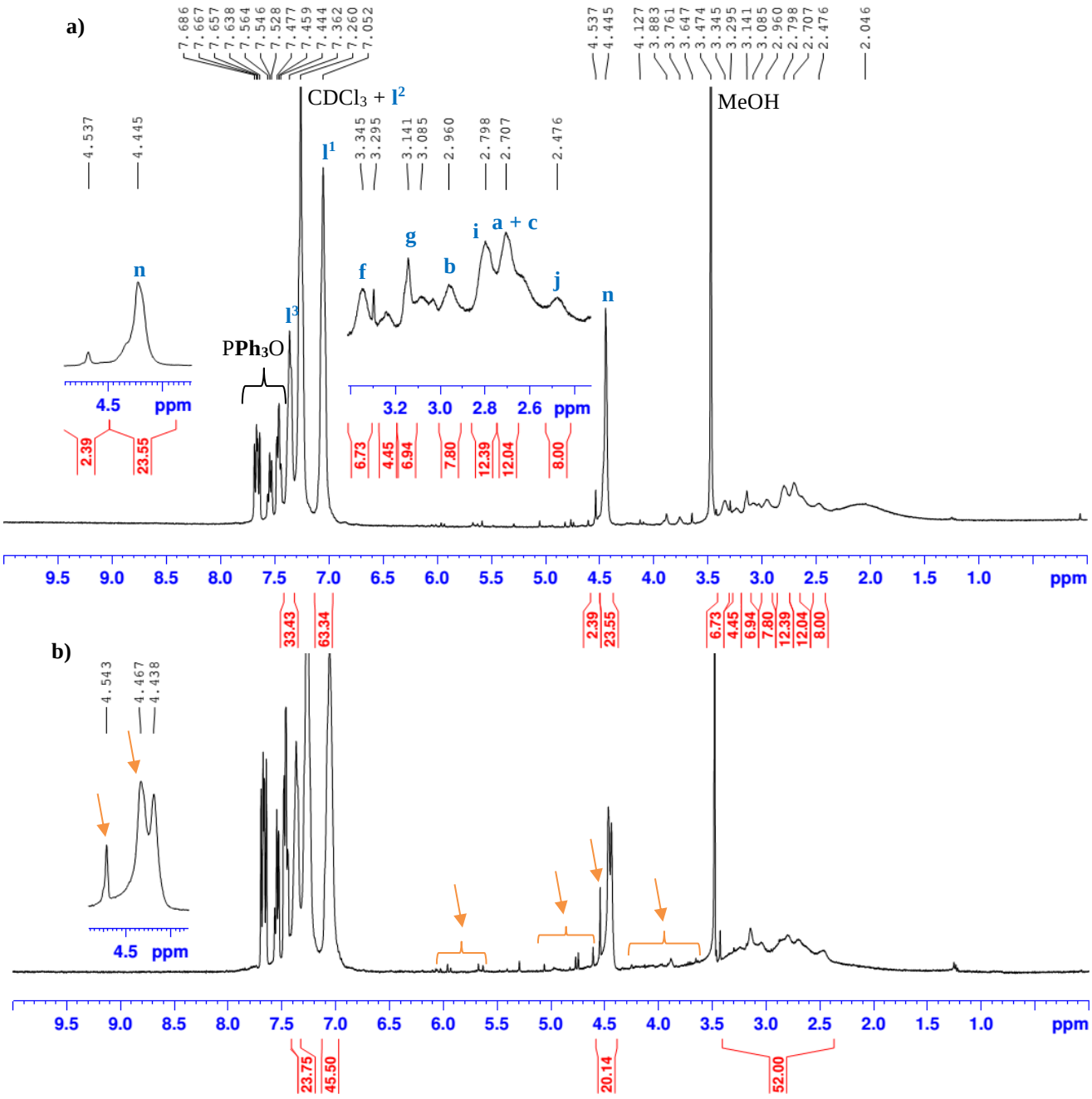

Figure 33 - ^{1}H-NMR spectra of the obtained products from the synthesis reaction of G0-$(CNRuCp(PPh_3)_2)_4(CF_3SO_3)_4$: a) the crude fraction after 22h of reaction and **b)** the brown powder after filtration; in $CDCl_3$. Each signal is marked with the respective type of protons that are represented with a unique letter (see scheme 1 and 3). The orange arrows points to the impurities/side-products that are needed to be removed.

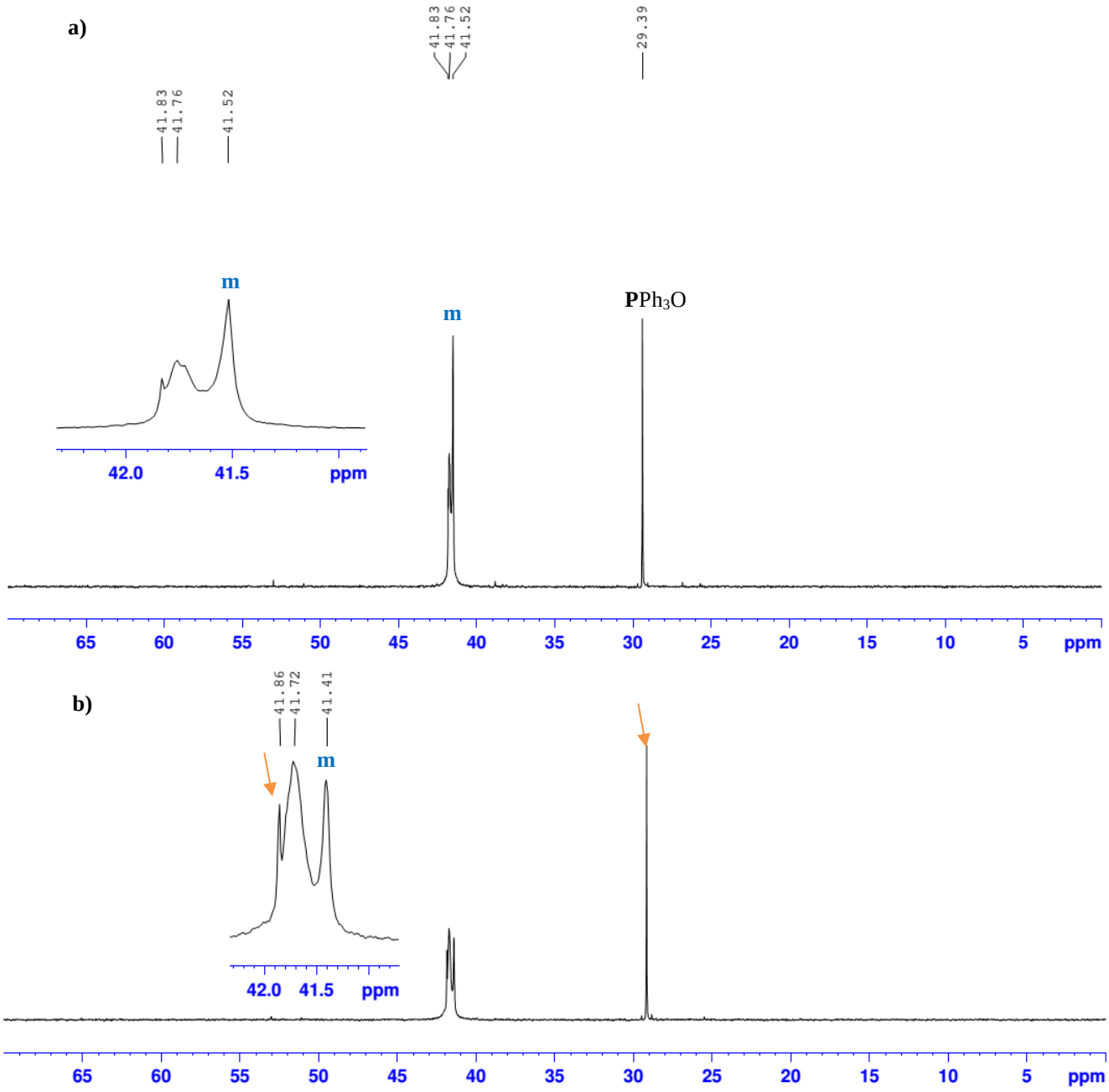

Figure 34 - ^{31}P-NMR spectrums of the corresponding samples from fig. 33; in $CDCl_3$. The "m" signal corresponds to the phosphorus from the G0-$(CNRuCp(PPh_3)_2)_4(CF_3SO_3)_4$ metallodendrimer (see scheme 1). The orange arrows points to the impurities/side-products that are needed to be removed.

After extraction with DCM and Et_2O washing (^{1}H and ^{31}P-NMR represented in figs. 35a) and 36a), respectively) it was still needed to remove the PPh_3O and the undesired side-products and/or impurities that were previously mentioned and that was still present. Thus, the powder was dissolved in 15 mL of DCM and precipitated with Et_2O. After being at -20°C overnight, the solution was filtered (bronze colour) and the brown precipitate was dried under vacuum. It

was possible to obtain 1.9 g (0.53 mmol) of a dark-brown powder with 96% of yield. The analysis of the performed ^{1}H and ^{31}P-NMR (figs. 35b) and 36b), respectively) have shown that, besides this purification process have removed the greater part of the PPh_3O and the sub-products/impurities, it was needed to repeat this process. Doing so, after the second purification, it was obtained 1.6 g (0.53 mmol) of it with a good yield of 84% (the performed ^{1}H and ^{31}P-NMR are represented in figs. 35c) and 36c), respectively). After the third purification, it was possible to obtain 1.5 g (0.4 mmol, 79 % of yield) of the metallodendrimer without PPh_3O (the performed ^{1}H and ^{31}P-NMR are represented in figs. 35d) and 36d), respectively). Through the analysis of all the ^{1}H-NMR of the metalodendrimer that was done so far, it was easy to identify that the singlet from the Cp-ring (the "n" signal), since the ^{1}H-NMR of the crude fraction (fig. 35a)), became a duplet with the same integration than before. This result diverges from the expected and reported from our group with similar compounds (183, 184): the presence of only one Cp-ring signal around 4.5 ppm in the ^{1}H-NMR spectrum and only one phosphorous signal in the ^{31}P-NMR around 42 ppm lead to the conclusion that all the ruthenium moieties were equivalently coordinated to the cores. In this work, the Cp-ring and the phosphorous signal from the $-PPh_3$ ligands ("m" signal), although not a singlet, have maintained the same arrangement during the three purification procedures. This fact, together with the adequate integration (20 protons) of the "n" signal, could emphasize that the G0-$(CNRuCp(PPh_3)_2)_4(CF_3SO_3)_4$ metallodendrimer was prepared as a unique compound with equivalent ruthenium moieties and not as a mixture of partially-functionalized metallodendrimers. Why? A possible explanation is given by the existence of intramolecular non-covalent interactions: *a)* arene-Arene interactions (212) between the aromatic π-systems (Cp and Ph rings); *b)* π-hydrogen bonds (213, 214) between these aromatic rings and the protons from the amide and secondary amine groups; *c)* aryl-heteroatom interactions (215) (although less frequent) accomplished with the nonbonding electrons of the oxygen and nitrogen (from the amide, secondary amines groups and even tertiary amines of the core) and these π-systems; and *d)* possibly dipole-dipole interactions between the ruthenium and the partial negative charge of the –NH and –(C=O)NH groups of the PAMAM dendrimer (216). To prove this hypothesis, it was performed a ^{13}C-NMR (fig. 37 and data in table 9, including the ^{1}H, ^{31}P-NMR data), an HSQC (fig. 38) and FTIR (fig. 5A and table 10) analysis. However, an analysis from MS and elemental analysis are still needed to support the obtained results. This work is ongoing.

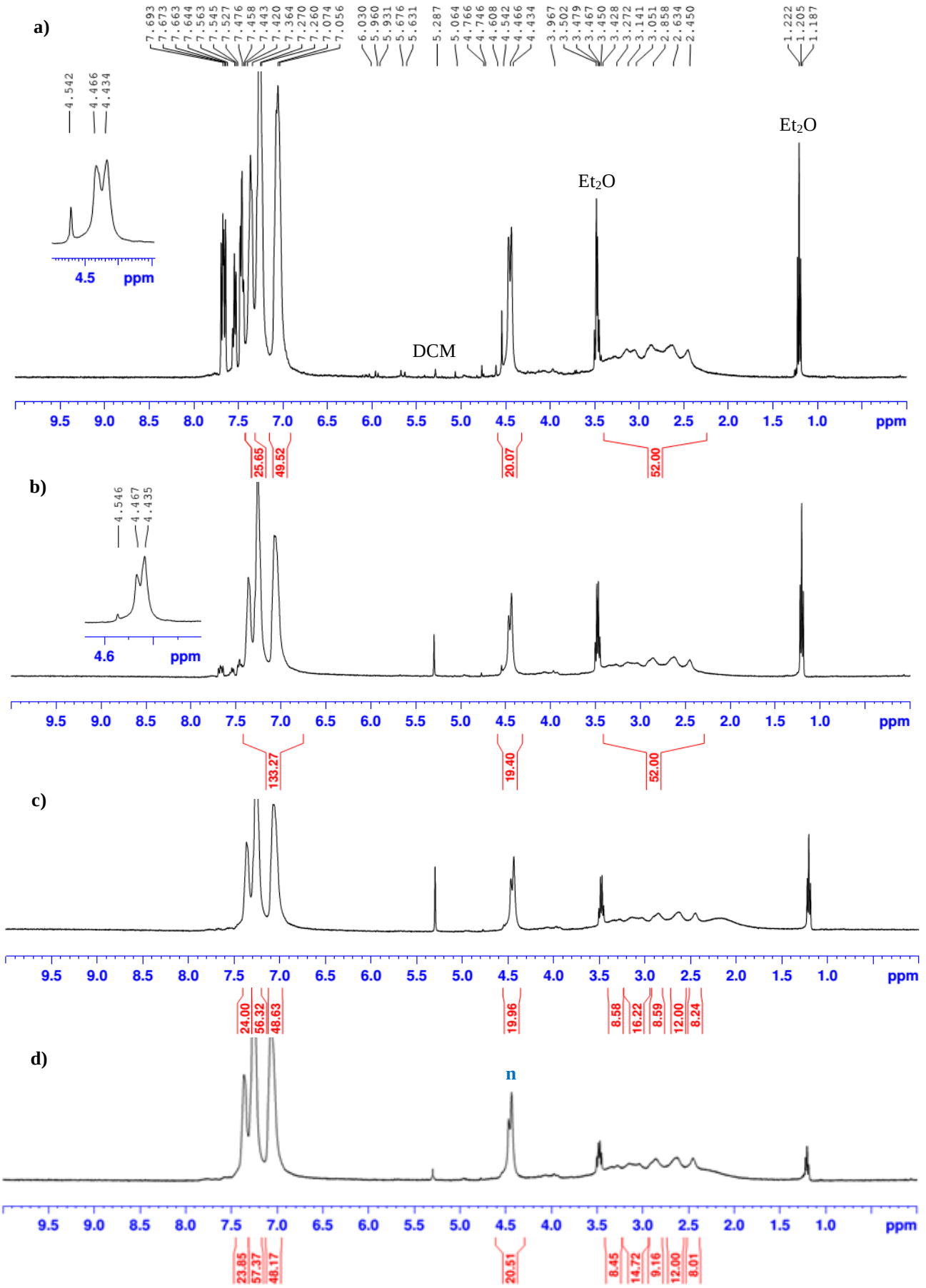

Figure 35 - ^{1}H-NMR spectra of the obtained products from the synthesis reaction of G0-$(CNRuCp(PPh_3)_2)_4(CF_3SO_3)_4$: a) after extracted by DCM and washed by Et_2O; b) after dissolved in DCM and precipitated with Et_2O; c) after the second precipitation with Et_2O; d) after the third precipitation; in $CDCl_3$.

The performed ^{13}C-NMR and HSQC spectra, besides showing the presence of all the carbon signals of the molecule, have exposed that the carbons from the Cp ring ("n" signal), the nitrile group ("k" signal), the **C**-NH- ("g" signal), the **C**-NH(C=O) ("f" signal), the **C**-C=O ("c" signal) and the **C**-N- ("b" signal) are all shifted when compared with the free nitrile dendrimer (G0-$(CN)_4$). These results indicate that, besides the adequate functionalization of the ruthenium moiety in the tetra-nitrile dendrimer by a covalent bond of the ruthenium with the nitrile groups, probably the abovementioned intramolecular non-covalent interactions are also present. This conclusion is supported by the presence of similar shifts in the ^{1}H-NMR spectrum (fig. 35d)) of the same sample (from the "j", "g", "i", "n" and "a" to "c" signals) and shifts from the stretch bands of the C≡N, (C=O)N–H, N–H (secondary amines), C=O and C–N in the FTIR spectrum. The most distinguished shifts are from the first tree signals and functional groups which reveals the coordination with the -RuCp moiety and that, probably, the most frequent non-covalent intramolecular interactions are the arene-arene, π-hydrogen bonds and dipole-dipole interactions between the metal and the partial negative charge of the amides and secondary amines of the dendrimer. These interactions certainly have influenced the metallodendrimer synthesis, its own crystallinity and particularly the molecular rearrangement of the molecule (217).

The study of the shifts observed from the stretch nitrile band (ν_{CN}) of the organonitriles after coordination with a metal centre, to higher or lower energies when compared with the free nitrile, can provide valuable information about the type of bond between the metal and the ligand (M-L), and the effect of the nitrile groups in the bond, as well as the other ligands of the molecule (in this particular case, the phosphines) (218). Accordingly, the increase in the CN stretching frequency, above that found for the free nitrile, in the order of 30 – 110 cm^{-1}, is a common feature exhibited by N-bonded nitrile complexes (219). These results indicate that the nitrile groups are coordinated with the metal centre through the nonbonding electrons of the nitrogen atom – linear coordination (218). Similar results were obtained for the G0-$(CNRuCp(PPh_3)_2)_4(CF_3SO_3)_4$ metallodendrimer in the FTIR spectrum, where the stretching nitrile band is shifted in 80 cm^{-1} when compared to the free nitrile ($\Delta\nu = \Delta\nu_{CN\ coordinated} - \Delta\nu_{CN\ free} = 2328 - 2248 = 80\ cm^{-1}$). Yet in the FTIR spectrum, it was also possible to detect several typical bands of the aromatic rings from the functionalized ruthenium moiety (see the values in cm^{-1} for aryl C=C and aryl–H in table 10) and, additionally, the characteristic bands of the $[CF_3SO_3^-]$ counterions was also present (≈ 1265 and 747 cm^{-1}).

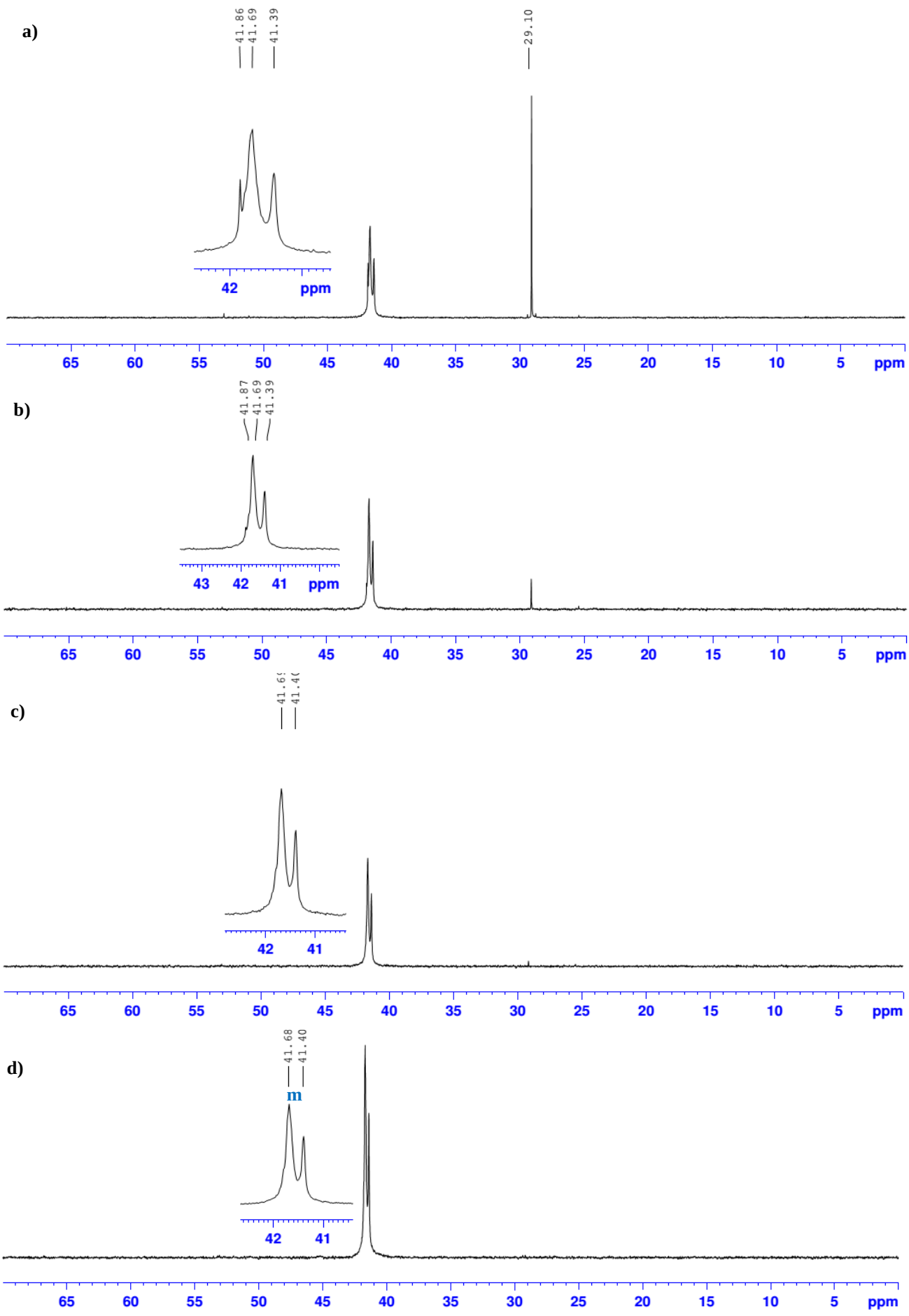

Figure 36 - ^{31}P-NMR spectrums of the corresponding samples from fig. 35; in $CDCl_3$.

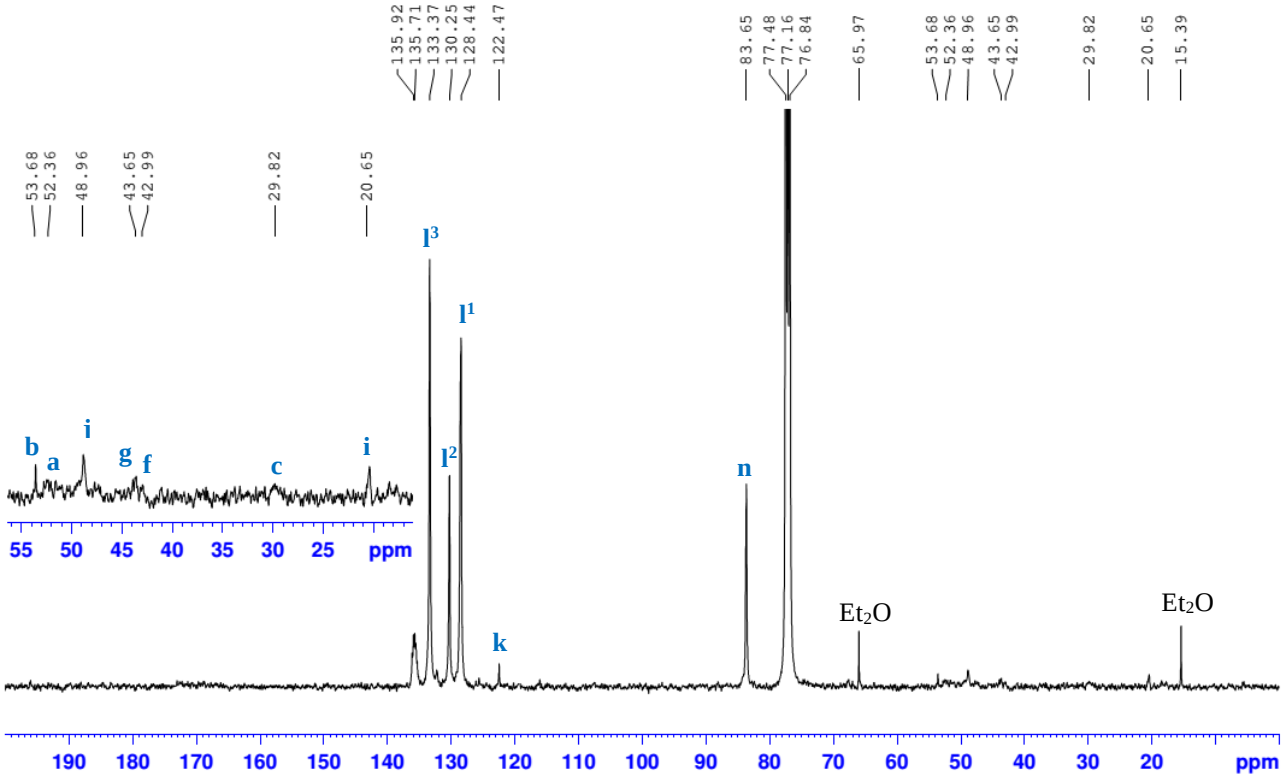

Figure 37 - ^{13}C-NMR spectrum of purified G0-$(CNRuCp(PPh_3)_2)_4(CF_3SO_3)_4$, in $CDCl_3$. Each signal is marked with the respective type of carbons that are represented with a unique letter (see scheme 1).

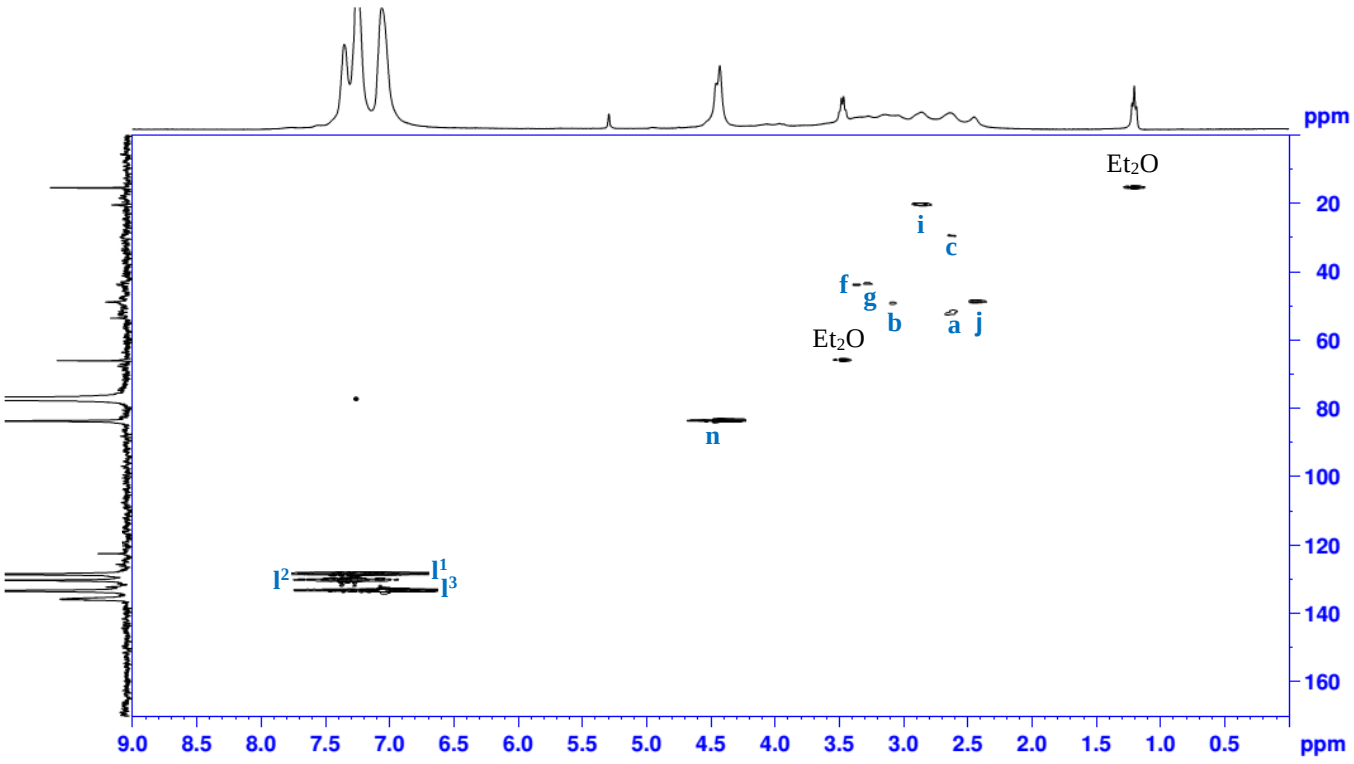

Figure 38 - HSQC spectrum of purified G0-$(CNRuCp(PPh_3)_2)_4(CF_3SO_3)_4$, in $CDCl_3$. Each signal is marked with the respective type of protons and type of carbon they are directly linked with. Each type is represented with a unique letter (see scheme 1).

Table 9 - ^{1}H, ^{31}P and ^{13}C-NMR data, of the corresponding spectrums represented in figs. 35d), 36d) and 37 for the purified G0-$(CNRuCp(PPh_3)_2)_4(CF_3SO_3)_4$. $CDCl_3$ was the NMR solvent. The ^{1}H and ^{31}P chemical shifts values are averages.

C atom	*^{1}H chemical shift (ppm)*	*Integral*		*^{31}P chemical shift (ppm)*	*^{13}C chemical shift (ppm)*
		Expected	*Obtained*		
a	Overlapped with "c"	4	*		52.36
b	3.042	8	#		53.68
c	2.619	8	*		29.82
d	-		-		Not detected in this concentration
e	Not detected in this concentration		-		-
f	3.337	8	8	-	42.99
g	3.146	8	#		43.65
h	Not detected in this concentration				
i	2.854	8			20.65
j	2.447	8	8		48.96
k	-		-		122.47
m	-		-	41.54	-
n	4.451	20	20		83.65
l^1	7.071	48	48		128.44
l^2	Overlapped with $CDCl_3$	48	-	-	130.25
l^3	7.362	25	24		133.37

*Sum of obtained integrals for "a" and "c": 12; expected sum: 12; # Sum of obtained integrals for "b" and "g": 15; expected sum: 16

Table 10 - Main characteristic bands (cm^{-1}), obtained by FTIR, for each functional group of the purified G0/G1-(CNRuCp(PPh$_3$)$_2$)x(CF$_3$SO$_3$)x. The type of vibration is also showed.

Functional group	***band (cm^{-1})***		***Type of vibration****
	G0	**G1**	
C(=O)N–H	3325	3332	Str
C=O of the amide	1634	1647	str
C–N	1159	1158	str
C≡N	2328	2343	str
–CH$_2$ (acyclic)	2931	2925	asym str
	2849	2848	sym str
N–H of the secondary amine	3472	3475	str
		1550	bend
Aryl C=C	1436	1435	str
	516	516	ring bend
Aryl–H	3058	3062	str
	1029	1028	in-plane bend
	696	696	out-of-plane bend
	638	637	
C–S	747	749	str
C–F	1265	1265	str

*str: stretch; asym str: asymmetric stretch; sym str: symmetric stretch

The successfully prepared compounds from generation 0 with optimized procedures press forward for the synthesis of similar compounds from generation 1. The G1-(CN)$_8$ and G1-(RuCp(PPh$_3$)$_2$)$_8$ were prepared as it is specified in scheme 2.

From 1.74 g (1.22 mmol; 1 eq. mol) of G1-PAMAM (golden oil) it was obtained 2.23 g (1.20 mmol; 99% of yield) of crude G1-(CN)$_8$ as a dark yellow oil. The corresponding ^{1}H-NMR is represented in fig. 39a). The spectrum is similar to the one obtained for G0-(CN)$_4$ (fig. 25a)) and the differences encountered between them was already discussed for the characterization of the G1-PAMAM.

After purification, it was obtained 2.12 g (1.14 mmol) of G1-(CN)$_8$ with a very good yield of 94 % as a dark yellow oil. The ^{1}H, ^{13}C-NMR, COSY, HSQC and FTIR spectra of this purified compound are represented in figs. 39b), c) (data organized in table 11); 40, 41 and 4A (data organized in table 7), respectively.

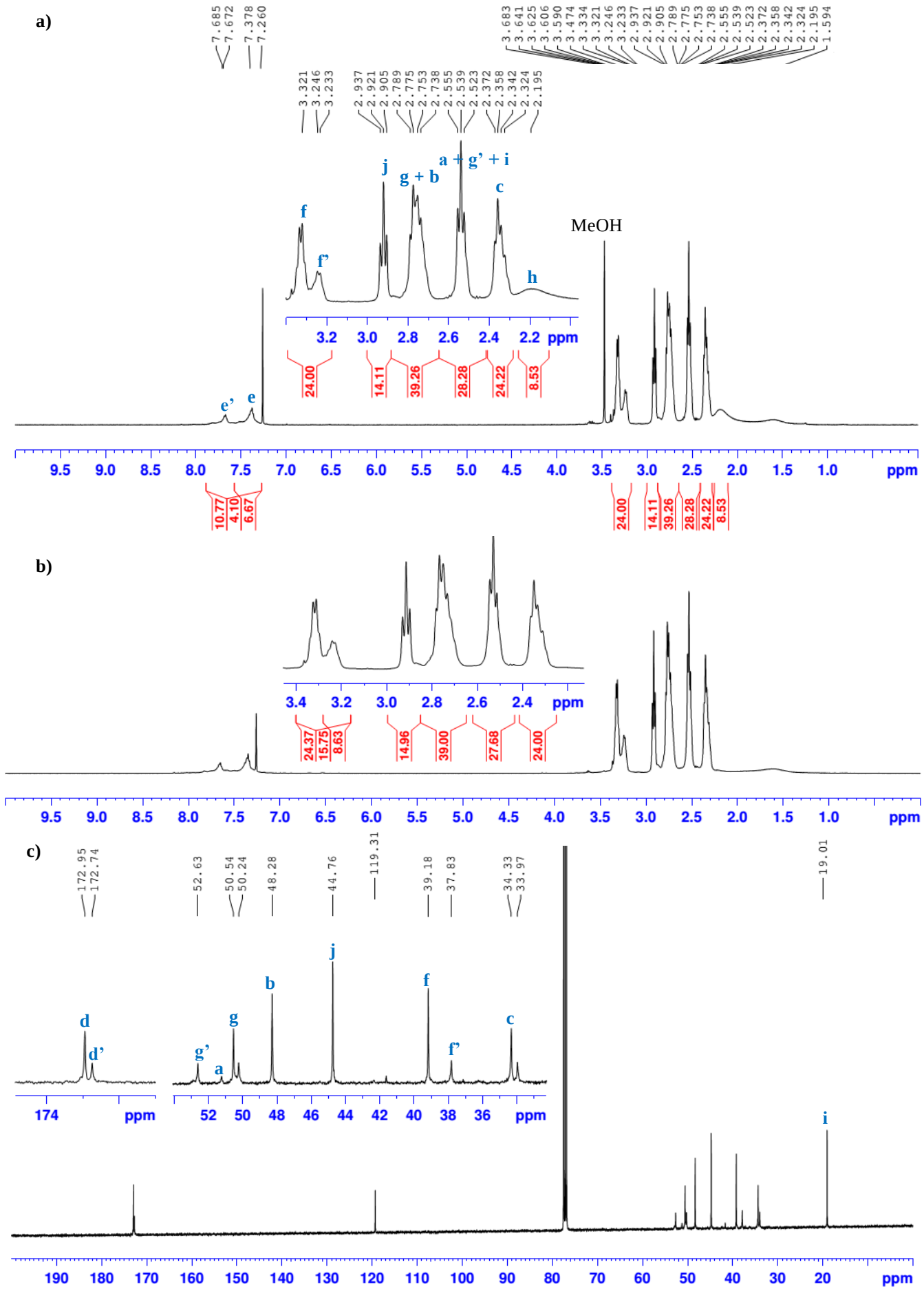

Figure 39 - NMR spectra of G1-$(CN)_8$: a) ^{1}H-NMR of the crude and b) the purified product; c) ^{13}C-NMR after purified; in $CDCl_3$. The red star represents the absence of MeOH.

Table 11 - ^{1}H and ^{13}C-NMR data, of the corresponding spectra represented in figs. 39b) and c), for purified G1-$(CN)_8$. $CDCl_3$ was the NMR solvent. The ^{1}H chemical shifts values are averages.

C atom	*^{1}H chemical shift (ppm)*	*Multiplicity*	*Integral*		*^{13}C chemical shift (ppm)*
			Expected	*Obtained*	
a	Overlapped with "i"		4	*	51.54
b	2.757	4	24	#	48.28
c	2.339	4	24	24	34.33
d	-	-	-	-	172.95
d'	-	-	-	-	172.74
e	7.348	3	8	7	-
e'	7.651	3	4	4	-
f	3.375	4	16	*[1]	39.18
f'	3.234	4	8	*[1]	37.83
g	Overlapped with "b"		16	#	50.54
g'	Overlapped with "i"		8	*	52.63
h	2.195	1	8	-	-
i	2.529	3	16	*	19.01
j	2.914	3	16	15	44.76
k	-	-	-	-	119.24

*Sum of obtained integrals for "a", "g'" and "i": 28; expected sum: 28; #Sum of obtained integrals for "b" and "g": 39; expected sum: 40; *[1]Sum of obtained integrals for "f" and "f'": 24; expected sum: 24

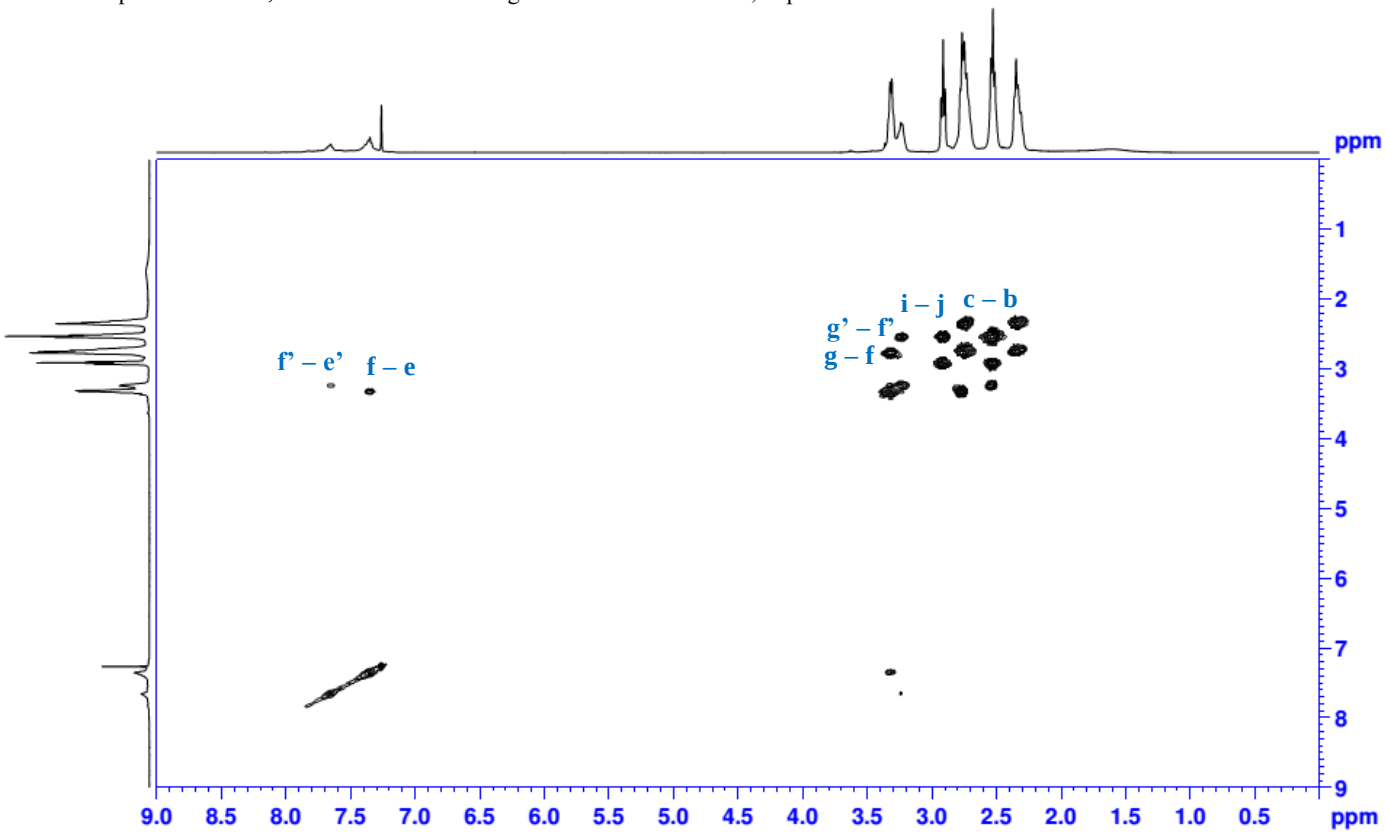

Figure 40 - COSY spectrum of purified G1-$(CN)_8$, in $CDCl_3$. Each signal is marked with the respective group of protons that are neighbours and linked to each other by a carbon bond. Each type of protons is represented with a unique letter (see scheme 2).

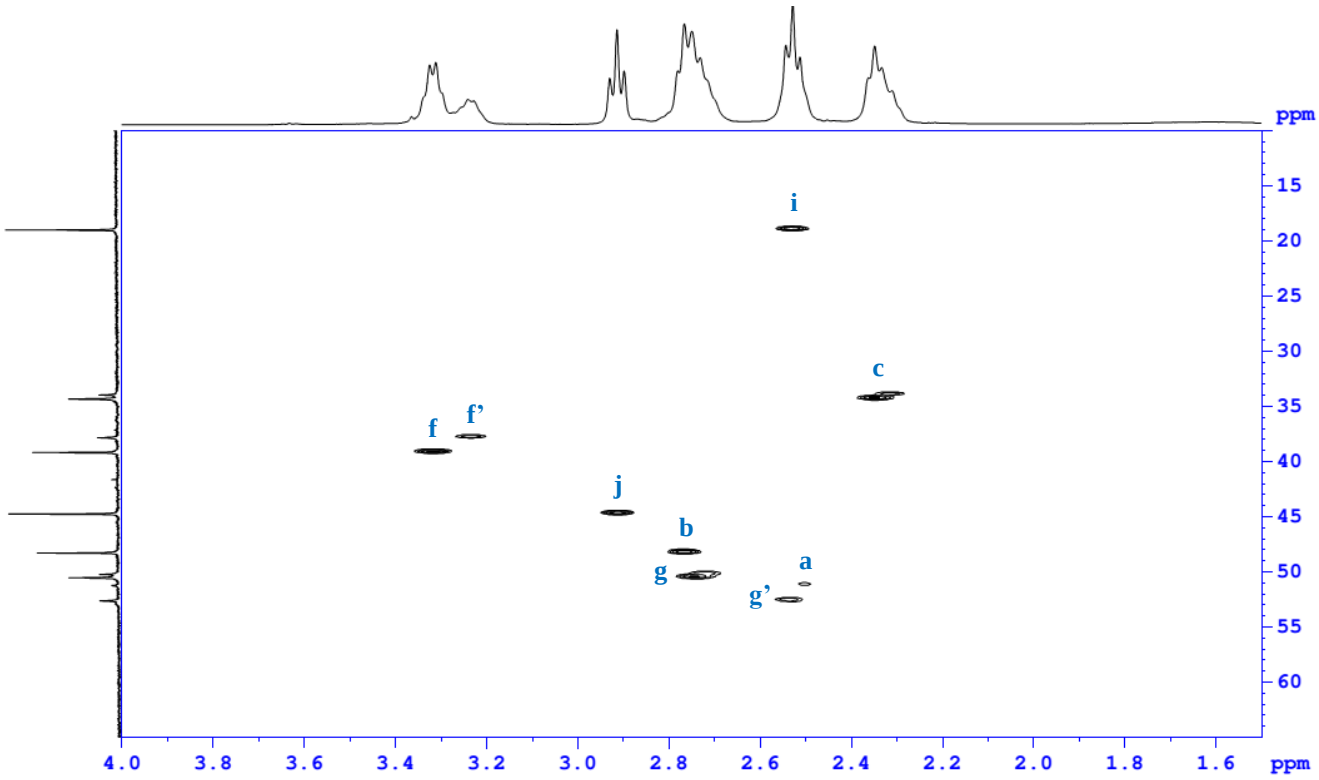

Figure 41 - HSQC spectrum of purified G1-$(CN)_8$, in $CDCl_3$. Each signal is marked with the respective type of protons and type of carbon they are directly linked with. Each type is represented with a unique letter (see scheme 2).

From 0.52 g (0.28 mmol, 1 eq. mol) of G1-$(CN)_8$, 1.66 g (2.28 mmol, 8.1 eq. mol) of $[RuCp(PPh_3)_2Cl]$ and 0.68 g (2.65 mmol, 9.4 mmol) of $AgCF_3SO_3$, and 24h of reaction at room temperature with protection from the light, it was possible to synthetize the crude G1-$(CNRuCp(PPh_3)_2)_8(CF_3SO_3)_8$ as a brown powder. The performed ^1H and ^{31}P-NMR (figs. 42a) and 43a), respectively) revealed that the synthesis was certainly completed. The characteristic signals from the G1-$(CNRuCp(PPh_3)_2)_8(CF_3SO_3)_8$ metallodendrimer were present: in the ^1H-NMR, the Cp-ring signal with $\delta \approx 4.4$ ppm ("n" signal); the phenyl protons ("l" signals) with $\delta \approx 7.0 - 7.4$ ppm and all the group of protons of the core between $\delta \approx 2.4 - 3.3$ ppm, and the phosphorous signal with $\delta \approx 41.6$ ppm ("m" signal) in the ^{31}P-NMR. The "n", "m" and "l" signals, in comparison with the free -RuCp moiety, are all shifted and also the downfield shift of the "j" signal when compared with the free octa-nitrile also confirms that the G1-metallodendrimer was synthesized with success. After extraction, washing and purification by precipitation (^1H and ^{31}P-NMR spectra of the washed and purified compound in figs. 42 b),c) and 43b),c), respectively) it was obtained 1.6 g (0.23 mmol) of the G1-$(CNRuCp(PPh_3)_2)_8(CF_3SO_3)_8$, as a dark-brown microcrystalline powder, with a good yield of

77%. The NMR data from it is organized in table 12. It was performed a FTIR spectrum, in a KBr pellet (fig. 5A and data in table 10), a ^{13}C-NMR (fig. 44 and data in table 12) and an HSQC (fig. 45). The obtained results agree with the acquired results for the G0-$(CNRuCp(PPh_3)_2)_4(CF_3SO_3)_4$ that were already discussed. In the FTIR spectrum, a similar increase in the CN stretching frequency (when compared to the free nitrile) was found, in the order of 96 cm^{-1} ($\Delta\nu$ = 2343 – 2247 = 96 cm^{-1}), which also indicates a linear coordination between the nitrile group and the metal centre. It is also important to emphasize that the analysis of the ^{1}H, ^{13}C-NMR and FTIR spectra, likewise what was observed for the G0-metallodendrimer, indicates that probably occurs non-covalent intramolecular interactions, specifically the arene-arene, π-hydrogen bonds and dipole-dipole (between the ruthenium and the partial negative charge of the amide and amine groups) because of the observed shifts from the "c", "g" and "i" signals and the shifts from the stretch bands of the (C=O)N–H and N–H. The only encountered difference was the less evidence of dipole-dipole interactions of ruthenium with the non-bonding electrons from the C=O and C–N groups of the core: in the ^{1}H-NMR spectra, the "a" and "b" group of protons have similar chemical shifts (compare table 11 with 12) and, in the FTIR spectrum, the stretching band for the C=O group has similar frequencies of vibration when compared with the free G1-$(CN)_4$ (compare table 7 with 10). This happen probably because of the increasing number of bonds between the C=O and C–N groups of the core and the metallic end group (15 and 18 bonds for the G1, and 8 and 11 for the G0, respectively) and, additionally, the bonds of the core becomes more stretched with the increase of the generation number when the dendrimer is in solution with a good solvent. This last hypothesis is supported by the structural information of the PAMAM dendrimers obtained from extensive molecular dynamics (MD) simulations in explicit solvent – studies of P. K. Maiti *et al.* (220).

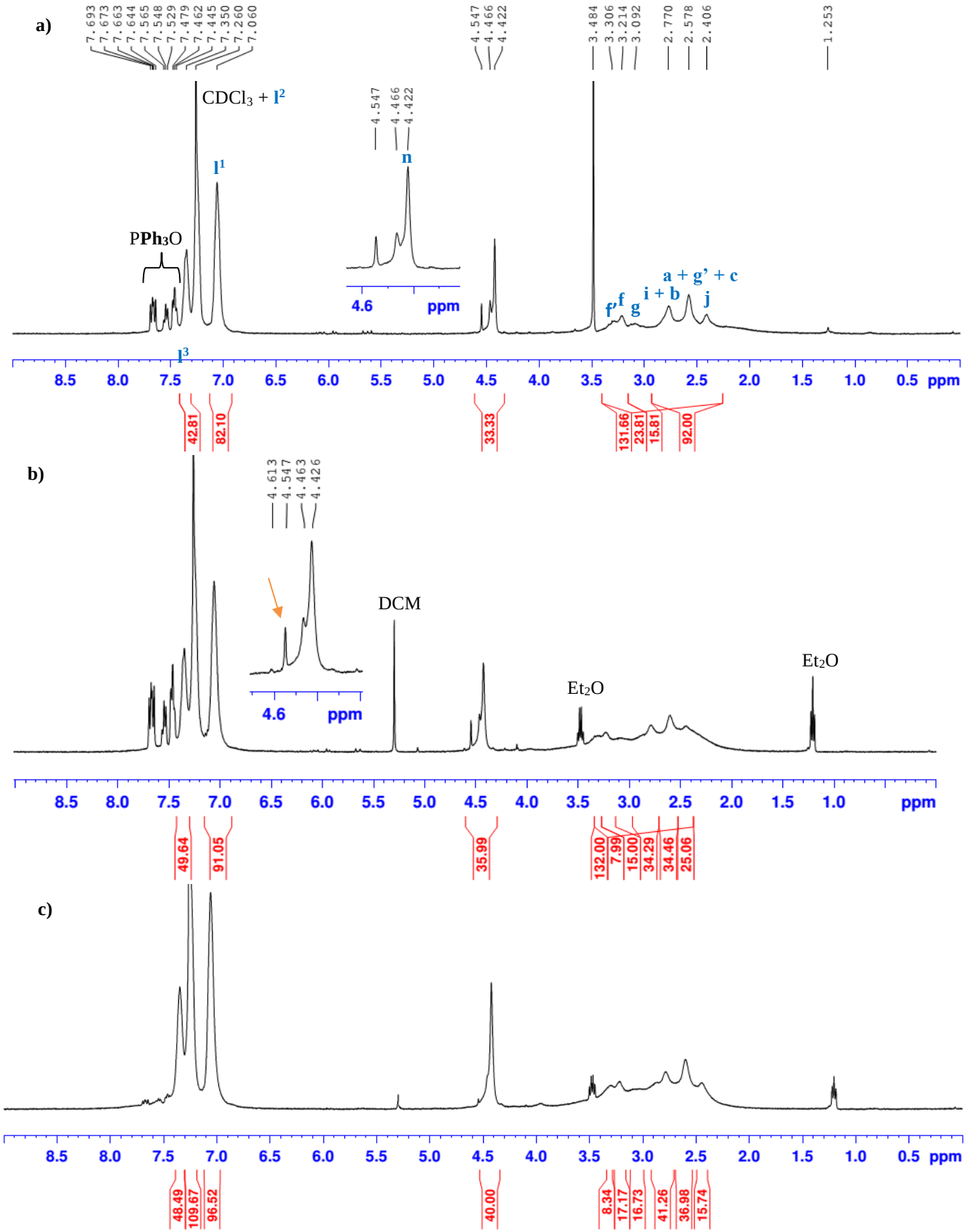

Figure 42 - ^{1}H-NMR spectra of the a) crude, b) extracted by DCM and washed by Et_2O and c) purified G1-$(CNRuCp(PPh_3)_2)_8(CF_3SO_3)_8$, in $CDCl_3$. Each signal is marked with the respective type of protons that are represented with a unique letter (see scheme 2 and 3). The orange arrow represents the impurity/sub-product that was removed after the purification.

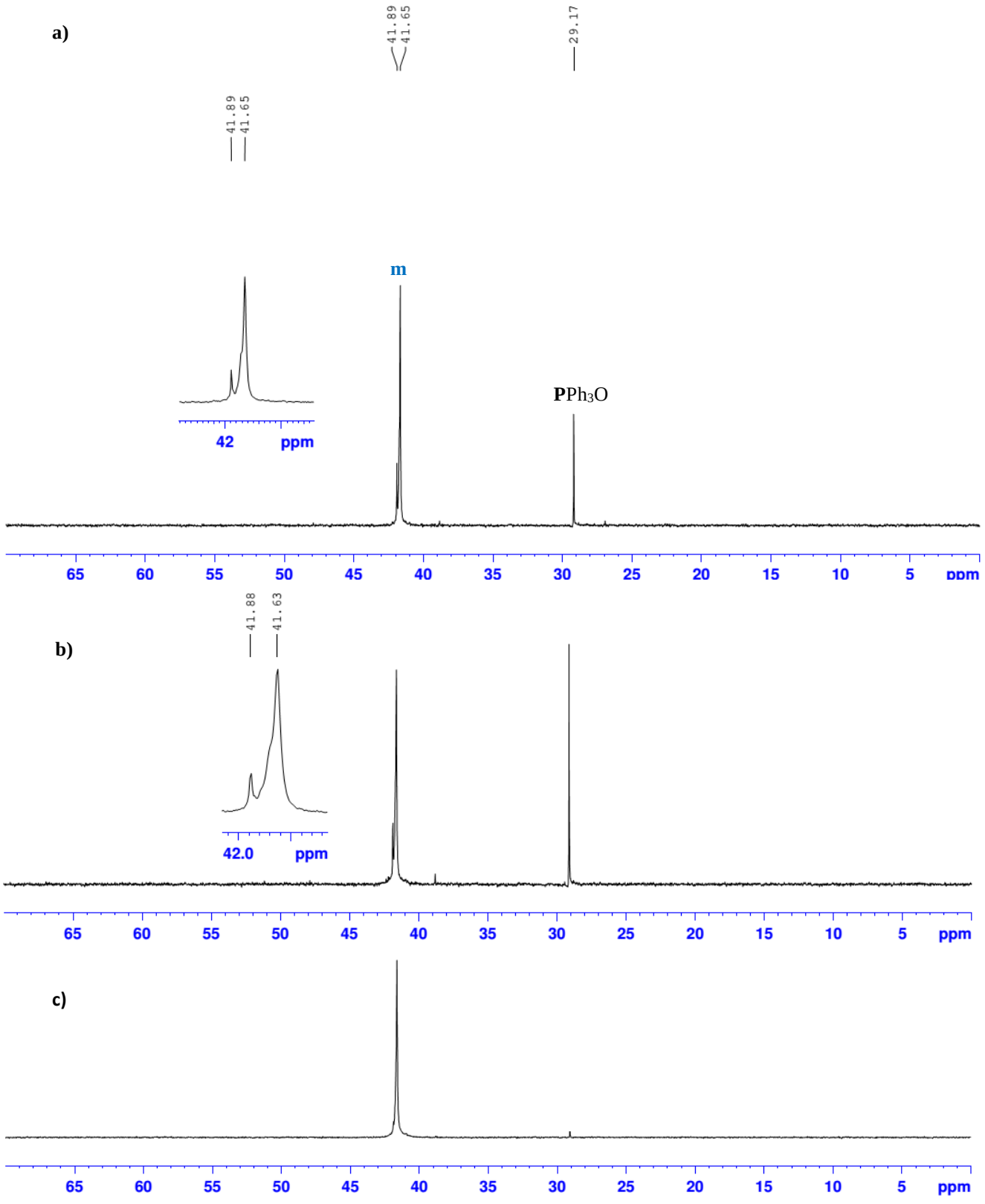

Figure 43 - ^{31}P-NMR spectra of the corresponding samples from fig. 42; in $CDCl_3$.

Table 12 - ^{1}H, ^{31}P, and ^{13}C-NMR data, of the corresponding spectra represented in figs. 42c), 43c) and 44 for the purified G1-(CNRuCp(PPh$_3$)$_2$)$_8$(CF$_3$SO$_3$)$_8$. CDCl$_3$ was the NMR solvent. The ^{1}H chemical shifts values are averages.

C atom	*^{1}H chemical shift (ppm)*	*Integral*		*^{31}P chemical shift (ppm)*	*^{13}C chemical shift (ppm)*
		Expected	*Obtained*		
a	Overlapped with "c"	4	*		52.33
b	2.784	24	#		50.44
c	2.599	24	*		31.43
d	-	-			173.48
d'	-	-			173.04
e	Not detected in this concentration	-			-
f	3.222	16	17		39.70
f´	3.293	8	8	-	38.71
g	3.080	16	17		48.37
g'	Overlapped with "c"	8	*		53.58
h	Not detected in this concentration	-			-
i	Overlapped with "b"	16	#		20.83
j	2.448	16	16		44.17
k	-	-			122.45
m	-	-		41.60	-
n	4.422	40	40	-	83.52
l^1	7.055	96	96		128.44
l^2	Overlapped with CDCl$_3$	96	-	-	130.21
l^3	7.344	48	48		133.32

*Sum of obtained integrals for "a", "c" and "g'": 37; expected sum: 36; # Sum of obtained integrals for "b" and "i": 41; expected sum: 40

In this way, probably the most frequent type of non-covalent intramolecular interactions in the G1-metallodendrimer is the arene-arene interactions and the π-hydrogen bonds among the periphery that are weaker when compared to the dipole-dipole interactions. Thus, the total influence on the multiplicity of the "n" and "m" signals of the G1-(CNRuCp(PPh$_3$)$_2$)$_8$(CF$_3$SO$_3$)$_8$ is lower when compared to the same compound from generation 0 and probably, that´s why their multiplicity is slightly different (compare figs. 35d) and 36d) with 42c) and 43b). However, this hypothesis must be supported from the MS and elemental analysis, which are ongoing.

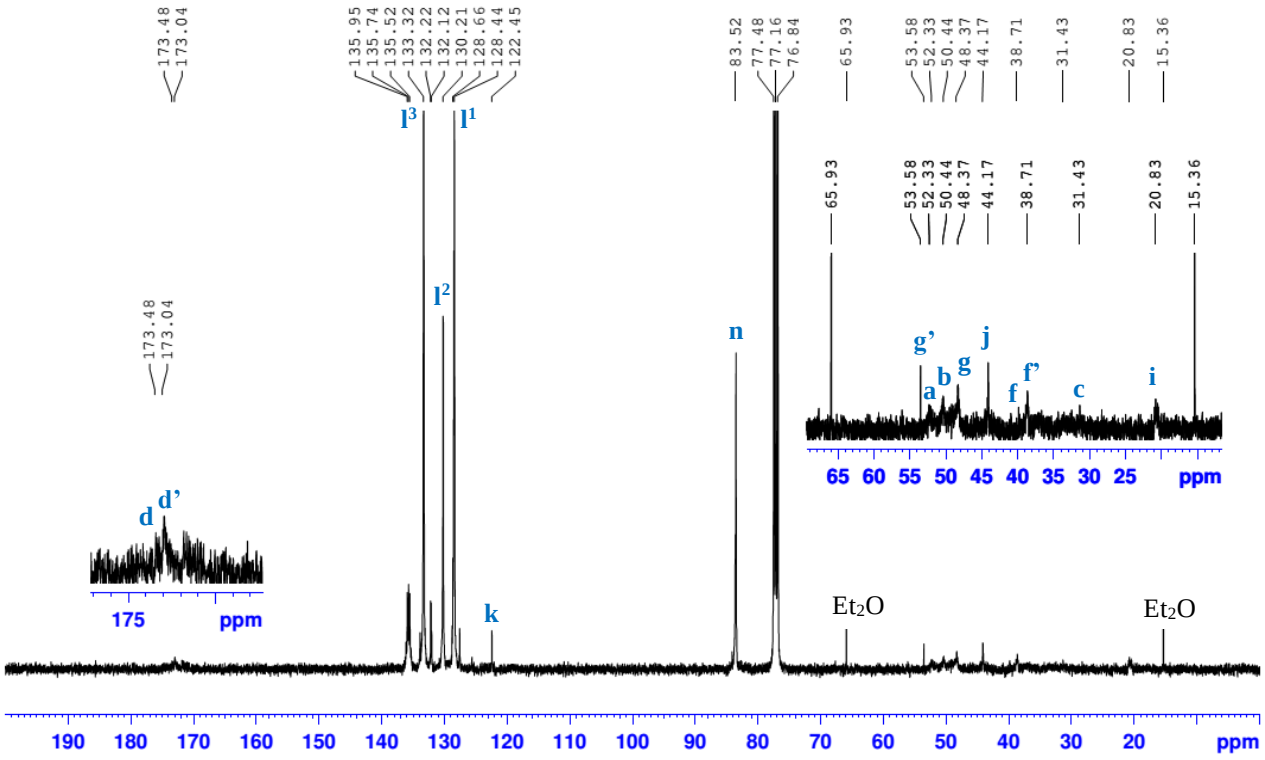

Figure 44 - ^{13}C-NMR spectrum of G1-$(CNRuCp(PPh_3)_2)_8(CF_3SO_3)_8$, in $CDCl_3$. Each signal is marked with the respective type of carbons that are represented with a unique letter (see scheme 2).

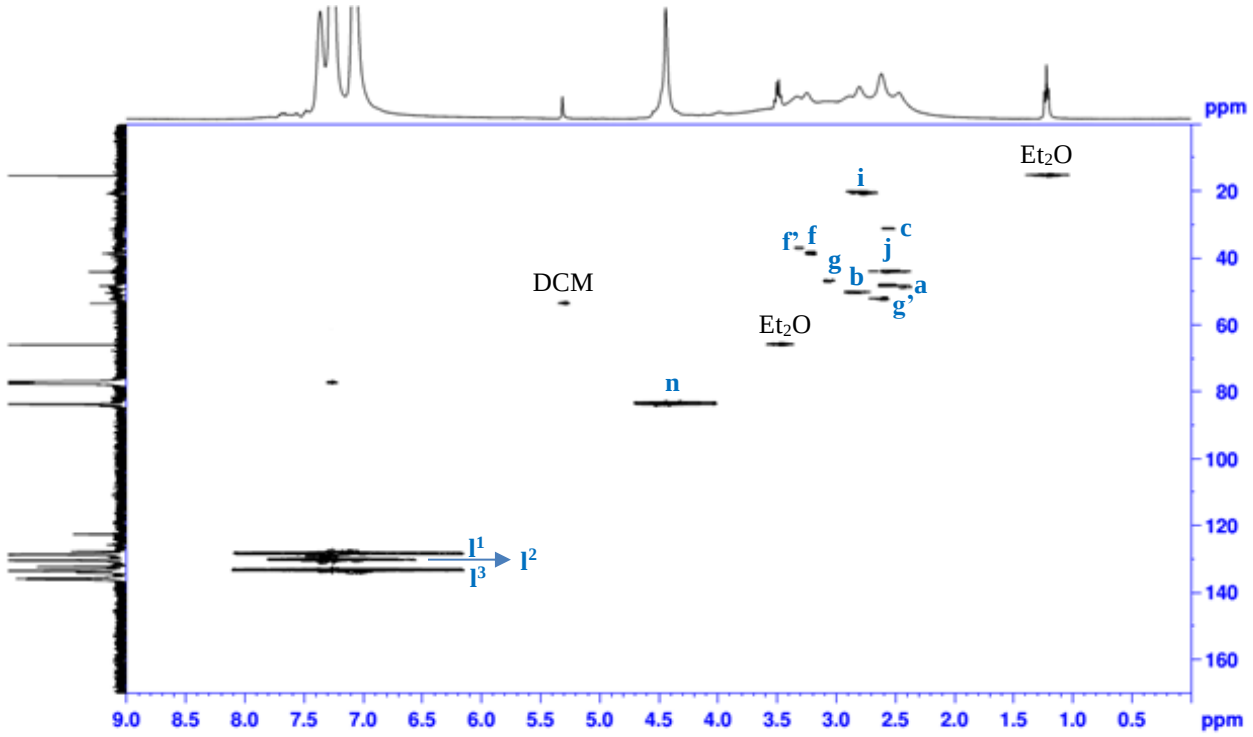

Figure 45 - HSQC spectrum of purified G1-$(CNRuCp(PPh_3)_2)_8(CF_3SO_3)_8$, in $CDCl_3$. Each signal is marked with the respective type of protons and type of carbon they are directly linked with. Each type is represented with a unique letter (see scheme 2).

5. ORGANIC COMPOUNDS

In this section, the developed methodology for the preparation of the hydroxyl dendrimers G0-$(OH)_8$ and G1-$(OH)_{16}$ will be presented and discussed.

5.1. Materials and methods

5.1.1. Reagents and solvents

All chemicals were purchased from commercial sources and used as received, with the exception of THF (C_4H_8O, 99.9%, CAS No. 109-99-9, HPLC grade, Fisher Chemical) that was dried by the solvent purification system mBRAUN MB SPS-800. The other chemicals that were used are listed: *Tert*-Butyl acrylate (98%, CAS No. 1663-39-4, Fluka); MeOH (99.9%, CAS No. 67-56-1, Fisher Chemical and 99.99%, HPLC grade from ACROS Organics); $LiAlH_4$ (95%, CAS No. 16853-85-3, Fisher Chemical); $CDCl_3$ (99.8 atom %D, CAS No. 865-49-6, Merck) and D_2O (99.8 atom %D, CAS No. 7789-20-0, ACROS Organics).

5.1.2. Samples preparation

The G0/G1-PAMAM dendrimer commercial solution (in MeOH; 4.40 mL for G0 – 54.95 % w/w) and 10.5 mL for G1 – 36.25 % w/w) were dried, dissolved in water and lyophilized.

5.1.3. Synthesis of poly-ester dendrimers G0/G1-$CO_2{}^tBu$

The G0-PAMAM dendrimer (1.71 g; 3.32 mmol; 1 eq. mol) was dissolved in 15 mL of MeOH. It was stirred until complete dissolution to be added *tert*-butyl acrylate (27.19 mmol; 8.2 eq. mol), dropwise. This mixture stayed under stirring for 44h, and the solvent was removed in the rotatory evaporator and then dried under vacuum. It was obtained 4.66 g (3.02 mmol; 91% of yield) of G0-$(CO_2{}^tBu)_8$ as a yellowish oil. The ^{1}H-NMR (in $CDCl_3$) spectrum of the crude product revealed the need to purify the prepared compound. In this way, it was performed a L-L extraction with Hex/9:1 MeOH:H_2O and, subsequently, the dried G0-$(CO_2{}^tBu)_8$ was washed with distilled water and partially dissolved in it to be lyophilized. This last procedure was repeated. The purified compound (4.46 g; 2.89 mmol; 87% of yield) was characterized by

^{1}H, ^{13}C-NMR, COSY, HSQC, FTIR, and MS. ^{1}H-NMR (400 MHz, $CDCl_3$): δ = 3.290 (m (multiplet), 9 H), 2.838 and 2.740 (t, 26 H), 2.541 (t, 8 H), 2.405 and 2.364 (t, 25 H), 1.440 (s, 72 H, $–CO_2C(CH_3)_3$) ppm. ^{13}C-NMR (100 MHz, $CDCl_3$): δ = 172.98 ($–HNC=O$), 172.19 ($–CO_2C(CH_3)_3$), 80.65 ($–CO_2C(CH_3)_3$), 52.88, 50.33, 49.49, 45.05, 37.59, 35.96, 33.87, 28.28 ($–CO_2C(CH_3)_3$) ppm. COSY (400 MHz, $CDCl_3$): three signals. HSQC (100 e 400 MHz, $CDCl_3$): eight signals. FTIR (KBr cells): $\tilde{\nu}$ = 1726 ($\nu_{–COOtBu}$) cm^{-1}. LC-MS/MS (ESI+): *m/z* = 1537.4 $[M]^+$, 643.4 (base peak).

With the G1-PAMAM dendrimer (2.98 g; 2.09 mmol; 1 eq. mol) it was applied the same procedure: 33.8 mmol (16.2 eq. mol) of *tert*-butyl acrylate was added, and after 44h it was obtained 6.25 g (1.80 mmol; 86% of yield) of crude G1-$(CO_2{}^tBu)_{16}$ as a dark yellow oil. After purification, it was possible to obtain 6.03 g (1.73 mmol) with 83 % of yield. The abovementioned spectroscopic methods have characterized it, except MS. ^{1}H-NMR (400 MHz, $CDCl_3$): δ = 3.303 (m, 25 H), 2.815 and 2.731 (t, 60 H), 2.538 (t, 24 H), 2.406 and 2.344 (t, 57 H), 1.438 (s, 144 H, $–CO_2C(CH_3)_3$) ppm. ^{13}C-NMR (100 MHz, $CDCl_3$): δ = 172.98 ($–HNC=O$), 172.26 ($–CO_2C(CH_3)_3$), 80.68 ($–CO_2C(CH_3)_3$), 52.77, 50.30, 49.41, 45.02, 37.57, 35.80, 33.83, 28.27 ($–CO_2C(CH_3)_3$) ppm. COSY (400 MHz, $CDCl_3$): three signals. HSQC (100 e 400 MHz, $CDCl_3$): eight signals. FTIR (KBr cells): $\tilde{\nu}$ = 1727 ($\nu_{–COOtBu}$) cm^{-1}.

5.1.4. Synthesis of poly-hydroxyl dendrimers G0/G1-OH

It was prepared, in advance, a suspension of $LiAlH_4$ (1.43 g; 37.6 mmol; 16 eq. mol), dissolved in 150 mL of dried THF in the N_2 atmosphere. Then, G0-$(CO_2{}^tBu)_8$ (3.63 g; 2.35 mmol; 1 eq. mol), previously dissolved in 50 mL of dried THF, was added dropwise to the lithium solution, at 0°C. It was added more 50 mL of dried THF to the reaction mixture to avoid the formation of a compact paste and to allow the reagents to react freely. It was firstly stirred at 0°C, for 1 hour, and then was left under stirring, at room temperature, for 26h. It was cooled to 0°C, quenched with ice and left until the gray residue became a free white suspension and settled. After the neutralization, the suspension was filtered, the obtained paste was dissolved in distilled water and stirred overnight. Then, after filtration, the solution was lyophilized. It was obtained 2.14 g (2.18 mmol; 93% of yield) of G0-$(OH)_8$ as a light yellow spongy, sticky oil. It was characterized by ^{1}H, ^{13}C-NMR, COSY, HSQC, FTIR and MS. ^{1}H-NMR (400 MHz, $CDCl_3$): δ = 3.650 (q, 16 H, $–CH_2OH$), 3.334 (q, 8 H), 2.819 (t, 10 H), 2.715 and 2.643 (t and

m, 30 H), 2.435 (t, 8 H), 1.752 (m, 16 H, –C*H*$_2$CH$_2$OH) ppm. ^{13}C-NMR (100 MHz, $CDCl_3$): δ = 174.69 (–HN*C*=O), 60.36 (–*C*H$_2$OH), 51.59, 50.54, 50.39, 49.16, 36.47, 32.67, 27.99 (–*C*H$_2$CH$_2$OH) ppm. COSY (400 MHz, $CDCl_3$): four signals. HSQC (100 e 400 MHz, $CDCl_3$): seven signals. FTIR (KBr cells): $\tilde{\nu}$ = 3676 (ν_{OH}), 1061 ($\nu_{C–OH}$) cm^{-1}. LC-MS/MS (ESI+): *m/z* = 981.7 [M]$^+$, 751.5.

For the preparation of the G1-hydroxyl dendrimer, it was followed the abovementioned procedure with 1.52 g of $LiAlH_4$ (40.03 mmol; 32 eq. mol) for 4.35 g (1.25 mmol; 1 eq. mol) of G1-($CO_2{}^t$Bu)$_{16}$ to be obtained 2.62 g (1.11 mmol; 89% of yield) of pure G1-(OH)$_{16}$ as a yellow spongy sticky oil. It was characterized by the same methods than G0-(OH)$_8$, except MS. ^{1}H-NMR (400 MHz, $CDCl_3$): δ = 3.654 (q, 33 H, –C*H*$_2$OH), 3.345 (q, 24 H), 2.810 (t, 24 H), 2.718 and 2.638 (t and m, 60 H), 2.445 (t, 24 H), 1.741 (m, 33 H, –C*H*$_2$CH$_2$OH) ppm. ^{13}C-NMR (100 MHz, $CDCl_3$): δ = 175.07 (–HN*C*=O), 60.36 (–*C*H$_2$OH), 51.70, 51.32, 50.41, 49.09, 36.46, 32.80, 28.01 (–*C*H$_2$CH$_2$OH) ppm. COSY (400 MHz, $CDCl_3$): four signals. HSQC (100 e 400 MHz, $CDCl_3$): seven signals. FTIR (KBr cells): $\tilde{\nu}$ = 3432 (ν_{OH}), 1058 ($\nu_{C–OH}$) cm^{-1}.

5.1.5. Characterization

The prepared four prepared dendrimers were characterized by ^{1}H, ^{13}C-NMR, HSQC, COSY and FTIR. The G0-(OH)$_8$ and G0-($CO_2{}^t$Bu)$_8$ were additionally characterized by MS spectroscopy. It was not possible to perform the MS spectra of the G1-(OH)$_{16}$ and G1-($CO_2{}^t$Bu)$_{16}$ due to a malfunction of the equipment.

The NMR (^{1}H, ^{13}C, HSQC, and COSY) characterization was performed with ≈ 10 mg of each compound dissolved in 550 μL of solvent: $CDCl_3$ for G0/G1-$CO_2{}^t$Bu and D_2O for G0/G1-OH. The NMR spectra were recorded with a Bruker Avance II+ 400 at 299 K (probe temperature) spectrometer. All chemical shifts are reported in parts per million (δ, ppm) with reference to Me_4Si.

FTIR spectra were recorded on a Nicolet Avatar 360 FTIR spectrometer. About 5 to 10 mg of each oily sample were analysed in KBr cells (25 x 4 mm). The main characteristics bands are reported in cm^{-1}, and the type of vibration of each are also showed. Only the significant bands are cited in the text.

The MS spectra were performed with filtered samples of 1 g/L of G0-(OH)$_8$ and 2 g/L of G0-($CO_2{}^t$Bu)$_8$ in MeOH. It were used syringe filters PTFE hydrophilic with 0.22 μm of pore

from SPECANALITICA. The spectra were recorded with a Bruker Esquire 6000/Dionex ESI LC-ESI-MS/MS spectrometer, between 30 minutes. Only one of the various obtained spectra of +MS, +MS2 and +MS3, is presented in this work, and likewise, only the significant *m/z* values are cited in the text.

5.2. Results and discussion

The preparation of G0/G1-OH as final compounds was accomplished by adapting the reported methodology of T. Krishna and N. Jayaraman (1) and G. Jayamurugan and N. Jayaraman (2) (amine → ester → alcohol) to increase the length of the lateral chains of the core by incorporating different functional groups at the periphery of the dendrimers. The precursors G0/G1-$CO_2{}^t$Bu were synthetized by a Michael addition (N-alkylation) of *tert*-butyl acrylate, that was followed by the reduction of the resulting *tert*-butyl to give the respective alcohol (Scheme 6 and 7), the desired compound.

In the synthesis reaction of G0/G1-$CO_2{}^t$Bu, the Michael donor is the $–NH_2$ groups of the G0/G1-PAMAM dendrimers and the Michael acceptor is the unsaturated α, β-carbons of the *tert*-butyl acrylate. The mechanism of the reaction is similar to the aza-Michael reaction previously discussed for the synthesis reaction of G0/G1-CN. Accordingly, for the synthesis of the G0-$(CO_2{}^t Bu)_8$ dendrimer (scheme 6), it was obtained 4.66 g (3.02 mmol; 91% of yield) of the crude product as a yellowish oil, from 1.71 g (3.32 mmol) of G0-PAMAM. The product was characterized by ^{1}H-NMR (fig. 46a)) to confirm its identity and to identify the presence or absence of a solvent. From its analysis it was possible to conclude that MeOH (the solvent of the reaction, 3.479 ppm) is, often, not entirely removed by the rotatory evaporator and even under vacuum. A closer analysis revealed that the product was indeed the desired ester moiety with eight peripherals ester groups instead of the terminal primary amine groups of the starting dendrimer, although being still present vestigial amounts of unreacted *tert*-butyl acrylate that was in excess (see the red box in the fig. 46 a)). The structure of the dendrimer was confirmed by the presence of the three new groups of protons from the functionalized ester groups – μ, ε and θ – with adequate multiplicity and integration values. All the other typical group of protons of the core are also present likewise in G0-PAMAM. Nevertheless, it was necessary to purify the compound: it was performed a L-L extraction with hexane/9:1 MeOH: H_2O because of the differences in solubility of *tert*-butyl acrylate and the dendrimer. The *tert*-butyl acrylate is very

soluble in hexane, and the dendrimer is insoluble in this solvent but soluble in MeOH. The incorporation of water in the polar fraction was to decrease the solubility of tert-butyl acrylate in it (the solution that contains the dendrimer) by increasing the difference of polarity of the extraction solvents. The performed ^{1}H-NMR spectrum (fig. 46b)) of the purified compound has shown that the applied purification process was a success because of the absence of the typical signals for the *tert*-butyl acrylate. It was still needed to remove the traces of MeOH from the product. It was implemented a simple procedure: washing the dendrimer with few amounts of distilled water at a time and lyophilized it. The poor solubility of the ester dendrimer and the high solubility of MeOH in water should enhance the separation of the remaining MeOH from the dendrimer with this purifying step. It was needed to repeat this step. The final ^{1}H-NMR spectrum (fig. 46c)) have shown that finally the dendrimer was purified. It was obtained 4.46 g of it (2.89 mmol) with a good yield of 87%. The purified product was fully characterized by ^{13}C-NMR, FTIR, MS, COSY and HSQC. The obtained spectra are represented in figs. 47, 6A (in section 7.1.4. of attachment), 48, 49 and 50, respectively, with data summarized in tables 13 and 14. A closer analysis of the ^{1}H-NMR spectrum (fig. 46c)) have shown that the only signal that is not detected is the signal from the –NH of the amide ("e" signal) that is almost absent (red arrow). It is possible that the functionalization with the ester group interferes with the detection of this signal. One reason for this occurrence could be the increase of the molecular weight of the dendrimer because of the addition of the *tert*-butyl ester group in each "arm" that, possibly, enhance the conformational changes with the back folding of the molecule because of the probable hydrogen bonding between the protons of the amide groups and the oxygen from the ester groups (216).

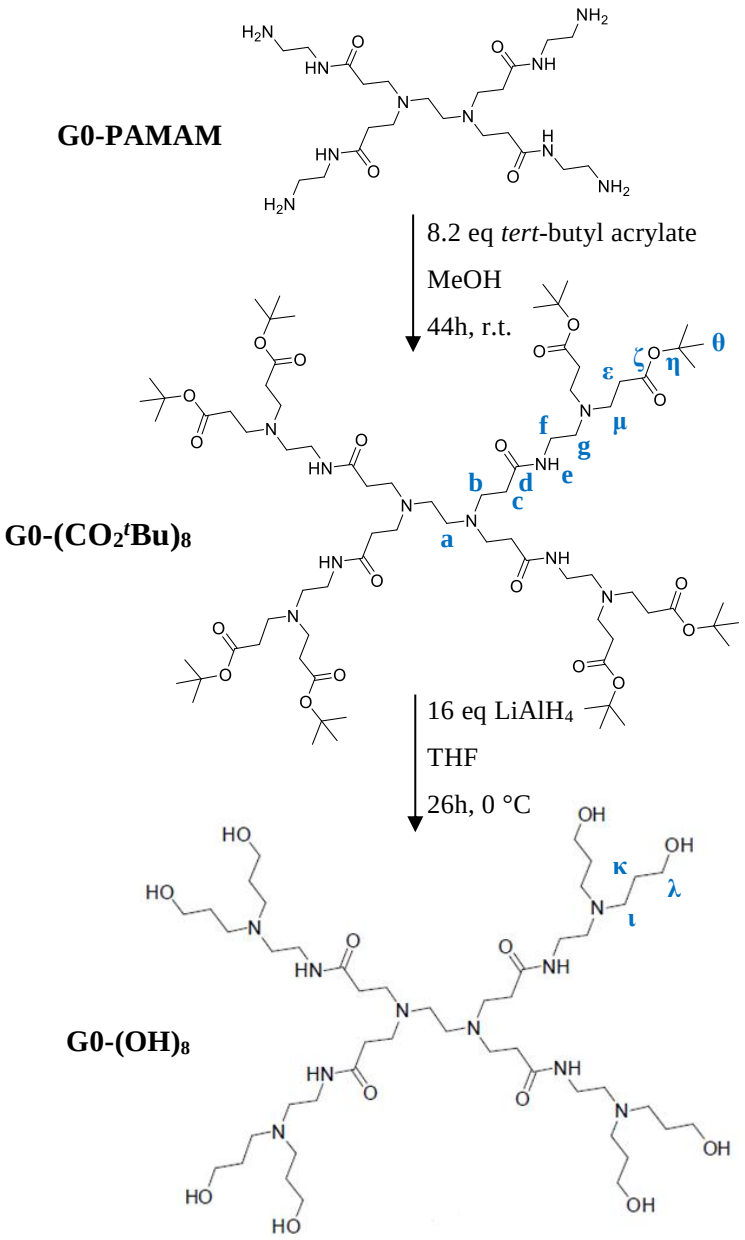

Scheme 6 - Synthetic routes for the preparation of G0-$(OH)_8$ dendrimer.

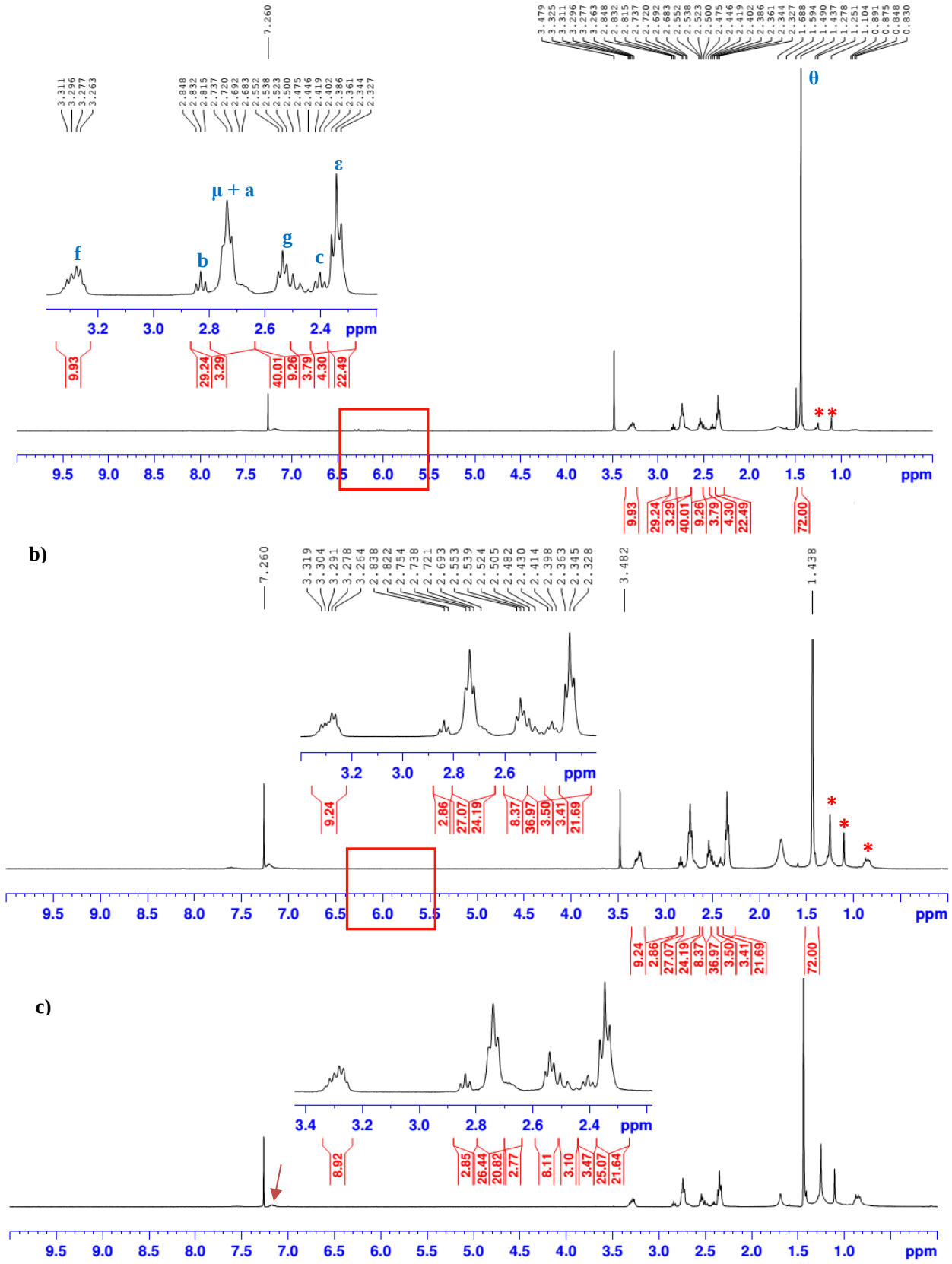

Figure 46 - ^{1}H-NMR spectrum of G0-(CO$_2$^{t}Bu)$_8$: a) crude, b) purified by the L-L extraction and c) washed by H_2O and lyophilized, in $CDCl_3$. Each signal is marked with the respective type of protons that are represented with a unique letter (see scheme 6). The red box point to the vestigial amounts of unreacted *tert*-butyl acrylate and the red stars represents the impurities of $CDCl_3$ (^{1}H-NMR in fig. 7A in attachment).

The protons represented by the letter "a" (N-CH_2-CH_2-N, see scheme 6), that usually appear with a chemical shift of 2.413 ppm in the G0-PAMAM (see table 1), possibly gave rise to a singlet with an integral of 4 that is overlapped with the μ signal between 2.683 and 2.737 ppm (the HSQC spectra, fig. 50, have confirmed this conclusion). These protons of the core are downfield shifted probably because of the abovementioned back folding of the molecule due to possible intramolecular interations – dipole-induced dipole – between the polar ester groups and the protons from the –CH_2 of the core. The integral sum of these two signals with the "b" signal is ≈ 28 (see fig. 46b) and table 13) which can include the eight "b" protons, the sixteen μ protons and the four "a" protons. In the ^{13}C-NMR spectra (fig. 47) was detected the quaternary carbons from the ester groups of the dendrimer: ζ and η signals (see in scheme 6); the typical molecular ion (≈ 1537 *m/z*) and the base peak (≈ 643 *m/z*) were identified in the MS spectra (fig. 48) and are similar to the expected values of ≈ 1541 and 639 *m/z*, respectively; the COSY and HSQC spectra (fig. 49 and 50, respectively) have confirmed its molecular structure, and the characteristic bands from the *tert*-butyl ester groups (1726 and 2977 cm^{-1}) was observed in the FTIR spectrum (table 14 and fig. 6A in attachment).

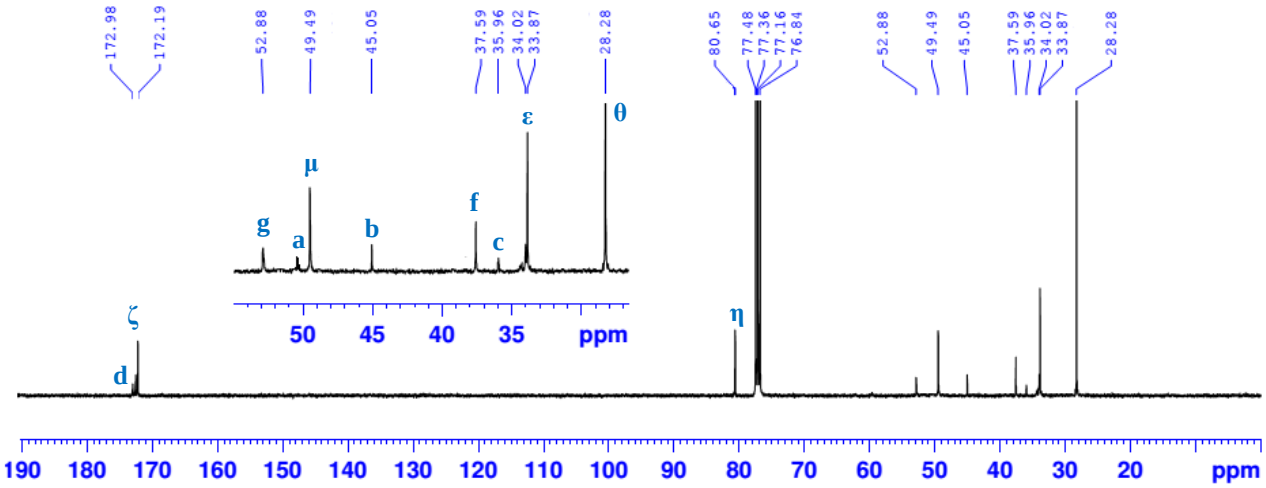

Figure 47 - ^{13}C-NMR spectrum of purified G0-$(CO_2{}^tBu)_8$, in $CDCl_3$. Each signal is marked with the respective type of carbons that are represented with a unique letter (see scheme 6).

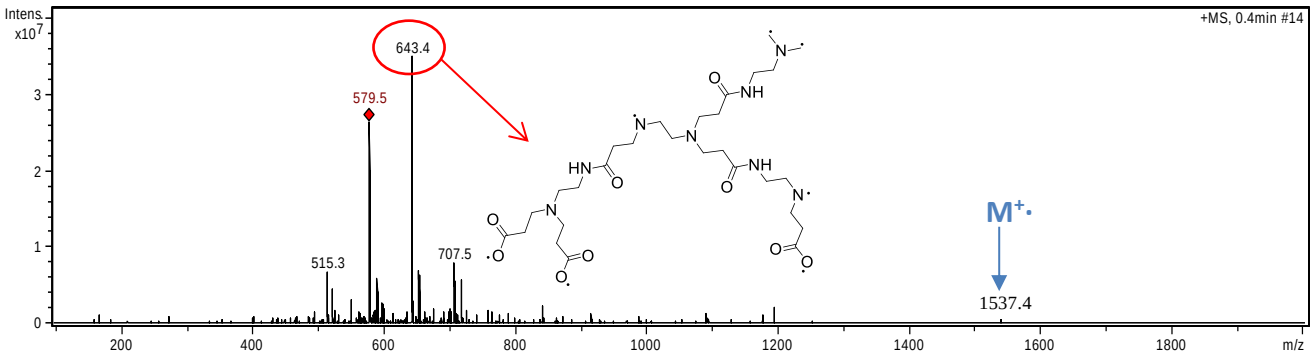

Figure 48 - +MS spectrum of purified G0-$(CO_2{}^tBu)_8$. The molecular ion ($M^+\cdot$) is represented in blue in the graphic area. The structure of the base peak (643.4 *m/z*) is also shown.

Table 13 - ^1H and ^{13}C-NMR data, of the corresponding spectra represented in figs. 46c) and 47 for the purified G0-$(CO_2{}^tBu)_8$, and in figs. 8Ab) and c) (in section 7.1.4. in attachment) for the purified G1-$(CO_2{}^tBu)_{16}$. $CDCl_3$ was the NMR solvent. The ^1H chemical shifts values are averages.

C atom	***^1H chemical shift (ppm)***		***Multiplicity***	***Integral***				***^{13}C chemical shift (ppm)***	
				Expected		***Obtained***			
	G0	***G1***		***G0***	***G1***	***G0***	***G1***	***G0***	***G1***
a	Overlapped by "μ"			4	4	*	*1	50.33	50.30
b	2.838	2.815	3	8	24	*	*1	45.05	45.02
c	2.405	2.406	3	8	24	#	#1	35.96	35.80
d	-		-	-		-		172.98	172.98
e	Not detectable							-	
f	3.290	3.303	m	8	24	9	25	37.59	37.57
g	2.541	2.538	3	8	24	8	24	52.88	52.77
μ	2.740	2.731	3	16	32	*	*1	49.49	49.41
ε	2.364	2.344	3	16	32	#	#1	33.87	33.83
ζ	-		-	-				172.19	172.26
η	-		-	-				80.65	80.68
θ	1.440	1.438	1	72	144	72	144	28.28	28.27

m: multiplet; *Sum of obtained integrals for "a", "b", "μ": 26; expected sum: 28; *1 - obtained sum: 60; expected sum: 60
#Sum of obtained integrals for "c" and "ε": 25; expected sum: 24; #1 - obtained sum: 57; expected sum: 56

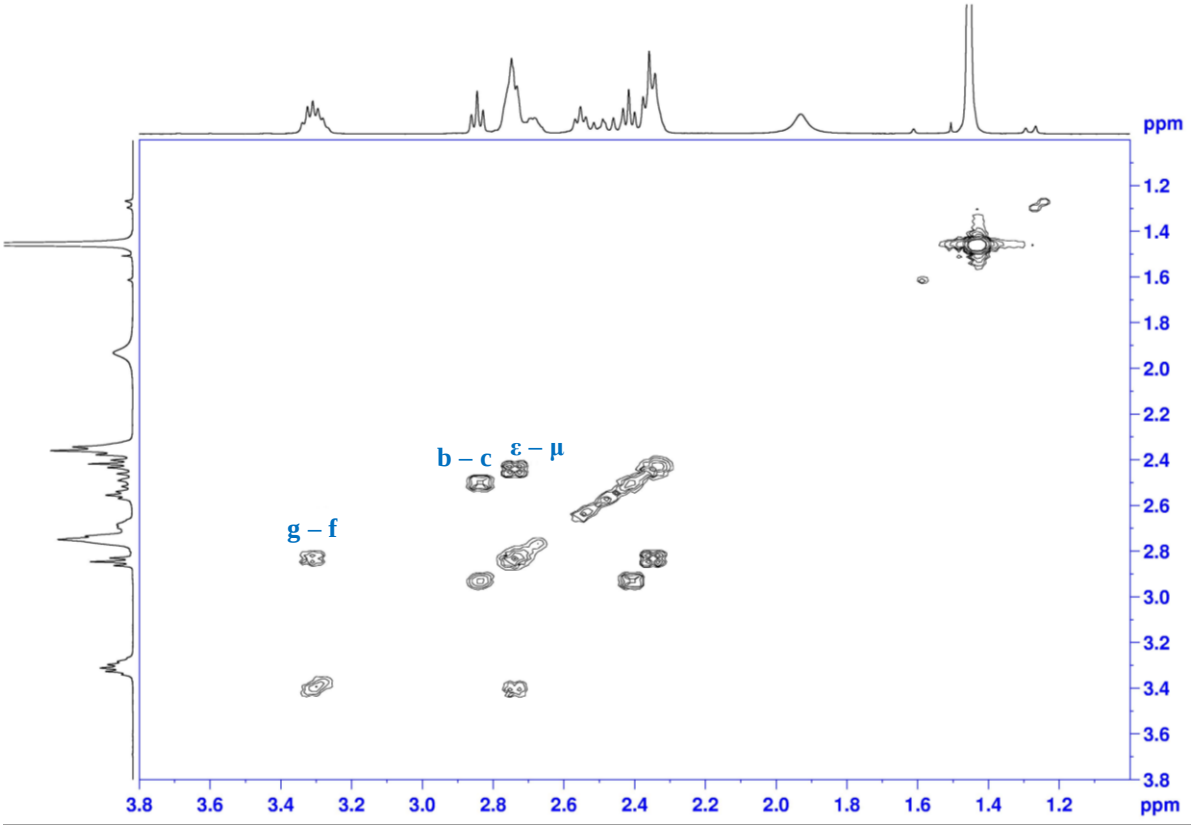

Figure 49 - COSY spectrum of purified G0-$(CO_2{}^tBu)_8$, in D_2O. Each signal is marked with the respective group of protons that are neighbours and linked to each other by a carbon bond. Each type of protons is represented with a unique letter (see scheme 6).

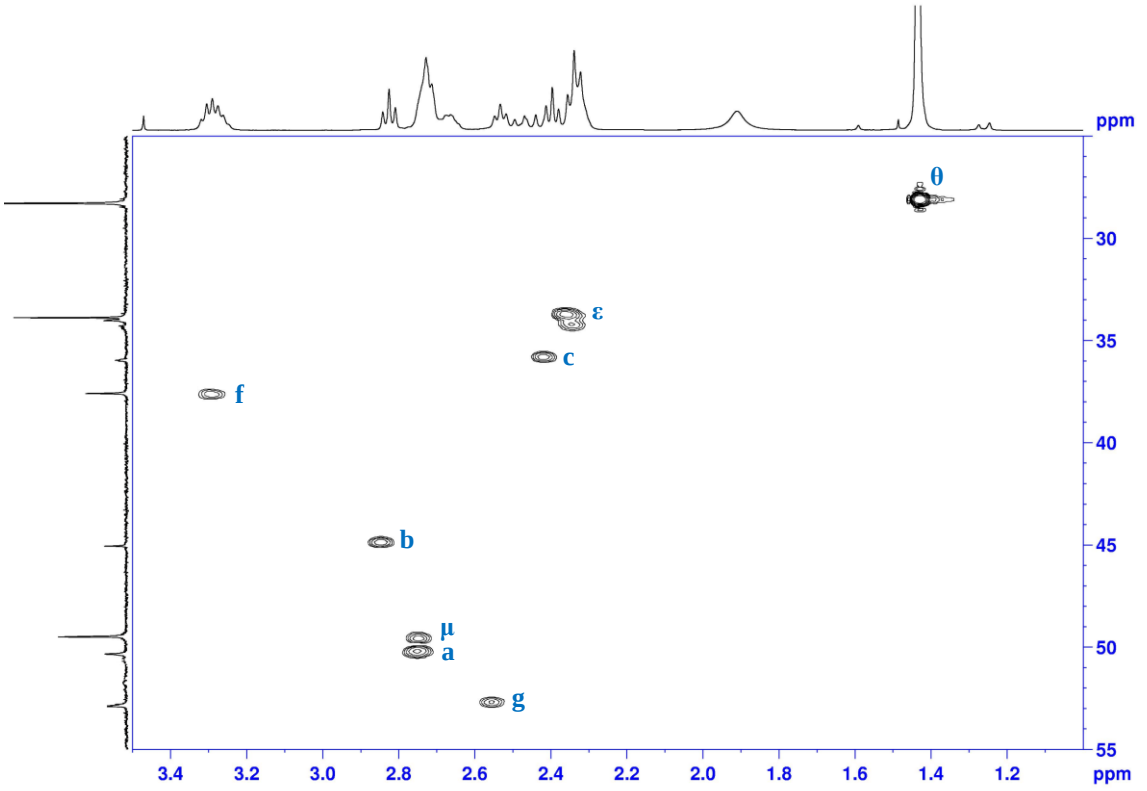

Figure 50 - HSQC spectrum of purified G0-$(CO_2{}^tBu)_8$, in D_2O. Each signal is marked with the respective type of protons and type of carbon they are directly linked with. Each type is represented with a unique letter (see scheme 6).

Table 14 - Main characteristic bands (cm^{-1}), obtained by FTIR, for each functional group of purified G0/G1-$CO_2{}^t$Bu. The type of vibration is also showed.

Functional group	*band (cm^{-1})*		*Type of vibration**
	G0	**G1**	
	3300	3297	str
C(=O)N–H	1551	1552	Comb C–N & N–H
	1461	1460	bend
C=O of the amide	1650	1651	str
–CO$_2{}^t$Bu	1726	1727	str
C–N	1039	1039	str
–CH$_3$	2977	2977	asym str
–CH$_2$ (acyclic)	2933	2934	asym str
–CH$_3$ or –CH$_2$ (acyclic)	2826	2830	sym str

*str: stretch; asym str: asymmetric stretch; sym str: symmetric stretch; comb: combination.

The preparation of the G0/G1-poly-hydroxyl dendrimers was accomplished by the reduction of the ester groups of the prepared G0/G1-$CO_2{}^t$Bu with $LiAlH_4$ as the reducing agent. The reduction is, in fact, a nucleophilic acyl substitution reaction in which H replaces –O*t*-Bu to give an aldehyde, which is further reduced to a primary alcohol by nucleophilic addition (mechanism of reaction in scheme 7). This intermediate reacts immediately and is not isolated because is much more reactive than the starting ester compound. The nucleophilic acyl substitution occurs on the carboxylate ion instead of the free carbonyl compound G0/G1-$CO_2{}^t$Bu to give a high-energy dianion intermediate because the hydride ion is a base as well as a nucleophile. In this intermediate, the two oxygens are certainly complexed to a Lewis acidic aluminum species (221, 222) .

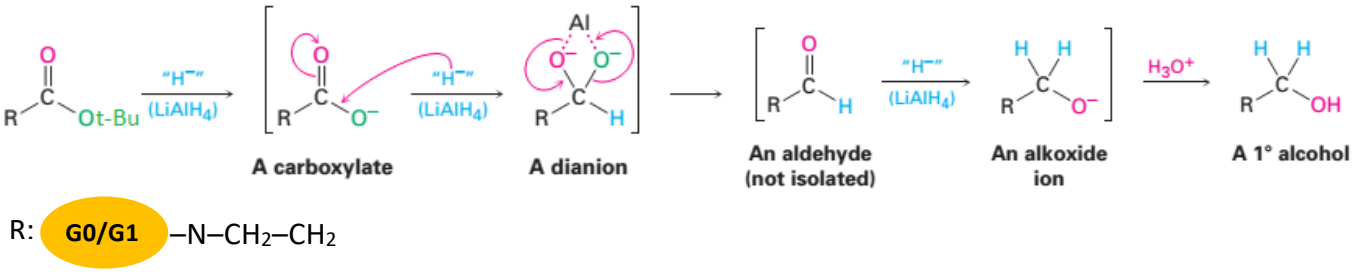

Scheme 7 - Mechanism of reaction of the reduction of the ester groups of G0/G1-$CO_2{}^t$Bu with $LiAlH_4$ to give the G0/G1-OH dendrimers (adapted from ref. (220)).

For the synthesis reaction of the G0-$(OH)_8$ dendrimer (scheme 6; fig. 51a)), it was used 3.63 g (2.35 mmol) of the previous prepared G0-$(CO_2{}^tBu)_8$, and it was obtained 2.14 g (2.18 mmol) of the desired hydroxyl dendrimer, as a light yellow spongy, sticky oil, with a very good yield of 93%. Nevertheless, this accomplishment was possible after the optimization of three reaction parameters: *a)* the eq. mol of $LiAlH_4$; *b)* the neutralization process of this reducing agent and *c)* the extraction of the obtained product with the adequate solvent. It was needed to increase the eq. mol of the reducing agent from 12 to 16 (8 eq. mol of excess); to quench the obtained reaction mixture with ice (fig. 51b)) instead of cold water; and to extract the obtained G0-$(OH)_8$ from the paste of the neutralized $LiAlH_4$ with distilled water with stirring, overnight. It was also important to do not use the plug of Celite® for the subsequent filtration to avoid the retention of product in it.

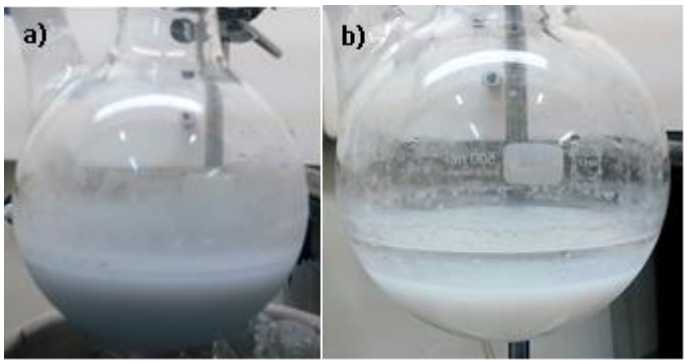

Figure 51 - Synthesis reaction of G0-$(OH)_8$: **a)** Grey suspension of the reaction mixture before neutralization of $LiAlH_4$; **b)** Settled white suspension of neutralized $LiAlH_4$.

In the past performed experiments the paste of neutralized $LiAlH_4$ was filtered, and the obtained solution of the product in THF (the solvent of the reaction) was dried. It was noticed that the G0-$(OH)_8$ could be synthesized but it was impure and the only discovered way to purified it was by dialysis. This method was not cost-effective because it was only possible to get yields of 9 to 19 % of the purified compound. It was needed to perform some solubility tests: the prepared hydroxyl dendrimer was highly soluble in H_2O and hardly solubilized in THF. Thus, with this simple outcome, it was possible to optimize the procedure. After the end of the reaction, the filtered solution was dried and analysed by ^{1}H-NMR (fig. 52a)). It was quickly noticed that this was the impure fraction of the product and it was obtained 168 mg (0.17 mmol; 7% of yield) of it as a dark yellow oil. The lyophilized light yellow spongy, sticky oil that corresponds to the pure fraction of the compound was characterized by ^{1}H, ^{13}C-NMR (data organized in table 15; figs. 52b) and c), respectively), COSY (fig. 53), HSQC (fig. 54), FTIR

(data in table 16; fig. 11A in section 7.1.5. of attachment) and MS (fig. 55). The ^1H and ^{13}C-NMR spectra shows the three signals of the functionalized hydroxyl groups ("ι", "κ" and "λ"; see scheme 6) with adequate integrations and multiplicities, besides all the other characteristics signals of the core. The COSY and HSQC spectra validate the structure of the dendrimer; in the FTIR spectrum were identified all the main characteristics bands, including the bands for the hydroxyl group of the surface: the stretching –OH (3676 cm^{-1}) and –COH (1061 cm^{-1}) and bands. The –OH band is sharp which indicates, accordingly to J. B. Lambert *et al*. (197) the absence of intramolecular hidrogens bonds. This fact (notwithstanding the abovementioned probable backfolding of the G0-$(CO_2{}^tBu)_8$) could explain the "open structure" that, normally, is expected in lower generations of PAMAM dendrimers, namely the generation 0, accordingly to the studies of P. K. Maiti *et al.* (220) obtained from extensive molecular dynamics (MD) simulations in explicit solvent . The C-N stretching band (of medium intensity) is not visible because is probably overlapped by the the strong band of –COH since they are detected in the same interval of frequencies. Finally, the exact mass of the dendrimer could be confirmed by the identification of the molecular ion (≈ 982 *m/z*) and the base peak (≈ 751 *m/z*) in the total fragmentation spectrum (fig. 55). These values are very similar to the expected values of ≈ 981 and 749 *m/z*, respectively.

Table 15 - ^1H and ^{13}C-NMR data, of the corresponding spectra represented in figs. 52 b) and c) for the pure fraction of G0-$(OH)_8$, and in figs. 12A b) and c) (section 7.1.5.) for G1-$(OH)_{16}$. D_2O was the NMR solvent. The ^1H chemical shifts values are averages.

C atom	*^1H chemical shift (ppm)*		*Multiplicity*	*Integral*				*^{13}C chemical shift (ppm)*	
				Expected		*Obtained*			
	G0	*G1*		*G0*	*G1*	*G0*	*G1*	*G0*	*G1*
a	Overlapped by "ι"			4	4	*	#	50.54	51.32
b	2.819	2.810	3	8	24	10	24	49.16	49.09
c	2.435	2.445	3	8	24	8	24	32.67	32.80
d	-		-	-		-		174.69	175.07
e	Not detectable							-	
f	3.334	3.345	4	8	24	8	24	36.47	36.46
g	2.715	2.718	3	8	24	*	#	51.59	51.70
ι	2.643	2.638	5	16	32	*	#	50.39	50.41
κ	1.752	1.741	5	16	32	16	33	27.99	28.01
λ	3.650	3.654	4	16	32	16	33	60.36	60.36

*Sum of obtained integrals for "a", "g" and "ι": 30; expected sum: 28. #Obtained sum: 60; expected sum: 60.

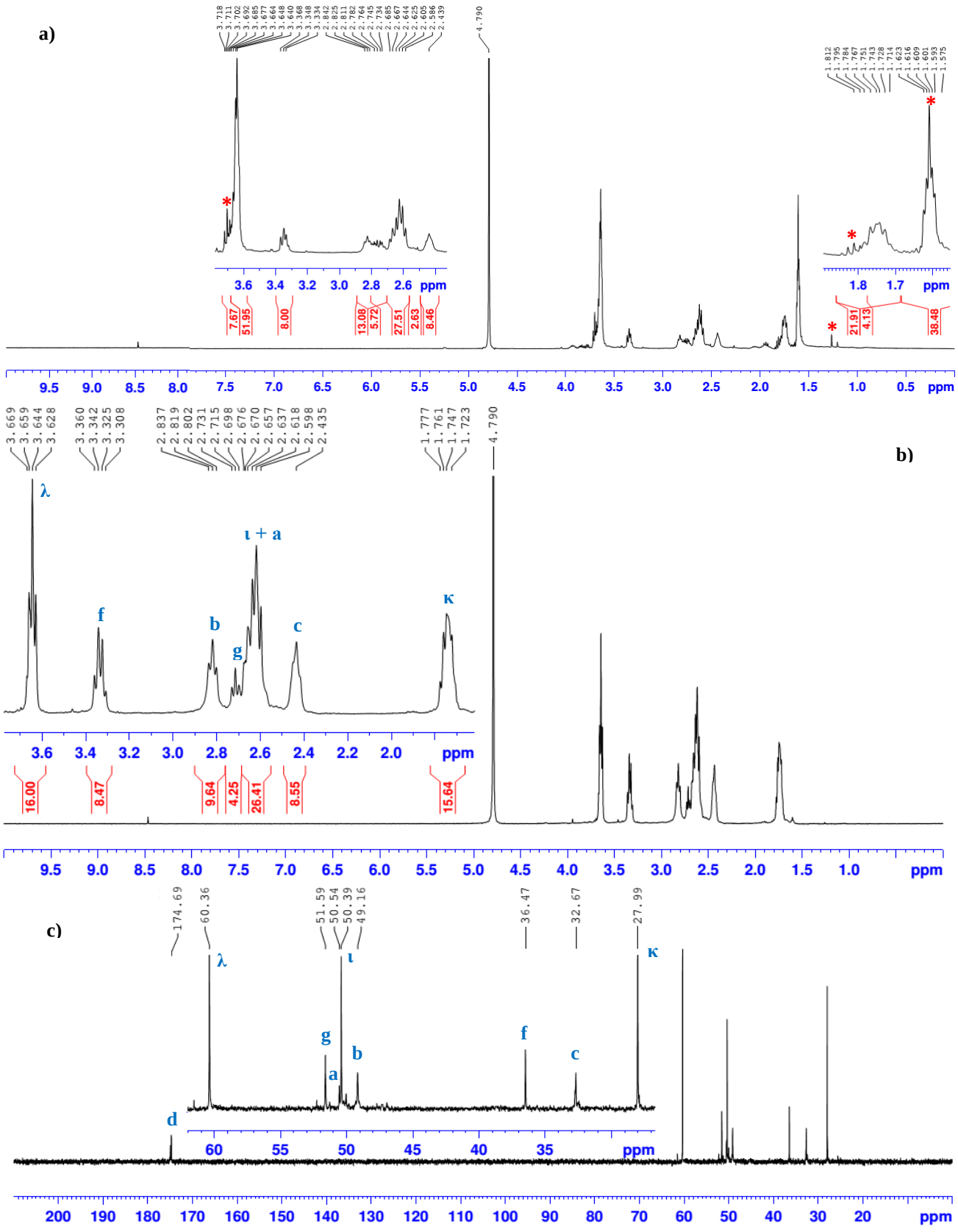

Figure 52 - NMR characterization of G0-(OH)$_8$: ^{1}H-NMR spectra of the a) impure fraction and b) pure fraction, and c) ^{13}C-NMR spectrum of the pure fraction, in D_2O. Each signal is marked with the respective type of protons that are linked to the corresponding carbon – they are represented with a unique letter (see scheme 6). The red stars represent the impurities on the not pure fraction.

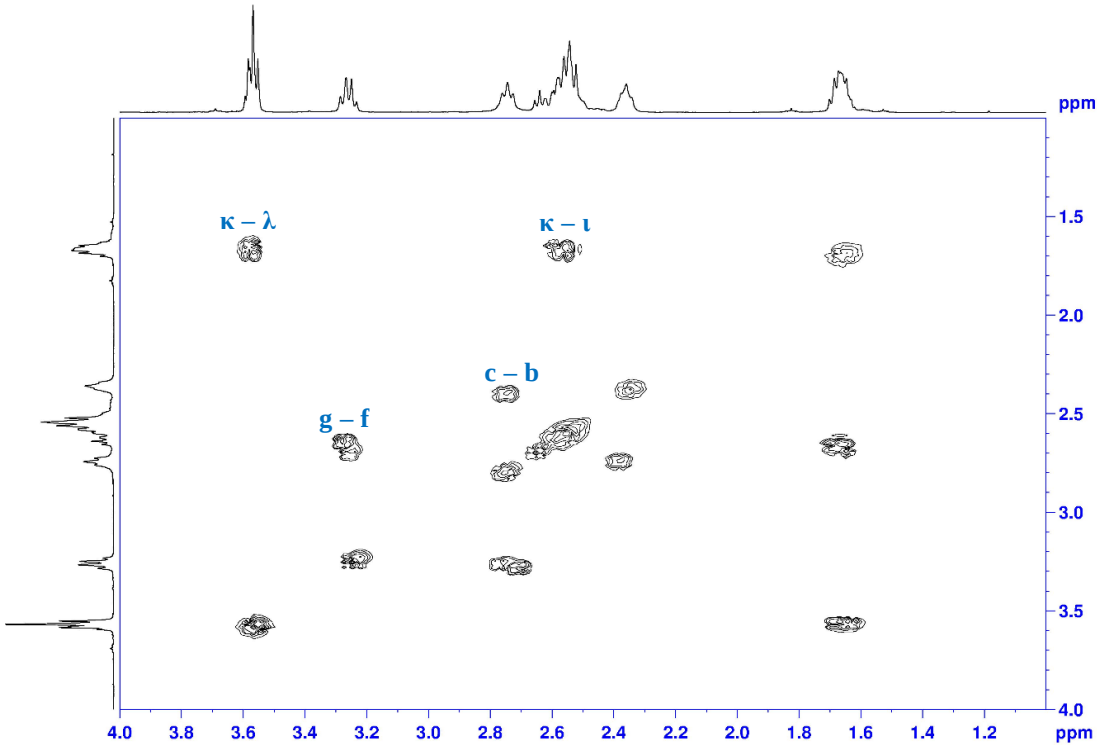

Figure 53 - COSY spectrum of the pure fraction of G0-$(OH)_8$, in D_2O. Each signal is marked with the respective group of protons that are neighbours and linked to each other by a carbon bond. Each type of protons is represented with a unique letter (see scheme 6).

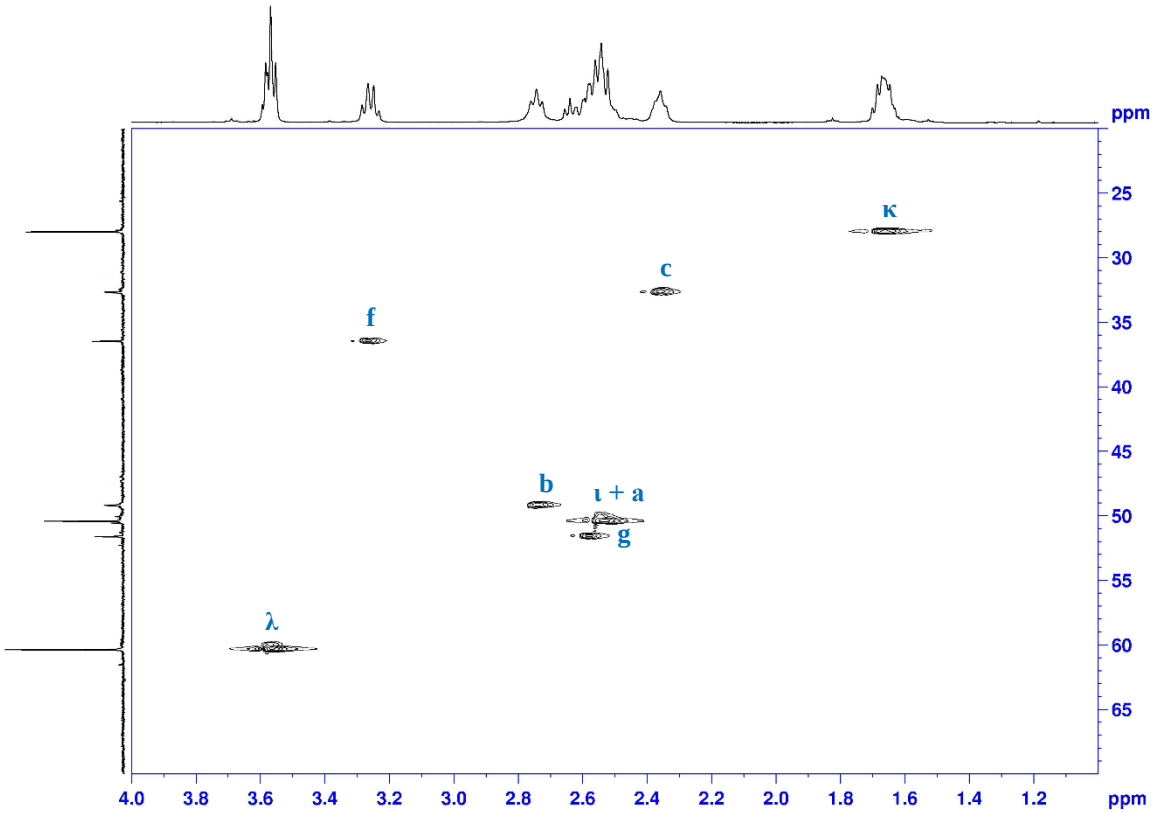

Figure 54 - HSQC spectrum of the pure fraction of G0-$(OH)_8$, in D_2O. Each signal is marked with the respective type of protons and type of carbon they are directly linked with. Each type is represented with a unique letter (see scheme 6).

Table 16 - Main characteristic bands (cm^{-1}), obtained by FTIR, for each functional group of the pure fraction of G0/G1-OH. The type of vibration is also showed.

Functional group	***band (cm^{-1})***		***Type of vibration****
	G0	**G1**	
C(=O)N–H	3284	Overlapped by O–H	str
	1463	1437	bend
	1557	1558	Comb C–N & N–H
C=O of the amide	1644	1634	str
O–H	3676 (sharp)	3432 (broad)	str
C–OH	1061	1058	str
–CH$_2$ (acyclic)	2942	2953	asym str
	2837	2851	sym str

*str: stretch; asym str: asymmetric stretch; sym str: symmetric stretch; comb: combination.

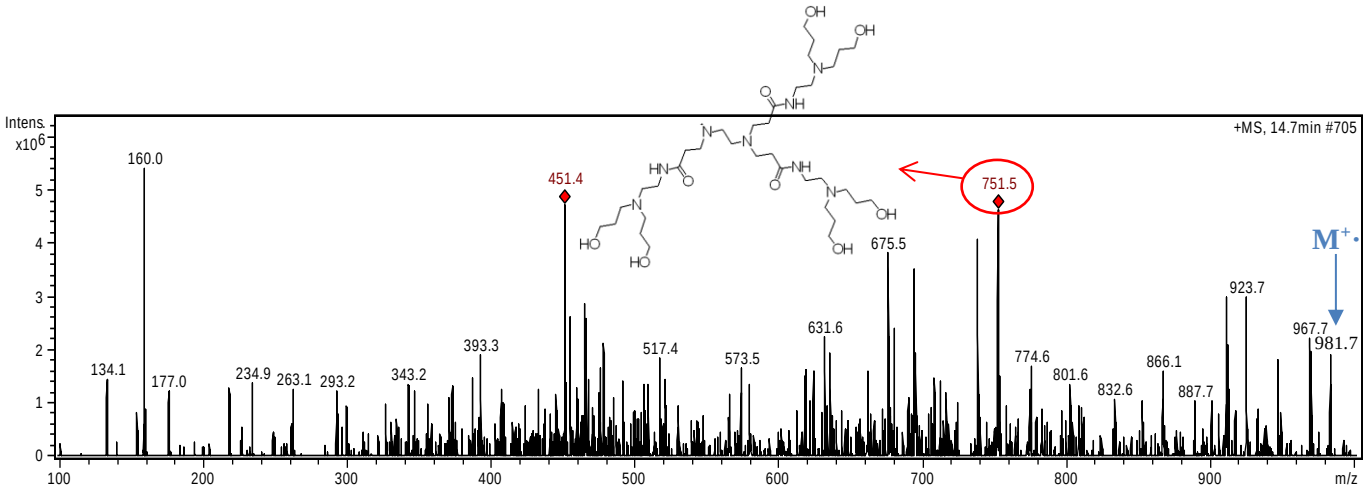

Figure 55 - +MS spectrum of the pure fraction of G0-(OH)$_8$. The molecular ion ($M^+\cdot$) is represented in blue in the graphic area. The structure of the base peak (751.5 *m/z*) is also shown.

The optimized synthesis of the ester and hydroxyl dendrimers from generation 0, open the way to the preparation of similar compounds but with higher generations. The G1-(CO$_2$^{t}Bu)$_{16}$ and G1-(OH)$_{16}$ were prepared as it is indicated in scheme 8.

G1-PAMAM

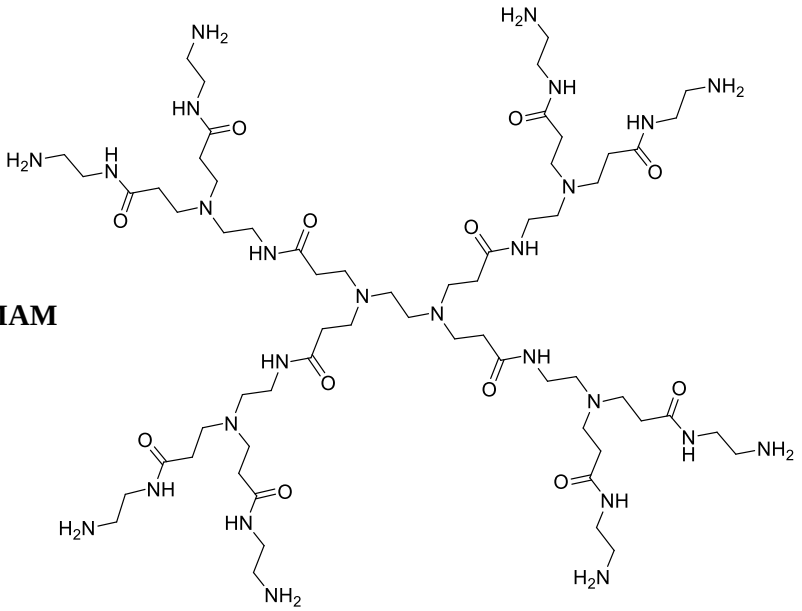

16.2 eq *tert*-butyl acrylate
MeOH
44h, r.t.

G1-$(CO_2{}^tBu)_{16}$

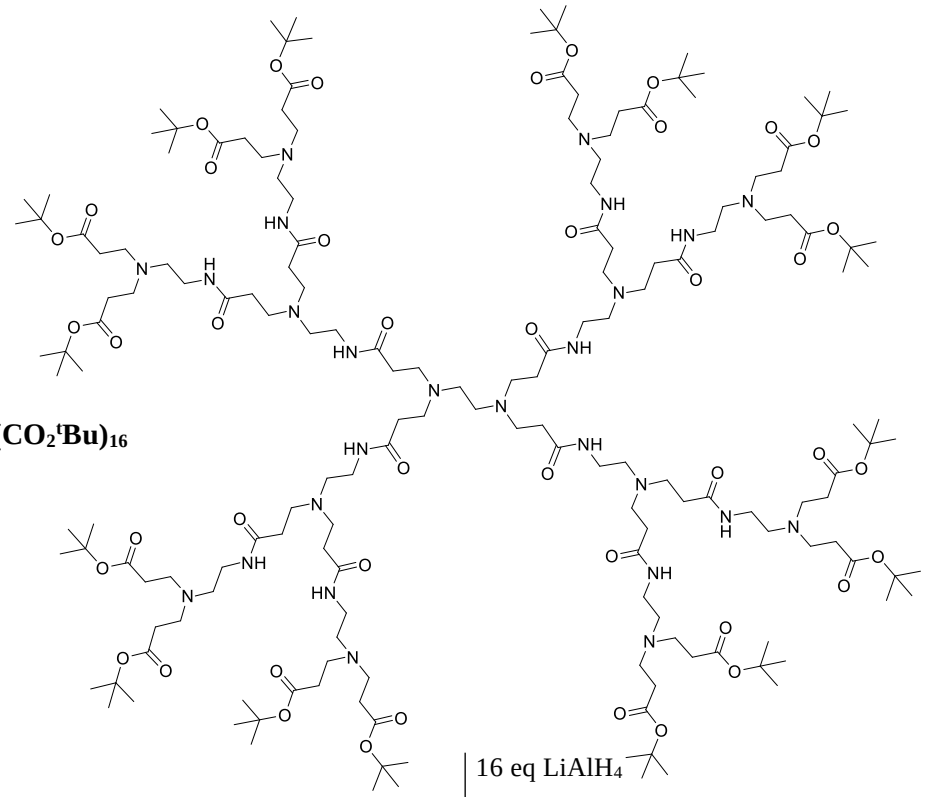

16 eq $LiAlH_4$
THF
26h, 0 °C

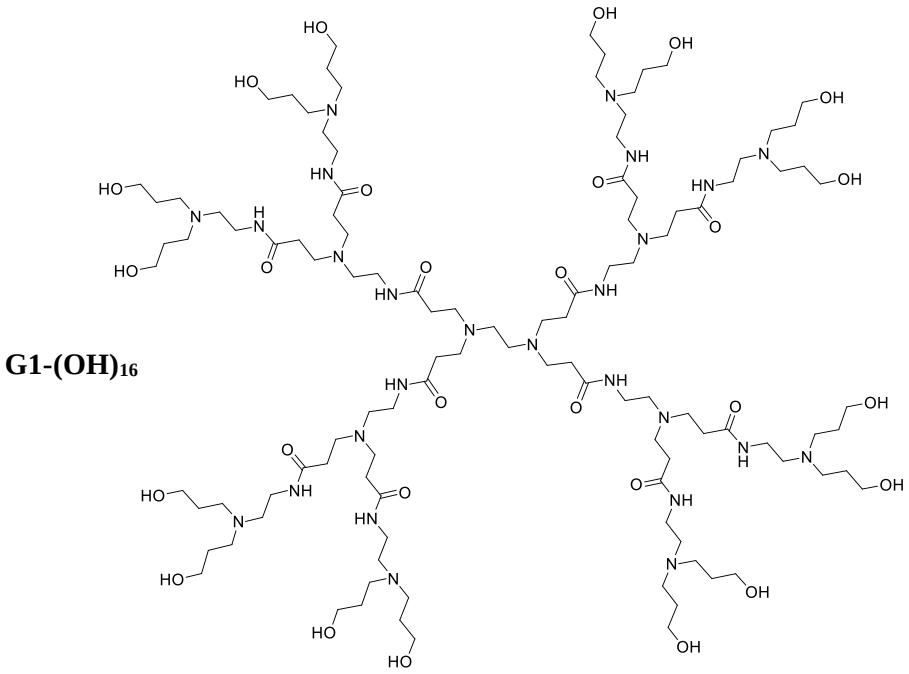

Scheme 8 - Synthetic routes for the preparation of G1-$(OH)_{16}$ dendrimer.

From 2.98 g (2.09 mmol) of G1-PAMAM (golden oil), it was obtained 6.25 g (1.80 mmol) of crude G1-$(CO_2{}^tBu)_{16}$, like a dark yellow oil, with 86 % of yield. The corresponding ^{1}H-NMR is represented in fig. 8Aa) (in section 7.1.4. in attachment). The spectrum is very similar to the one obtained for G0-$(CO_2{}^tBu)_8$ (fig. 46a)), as it was already expected, because of the equivalence of the group of atoms. The only difference is the integration values that increases with the increase of the generation number (see table 13). After being purified, it was obtained 6.03 g (1.73 mmol) of the G1-ester dendrimer with a good 83 % of yield. The ^{1}H, ^{13}C-NMR, COSY, HSQC and FTIR spectra of this purified compound are represented in figs. 8Ab), c) (data organized in table 13); 9A, 10A and 6A (data organized in table 14), respectively.

It was prepared 2.62 g (1.11 mmol) of "pure" G1-$(OH)_{16}$, as a yellow spongy, sticky oil, with a good yield of 89 %, from 4.35 g (1.25 mmol) of G1-$(CO_2{}^tBu)_{16}$. Firstly, it was obtained 354 mg (0.15 mmol; 11 % of yield) of an impure fraction of the product. From the performed ^{1}H-NMR (fig. 12Aa) in section 7.1.5. in attachment) it was already possible to conclude that the synthesis reaction was a success because of the similarity with the ^{1}H-NMR of the G0-$(OH)_8$ (fig. 52a)) and the adequate integration values of each signal. Thus, the "pure" G1-hydroxyl dendrimer was fully characterized by ^{1}H, ^{13}C-NMR (fig. 12Ab), c), respectively), COSY (fig. 13A), HSQC (fig. 14A) and FTIR (fig. 11A) spectroscopic methods and the obtained results were similar to the compound of generation 0 (see tables 15 and 16 and compare the spectra).

The only encountered differences was observed in the FTIR spectrum where the –OH stretching band, that is broad (in contrast with the sharp band observed for G0-$(OH)_8$), suffered a shift for lower frequencies (3432 cm^{-1} for G1-hydroxyl and 3676 cm^{-1} for G0). According to J. B. Lambert *et al*. (197), the broad –OH band when observed in the interval of 3400-3600 cm^{-1} is involved in intramolecular hydrogen bonds. In fact, it was expected that this type of interactions was present in the G1-$(OH)_{16}$ dendrimer due to the increase number of hydroxyl groups at the "surface" with the increase of the generation number. The bonds of the core become more stretched and the high volume of the periphery explains this structural behaviour. This fact is supported by the findings of P. K. Maiti *et al.* (220) that were already mentioned in the discussion of the results obtained for the G1-$(CNRuCp(PPh)_3)_8(CF_3SO_3)_8$.

PART III – CONCLUSIONS AND FUTURE PERSPECTIVES

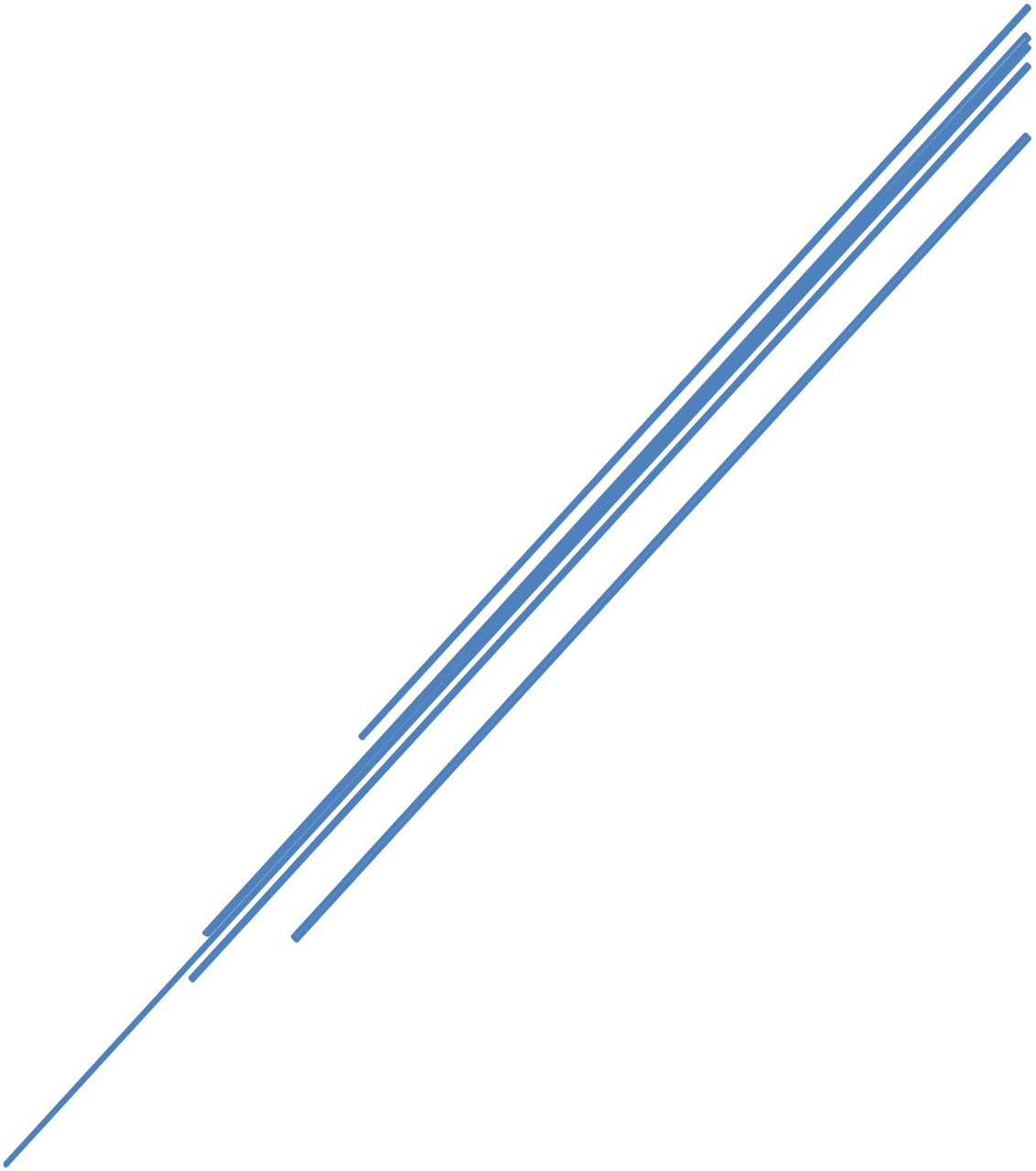

6. CONCLUSIONS

In this work, a series of new functionalized low generation PAMAM dendrimers – G0/G1-CN, G0/G1-(CNRu(η^5-C_5H_5)(PPh_3)$_2$)$_x$(CF_3SO_3)$_x$, G0/G1-$CO_2{}^t$Bu and G0/G1-OH – were successfully synthesized with good yields (77% – 94%) and characterized by NMR (^{1}H, ^{13}C, ^{31}P, COSY, HSQC) and FTIR spectroscopic techniques. The polynitrile PAMAM dendrimers (G0-$(CN)_4$ and G1-$(CN)_8$) was used as scaffolds for the preparation of new cationic ruthenium (II) cyclopentadienyl metallodendrimers from generation 0 (G0-(CNRu(η^5-C_5H_5)(PPh_3)$_2$)$_4$(CF_3SO_3)$_4$) and 1 (G1-(CNRu(η^5-C_5H)(PPh_3)$_2$)$_8$). They were obtained with good yields of 79% and 77%, respectively, from the reaction of the organometallic moiety [Ru(η^5-C_5H_5)(PPh_3)$_2$Cl] (also prepared with 54% of yield) with the organic core (with silver triflate as the chloride abstractor). The spectroscopic data lead to the conclusion that these two compounds were completely functionalized with the ruthenium cyclopentadienyl moieties equivalently coordinated to the core in a tetra- (for generation 0) and octa-coordination manner (for generation 1). Additionally, it was also possible to observe a strong evidence for the existence of intramolecular non-covalent interactions within these molecules that have influenced the optimization of the synthetic procedure and, mainly their structural arrangement. The most frequent type of interactions appears to be arene-arene between the aromatic π-systems (cyclopentadienyl and phenyl rings), π-hydrogen bonds between these aromatic rings and the protons from the amide and secondary amine groups of the organic scaffold and dipole-dipole interactions directly between the metal and the partial negative charge of these functional groups. This last hypothesis predicts a new type of interaction between the ruthenium and organic molecules that is not yet reported in the literature and, thus, demands more studies – such as, for example, elemental analysis and MS which are ongoing. Another hypothesis, that is supported by the spectroscopic data, is that the ruthenium metallodendrimer from generation 1 probably exhibit a reduced number of dipole-dipole interactions, when compared with the generation 0, because of the increase of the periphery volume and the "protection" of the core.

This novel metallodendrimers based on PAMAM cores has emerged from the previous work that was done by our group with poly(alkylidenamine) dendrimers and belongs to a scarce family of cationic ruthenium metallodendrimers that was prepared through coordination of the nitrile groups of the organic cores with the metal. These compounds are currently under *in vitro* studies for anticancer applications.

Regarding the poly-hydroxyl (G0/G1-OH) PAMAM dendrimers they were also successfully synthesized and characterized by NMR (^{1}H, ^{13}C, COSY, HSQC) and FTIR spectroscopic techniques. The G0-$(OH)_8$ and G0-$(CO_2{}^t Bu)_8$ dendrimers were also characterized by MS. They were prepared through a synthetic sequence that begun with an N-alkylation of the PAMAM surface amine groups that lead to the synthesis of the poly-ester dendrimers (G0-$(CO_2{}^t Bu)_8$ and G1-$(CO_2{}^t Bu)_{16}$) with very good yields – 87% for G0 and 83% for G1. In turn, the reduction of its ester groups lead to preparation of the hydroxyl dendrimers once again with attractive yields of 93% and 89% for generation 0 and 1, respectively. The obtained spectroscopic data have confirmed the adequate functionalization of each compound and the probable existence of surface intramolecular hydrogen bonds for the G1-$(OH)_{16}$ dendrimer. Thus, these new organic molecules are attractive scaffolds for the future preparation of a new family of ruthenium cyclopentadienyl metallodendrimers having acetylene groups as terminals, acting as a bridge between the organometallic moiety and the dendrimer scaffold.

The achieved success of this work was only possible through optimization tests that have involved different parameters: type and quantity of solvent, molar equivalents, time of reaction, temperature, the need of catalysts and purification procedures. However, all the spent time and effort revealed to be worth it at the end since the final compounds were prepared and purified with relatively easy, quick and cost-effective procedures. Therefore, this work confirms the versatility of using PAMAM dendrimers as a building block for the preparation of a variety of dendrimers with different surface groups, including nitrile derivatives as scaffolds for the preparation of ruthenium metallodendrimers.

7. FUTURE PERSPECTIVES

The suggested future perspectives of this work are the following:

- Characterize by MS the ruthenium metallodendrimers and the G0/G1-CN, G1-$(CO_2{}^tBu)_{16}$ and G1-$(OH)_{16}$ dendrimers;
- Characterize all the dendrimers by elemental analysis;
- Because the stability of the compounds is extremely important for biomedical applications, it is needed to perform stability tests of the prepared metallodendrimers in similar solutions of the biological assays, with different pH values in physiological temperature (37ºC);
- Synthesize the generation 2 of the prepared metallodendrimers: G2-(**CN**Ru(η^5-C_5H_5)$(PPh_3)_2)_{16}(CF_3SO_3)_{16}$ in order to evaluate the existence of intramolecular non-covalent interactions between the ruthenium moieties and the organic core and compare this results with the already prepared compounds of lower generations;
- Perform cytotoxic studies in several cancer cell lines to determine the anticancer activity of the prepared metallodendrimers in comparison with *cisplatin*;
- Apply a synthetic strategy to prepare novel acetylide ruthenium-based metallodendrimers (G0/G1-(CCRu(η^5-C_5H_5)$(PPh_3)_2)_x(CF_3SO_3)_x$) with the same organic cores than the prepared nitrile-based metallodendrimers G0/G1-(CNRu(η^5-C_5H_5)$(PPh_3)_2)_x(CF_3SO_3)_x$ in order to compare their anticancer activities.

As it is distinguished, a lot of work is forecasted for these new family of ruthenium (II) cyclopentadienyl metallodendrimers to considered them, in the future, potential anticancer agents. Although long, it is also forecasted an exciting and enthusiastic journey!

8. REFERENCES

1. Krishna TR, Jayaraman N. Synthesis of Poly(propyl ether imine) Dendrimers and evaluation of their cytotoxic properties. The Journal of Organic Chemistry. 2003;68(25):9694-704.

2. Jayamurugan G, Jayaraman N. Synthesis of large generation poly(propyl ether imine) (PETIM) dendrimers. Tetrahedron. 2006;62(41):9582-8.

3. Lainé A-L, Passirani C. Novel metal-based anticancer drugs: a new challenge in drug delivery. Current Opinion in Pharmacology. 2012;12(4):420-6.

4. Van Rijt SH, Sadler PJ. Current applications and future potential for bioinorganic chemistry in the development of anticancer drugs. Drug Discovery Today. 2009;14(23–24):1089-97.

5. Bruijnincx PCA, Sadler PJ. New trends for metal complexes with anticancer activity. Current Opinion in Chemical Biology. 2008;12(2):197-206.

6. Organization WH. Cancer - Fact sheet 2017 [updated February 10, 2017]. Available from: http://www.who.int/mediacentre/factsheets/fs297/en/.

7. Stewart BWKP, Wild CP. World cancer report 2014. Health. 2017.

8. Miller KD, Siegel RL, Lin CC, Mariotto AB, Kramer JL, Rowland JH, et al. Cancer treatment and survivorship statistics, 2016. CA: a Cancer Journal for Clinicians. 2016;66(4):271-89.

9. Siegel RL, Miller KD, Jemal A. Cancer statistics, 2016. CA: a Cancer Journal for Clinicians. 2016;66(1):7-30.

10. Marques MPM. Platinum and palladium polyamine complexes as anticancer agents: the structural factor. International Scholalry Research Notices Spectroscopy. 2013;2013:1-29.

11. Köpf H, Köpf-Maier P. Titanocene dichloride—the first metallocene with cancerostatic activity. Angewandte Chemie International Edition in English. 1979;18(6):477-8.

12. Jung Y, Lippard SJ. Direct cellular responses to platinum-induced DNA damage. Chemical Reviews. 2007;107(5):1387-407.

13. Hambley TW. Metal-based therapeutics. Science. 2007;318(5855):1392-3.

14. Dasari S, Tchounwou PB. Cisplatin in cancer therapy: molecular mechanisms of action. European Journal of Pharmacology. 2014;740:364-78.

15. Rosenberg B, Vancamp L. Platinum compounds: a new class of potent antitumour agents. Nature. 1969;222:385-6.

16. Prestayko AW, d'Aoust J, Issell B, Crooke S. Cisplatin (cis-diamminedichloroplatinum II). Cancer Treatment Reviews. 1979;6(1):17-39.

17. Kelland L. The resurgence of platinum-based cancer chemotherapy. Nature Reviews Cancer. 2007;7(8):573-84.

18. Tattersall MHN. Ovarian cancer chemotherapy: carboplatin as standard. The Lancet. 2002;360(9332):500-1.

19. André T, Boni C, Mounedji-Boudiaf L, Navarro M, Tabernero J, Hickish T, et al. Oxaliplatin, fluorouracil, and leucovorin as adjuvant treatment for colon cancer. New England Journal of Medicine. 2004;350(23):2343-51.

20. De Jongh F, Van Veen R, Veltman S, de Wit R, Van der Burg M, Van den Bent M, et al. Weekly high-dose cisplatin is a feasible treatment option: analysis on prognostic factors for toxicity in 400 patients. British Journal of Cancer. 2003;88(8):1199-206.

21. Al-Majed AA. Carnitine deficiency provokes cisplatin-induced hepatotoxicity in rats. Basic & Clinical pharmacology & Toxicology. 2007;100(3):145-50.

22. Florea AM, Büsselberg D. Cisplatin as an anti-tumor drug: cellular mechanisms of activity, drug resistance and induced side effects. Cancers. 2011;3:1351-71.

23. Shen D-W, Pouliot LM, Hall MD, Gottesman MM. Cisplatin resistance: a cellular self-defense mechanism resulting from multiple epigenetic and genetic changes. Pharmacological Reviews. 2012;64(3):706-21.

24. Galluzzi L, Vitale I, Michels J, Brenner C, Szabadkai G, Harel-Bellan A, et al. Systems biology of cisplatin resistance: past, present and future. Cell Death and Disease. 2014;5:e1257.

25. Gatzemeier U, Groth G, Butts C, Van Zandwijk N, Shepherd F, Ardizzoni A, et al. Randomized phase II trial of gemcitabine–cisplatin with or without trastuzumab in HER2-positive non-small-cell lung cancer. Annals of Oncology. 2004;15(1):19-27.

26. Gatzemeier U, Pluzanska A, Szczesna A, Kaukel E, Roubec J, De Rosa F, et al. Phase III study of erlotinib in combination with cisplatin and gemcitabine in advanced non–small-cell lung cancer: The Tarceva Lung Cancer Investigation Trial. Journal of Clinical Oncology. 2007;25(12):1545-52.

27. Kindler HL, Karrison TG, Gandara DR, Lu C, Krug LM, Stevenson JP, et al. Multicenter, double-blind, placebo-controlled, randomized phase II trial of gemcitabine/cisplatin plus bevacizumab or placebo in patients with malignant mesothelioma. Journal of Clinical Oncology. 2012;30(20):2509-15.

28. Pages BJ, Sakoff J, Gilbert J, Zhang Y, Li F, Preston D, et al. Investigating the cytotoxicity of platinum(II) complexes incorporating bidentate pyridyl-1,2,3-triazole "click" ligands. Journal of Inorganic Biochemistry. 2016;165:92-9.

29. Li J, Hu X, Liu M, Hou J, Xie Z, Huang Y, et al. Complex of cisplatin with biocompatible poly (ethylene glycol) with pendant carboxyl groups for the effective treatment of liver cancer. Journal of Applied Polymer Science. 2014;131(18).

30. van Rijt SH, Peacock AF, Johnstone RD, Parsons S, Sadler PJ. Organometallic osmium (II) arene anticancer complexes containing picolinate derivatives. Inorganic Chemistry. 2009;48(4):1753-62.

31. Peacock AF, Sadler PJ. Medicinal organometallic chemistry: designing metal arene complexes as anticancer agents. Chemistry–An Asian Journal. 2008;3(11):1890-9.

32. Chen J, Li J, Qian L, Zheng K. Electronic structures and SARs of the isomeric complexes α-, β-, γ-$[Ru(mazpy)_2Cl_2]$ with different antitumor activities. Journal of Molecular Structure. 2005;728(1):93-101.

33. Hotze AC, Caspers SE, de Vos D, Kooijman H, Spek AL, Flamigni A, et al. Structure-dependent in vitro cytotoxicity of the isomeric complexes $[Ru(L)_2Cl_2]$(L=*o*-tolylazopyridine and 4-methyl-2-phenylazopyridine) in comparison to $[Ru(azpy)_2Cl_2]$. Journal of Biological Inorganic Chemistry. 2004;9(3):354-64.

34. Chen H, Parkinson JA, Nováková O, Bella J, Wang F, Dawson A, et al. Induced-fit recognition of DNA by organometallic complexes with dynamic stereogenic centers. Proceedings of the National Academy of Sciences. 2003;100(25):14623-8.

35. Chen H, Parkinson JA, Parsons S, Coxall RA, Gould RO, Sadler PJ. Organometallic ruthenium (II) diamine anticancer complexes: arene-nucleobase stacking and stereospecific hydrogen-bonding in guanine adducts. Journal of the American Chemical Society. 2002;124(12):3064-82.

36. Aird R, Cummings J, Ritchie A, Muir M, Morris R, Chen H, et al. In vitro and in vivo activity and cross resistance profiles of novel ruthenium (II) organometallic arene complexes in human ovarian cancer. British Journal of Cancer. 2002;86(10):1652-7.

37. Galanski M, Arion V, Jakupec M, Keppler B. Recent developments in the field of tumor-inhibiting metal complexes. Current Pharmaceutical Design. 2003;9(25):2078-89.

38. Bindoli A, Rigobello MP, Scutari G, Gabbiani C, Casini A, Messori L. Thioredoxin reductase: a target for gold compounds acting as potential anticancer drugs. Coordination Chemistry Reviews. 2009;253(11):1692-707.

39. Sergeant CD, Ott I, Sniady A, Meneni S, Gust R, Rheingold AL, et al. Metallo-nucleosides: synthesis and biological evaluation of hexacarbonyl dicobalt 5-alkynyl-2′-deoxyuridines. Organic & Biomolecular Chemistry. 2008;6(1):73-80.

40. Saggioro D, Rigobello MP, Paloschi L, Folda A, Moggach SA, Parsons S, et al. Gold (III)-dithiocarbamato complexes induce cancer cell death triggered by thioredoxin redox system inhibition and activation of ERK pathway. Chemistry & Biology. 2007;14(10):1128-39.

41. Meggers E, Atilla-Gokcumen GE, Bregman H, Maksimoska J, Mulcahy SP, Pagano N, et al. Exploring chemical space with organometallics: ruthenium complexes as protein kinase inhibitors. Synlett. 2007;2007(08):1177-89.

42. Jakupec MA, Keppler BK. Gallium in cancer treatment. Current Topics in Medicinal Chemistry. 2004;4(15):1575-83.

43. Che CM, Sun RWY, Yu WY, Ko CB, Zhu N, Sun H. Gold(III) porphyrins as a new class of anticancer drugs: cytotoxicity, DNA binding and induction of apoptosis in human cervix epitheloid cancer cells. Chemical Communications. 2003(14):1718-9.

44. Nguyen A, Top S, Pigeon P, Vessières A, Hillard EA, Plamont MA, et al. Synthesis and structure–activity relationships of ferrocenyl tamoxifen derivatives with modified side chains. Chemistry–A European Journal. 2009;15(3):684-96.

45. Ernst RJ, Song H, Barton JK. DNA mismatch binding and antiproliferative activity of rhodium metalloinsertors. Journal of the American Chemical Society. 2009;131(6):2359-66.

46. Dougan SJ, Habtemariam A, McHale SE, Parsons S, Sadler PJ. Catalytic organometallic anticancer complexes. Proceedings of the National Academy of Sciences. 2008;105(33):11628-33.

47. Failes TW, Cullinane C, Diakos CI, Yamamoto N, Lyons JG, Hambley TW. Studies of a cobalt (III) complex of the MMP inhibitor marimastat: a potential hypoxia-activated prodrug. Chemistry–A European Journal. 2007;13(10):2974-82.

48. Cordier C, Pierre VC, Barton JK. Insertion of a bulky rhodium complex into a DNA cytosine− cytosine mismatch: an NMR solution study. Journal of the American Chemical Society. 2007;129(40):12287-95.

49. Hillard E, Vessières A, Thouin L, Jaouen G, Amatore C. Ferrocene-mediated proton-coupled electron transfer in a series of ferrocifen-type breast-cancer drug candidates. Angewandte Chemie International Edition. 2006;45(2):285-90.

50. Reedijk J. Metal-ligand exchange kinetics in platinum and ruthenium complexes. Platinum Metals Review. 2008;52(1):2-11.

51. Bergamo A, Gaiddon C, Schellens JHM, Beijnen JH, Sava G. Approaching tumour therapy beyond platinum drugs: status of the art and perspectives of ruthenium drug candidates. Journal of Inorganic Biochemistry. 2012;106(1):90-9.

52. Clarke M, Bitler S, Rennert D, Buchbinder M, Kelman A. Reduction and subsequent binding of ruthenium ions catalyzed by subcellular components. Journal of Inorganic Biochemistry. 1980;12(1):79-87.

53. Frasca D, Ciampa J, Emerson J, Umans R, Clarke M. Effects of hypoxia and transferrin on toxicity and DNA binding of ruthenium antitumor agents in HeLa cells. Metal-Based Drugs. 1996;3(4):197-209.

54. Clarke MJ. Ruthenium metallopharmaceuticals. Coordination Chemistry Reviews. 2003;236(1):209-33.

55. Kapitza S, Pongratz M, Jakupec M, Heffeter P, Berger W, Lackinger L, et al. Heterocyclic complexes of ruthenium (III) induce apoptosis in colorectal carcinoma cells. Journal of Cancer Research and Clinical Oncology. 2005;131(2):101-10.

56. Gatenby RA, Gillies RJ. Why do cancers have high aerobic glycolysis? Nature Reviews Cancer. 2004;4(11):891-9.

57. Antonarakis ES, Emadi A. Ruthenium-based chemotherapeutics: are they ready for prime time? Cancer Chemotherapy and Pharmacology. 2010;66(1):1-9.

58. Som P, Oster Z, Matsui K, Guglielmi G, Persson B, Pellettieri M, et al. 97Ru-transferrin uptake in tumor and abscess. European Journal of Nuclear Medicine and Molecular Imaging. 1983;8(11):491-4.

59. Vincent JB, Love S. The binding and transport of alternative metals by transferrin. Biochimica et Biophysica Acta−General Subjects. 2012;1820(3):362-78.

60. Brabec V. DNA modifications by antitumor platinum and ruthenium compounds: their recognition and repair. Progress in Nucleic Acid Research and Molecular Biology. 2002;71:1-68.

61. Brabec V, Nováková O. DNA binding mode of ruthenium complexes and relationship to tumor cell toxicity. Drug Resistance Updates. 2006;9(3):111-22.

62. Kapitza S, Jakupec MA, Uhl M, Keppler BK, Marian B. The heterocyclic ruthenium (III) complex KP1019 (FFC14A) causes DNA damage and oxidative stress in colorectal tumor cells. Cancer Letters. 2005;226(2):115-21.

63. Bergamo A, Sava G. Ruthenium anticancer compounds: myths and realities of the emerging metal-based drugs. Dalton Transactions. 2011;40(31):7817-23.

64. Keppler B, Rupp W, Juhl U, Endres H, Niebl R, Balzer W. Synthesis, molecular structure, and tumor-inhibiting properties of imidazolium trans-bis (imidazole) tetrachlororuthenate (III) and its methyl-substituted derivatives. Inorganic Chemistry. 1987;26(26):4366-70.

65. Sava G, Capozzi I, Bergamo A, Gagliardi R, Cocchietto M, Masiero L, et al. Down-regulation of tumour gelatinase/inhibitor balance and preservation of tumour endothelium by an anti-metastatic ruthenium complex. International Journal of Cancer. 1996;68(1):60-6.

66. Sava G, Zorzet S, Turrin C, Vita F, Soranzo M, Zabucchi G, et al. Dual action of NAMI-A in inhibition of solid tumor metastasis. Clinical Cancer Research. 2003;9(5):1898-905.

67. Garzon F, Berger M, Keppler B, Schmähl D. Comparative antitumor activity of ruthenium derivatives with 5′-deoxy-5-fluorouridine in chemically induced colorectal tumors in SD rats. Cancer Chemotherapy and Pharmacology. 1987;19(4):347-9.

68. Keppler BK, Henn M, Juhl UM, Berger MR, Niebl R, Wagner FE. New ruthenium complexes for the treatment of cancer. Ruthenium and other non-platinum metal complexes in cancer chemotherapy. Progress in Clinical Biochemistry and Medicine. 1989;10: 41-69.

69. Hartinger CG, Zorbas-Seifried S, Jakupec MA, Kynast B, Zorbas H, Keppler BK. From bench to bedside–preclinical and early clinical development of the anticancer agent indazolium trans-[tetrachlorobis (^{1}H-indazole) ruthenate (III)] (KP1019 or FFC14A). Journal of Inorganic Biochemistry. 2006;100(5):891-904.

70. Hartinger CG, Jakupec MA, Zorbas-Seifried S, Groessl M, Egger A, Berger W, et al. KP1019, a new redox-active anticancer agent–preclinical development and results of a clinical phase I study in tumor patients. Chemistry & Biodiversity. 2008;5(10):2140-55.

71. Bergamo A, Masi A, Jacupec MA, Keppler BK, Sava G. Inhibitory effects of the ruthenium complex KP1019 in models of mammary cancer cell migration and invasion. Metal-Based Drugs. 2009;2009:1-9.

72. Bratsos I, Gianferrara T, Alessio E, Hartinger CG, Jakupec MA, Keppler BK. Ruthenium and other non-platinum anticancer compounds. Bioinorganic Medicinal Chemistry: Wiley-VCH Verlag GmbH & Co. KGaA; 2011. p. 151-74.

73. Bergamo A, Sava G. Ruthenium complexes can target determinants of tumour malignancy. Dalton Transactions. 2007(13):1267-72.

74. Blunden BM, Rawal A, Lu H, Stenzel MH. Superior chemotherapeutic benefits from the ruthenium-based anti-metastatic drug NAMI-A through conjugation to polymeric micelles. Macromolecules. 2014;47(5):1646-55.

75. Trondl R, Heffeter P, Kowol CR, Jakupec MA, Berger W, Keppler BK. NKP-1339, the first ruthenium-based anticancer drug on the edge to clinical application. Chemical Science. 2014;5(8):2925-32.

76. Leijen S, Burgers SA, Baas P, Pluim D, Tibben M, van Werkhoven E, et al. Phase I/II study with ruthenium compound NAMI-A and gemcitabine in patients with non-small cell lung cancer after first line therapy. Investigational New Drugs. 2015;33(1):201-14.

77. Motswainyana WM, Ajibade PA. Anticancer activities of mononuclear ruthenium (II) coordination complexes. Advances in Chemistry. 2015;2015:1-21.

78. Allardyce CS, Dyson PJ. Metal-based drugs that break the rules. Dalton Transactions. 2016;45(8):3201-9.

79. Chang SW, Lewis AR, Prosser KE, Thompson JR, Gladkikh M, Bally MB, et al. CF3 derivatives of the anticancer Ru (III) complexes KP1019, NKP-1339, and their imidazole and pyridine analogues show enhanced lipophilicity, albumin interactions, and cytotoxicity. Inorganic Chemistry. 2016;55(10):4850-63.

80. Hayward R, Schornagel Q, Tente R, Macpherson J, Aird R, Guichard S, et al. Investigation of the role of Bax, p21/Waf1 and p53 as determinants of cellular responses in HCT116 colorectal cancer cells exposed to the novel cytotoxic ruthenium (II) organometallic agent, RM175. Cancer Chemotherapy and Pharmacology. 2005;55(6):577-83.

81. Bergamo A, Masi A, Peacock AF, Habtemariam A, Sadler P, Sava G. In vivo tumour and metastasis reduction and in vitro effects on invasion assays of the ruthenium RM175 and osmium AFAP51 organometallics in the mammary cancer model. Journal of Inorganic Biochemistry. 2010;104(1):79-86.

82. Scolaro C, Bergamo A, Brescacin L, Delfino R, Cocchietto M, Laurenczy G, et al. In vitro and in vivo evaluation of ruthenium (II) − arene PTA complexes. Journal of Medicinal Chemistry. 2005;48(12):4161-71.

83. Bergamo A, Masi A, Dyson PJ, Sava G. Modulation of the metastatic progression of breast cancer with an organometallic ruthenium compound. International Journal of Oncology. 2008;33(6):1281-9.

84. Nowak-Sliwinska P, van Beijnum JR, Casini A, Nazarov AA, Wagnieres G, van den Bergh H, et al. Organometallic ruthenium (II) arene compounds with antiangiogenic activity. Journal of Medicinal Chemistry. 2011;54(11):3895-902.

85. Weiss A, Ding X, Beijnum JR, Wong I, Wong TJ, Berndsen RH, et al. Rapid optimization of drug combinations for the optimal angiostatic treatment of cancer. Angiogenesis. 2015;18(3):233-44.

86. Weiss A, Berndsen RH, Dubois M, Müller C, Schibli R, Griffioen AW, et al. In vivo anti-tumor activity of the organometallic ruthenium (II)-arene complex [Ru(η^6-p-cymene)Cl_2(pta)] (RAPTA-C) in human ovarian and colorectal carcinomas. Chemical Science. 2014;5(12):4742-8.

87. Murray BS, Babak MV, Hartinger CG, Dyson PJ. The development of RAPTA compounds for the treatment of tumors. Coordination Chemistry Reviews. 2016;306:86-114.

88. Pettinari R, Marchetti F, Condello F, Pettinari C, Lupidi G, Scopelliti R, et al. Ruthenium (II)–arene RAPTA type complexes containing curcumin and bisdemethoxycurcumin display potent and selective anticancer activity. Organometallics. 2014;33(14):3709-15.

89. Pettinari R, Marchetti F, Pettinari C, Condello F, Petrini A, Scopelliti R, et al. Organometallic rhodium (III) and iridium (III) cyclopentadienyl complexes with curcumin and bisdemethoxycurcumin co-ligands. Dalton Transactions. 2015;44(47):20523-31.

90. Palmucci J, Marchetti F, Pettinari R, Pettinari C, Scopelliti R, Riedel T, et al. Synthesis, structure, and anticancer activity of arene–ruthenium (II) complexes with acylpyrazolones bearing aliphatic groups in the acyl moiety. Inorganic Chemistry. 2016;55(22):11770-81.

91. Meng X, Leyva M, Jenny M, Gross I, Benosman S, Fricker B, et al. A ruthenium-containing organometallic compound reduces tumor growth through induction of the endoplasmic reticulum stress gene CHOP. Cancer Research. 2009;69(13):5458-66.

92. Tomaz AI, Jakusch T, Morais TS, Marques F, De Almeida RF, Mendes F, et al. [Ru^{II}(η^5-C_5H_5)(bipy)(PPh_3)]$^+$, a promising large spectrum antitumor agent: Cytotoxic activity and interaction with human serum albumin. Journal of Inorganic Biochemistry. 2012;117:261-9.

93. Mavrynsky D, Rahkila J, Bandarra D, Martins S, Meireles M, Calhorda MJ, et al. Cytotoxicities of polysubstituted chlorodicarbonyl (cyclopentadienyl) and (indenyl) ruthenium complexes. Organometallics. 2013;32(10):3012-7.

94. Debreczeni JÉ, Bullock AN, Atilla GE, Williams DS, Bregman H, Knapp S, et al. Ruthenium half-sandwich complexes bound to protein kinase Pim-1. Angewandte Chemie International Edition. 2006;45(10):1580-5.

95. Maksimoska J, Feng L, Harms K, Yi C, Kissil J, Marmorstein R, et al. Targeting large kinase active site with rigid, bulky octahedral ruthenium complexes. Journal of the American Chemical Society. 2008;130(47):15764-5.

96. Hartinger CG, Metzler-Nolte N, Dyson PJ. Challenges and opportunities in the development of organometallic anticancer drugs. Organometallics. 2012;31(16):5677-85.

97. Tsai C-J, Nussinov R. The molecular basis of targeting protein kinases in cancer therapeutics. Seminars in Cancer Biology. 2013;23(4):235-42.

98. Hartinger CG, Dyson PJ. Bioorganometallic chemistry—from teaching paradigms to medicinal applications. Chemical Society Reviews. 2009;38(2):391-401.

99. Meggers E. Targeting proteins with metal complexes. Chemical Communications. 2009;(9):1001-10.

100. Morais TS, Silva TJ, Marques F, Robalo MP, Avecilla F, Madeira PJA, et al. Synthesis of organometallic ruthenium (II) complexes with strong activity against several human cancer cell lines. Journal of Inorganic Biochemistry. 2012;114:65-74.

101. Atilla-Gokcumen GE, Pagano N, Streu C, Maksimoska J, Filippakopoulos P, Knapp S, et al. Extremely tight binding of a ruthenium complex to glycogen synthase kinase 3. European Journal of Chemical Biology. 2008;9(18):2933-6.

102. Pagano N, Maksimoska J, Bregman H, Williams DS, Webster RD, Xue F, et al. Ruthenium half-sandwich complexes as protein kinase inhibitors: derivatization of the pyridocarbazole pharmacophore ligand. Organic & Biomolecular Chemistry. 2007;5(8):1218-27.

103. Smalley KS, Contractor R, Haass NK, Kulp AN, Atilla-Gokcumen GE, Williams DS, et al. An organometallic protein kinase inhibitor pharmacologically activates p53 and induces apoptosis in human melanoma cells. Cancer Research. 2007;67(1):209-17.

104. Bregman H, Meggers E. Ruthenium half-sandwich complexes as protein kinase inhibitors: an N-succinimidyl ester for rapid derivatizations of the cyclopentadienyl moiety. Organic Letters. 2006;8(24):5465-8.

105. Garcia MH, Morais TS, Florindo P, Piedade MFM, Moreno V, Ciudad C, et al. Inhibition of cancer cell growth by ruthenium (II) cyclopentadienyl derivative complexes with heteroaromatic ligands. Journal of Inorganic Biochemistry. 2009;103(3):354-61.

106. Moreno V, Lorenzo J, Aviles FX, Garcia MH, Ribeiro JP, Morais TS, et al. Studies of the antiproliferative activity of ruthenium (II) cyclopentadienyl-derived complexes with nitrogen coordinated ligands. Bioinorganic Chemistry and Applications. 2010;2010:1-11.

107. Moreno V, Font-Bardia M, Calvet T, Lorenzo J, Avilés FX, Garcia MH, et al. DNA interaction and cytotoxicity studies of new ruthenium (II) cyclopentadienyl derivative complexes containing heteroaromatic ligands. Journal of Inorganic Biochemistry. 2011;105(2):241-9.

108. Morais TS, Santos F, Côrte-Real L, Marques F, Robalo MP, Madeira PJA, et al. Biological activity and cellular uptake of $[Ru(\eta^5\text{-}C_5H_5)(PPh_3)(Me_2bpy)][CF_3SO_3]$ complex. Journal of Inorganic Biochemistry. 2013;122:8-17.

109. Valente A, Garcia MH, Marques F, Miao Y, Rousseau C, Zinck P. First polymer "ruthenium-cyclopentadienyl" complex as potential anticancer agent. Journal of Inorganic Biochemistry. 2013;127:79-81.

110. Florindo P, Marques IJ, Nunes CD, Fernandes AC. Synthesis, characterization and cytotoxicity of cyclopentadienyl ruthenium (II) complexes containing carbohydrate-derived ligands. Journal of Organometallic Chemistry. 2014;760:240-7.

111. Morais TS, Santos FC, Jorge TF, Corte-Real L, Madeira PJA, Marques F, et al. New water-soluble ruthenium (II) cytotoxic complex: biological activity and cellular distribution. Journal of Inorganic Biochemistry. 2014;130:1-14.

112. Florindo PR, Pereira DM, Borralho PM, Rodrigues CM, Piedade M, Fernandes AC. Cyclopentadienyl–ruthenium (II) and iron (II) organometallic compounds with carbohydrate derivative ligands as good colorectal anticancer agents. Journal of Medicinal Chemistry. 2015;58(10):4339-47.

113. Misra R, Acharya S, Sahoo SK. Cancer nanotechnology: application of nanotechnology in cancer therapy. Drug Discovery Today. 2010;15(19):842-50.

114. Mirtsching B, Cosgriff T, Harker G, Keaton M, Chidiac T, Min M. A phase II study of weekly nanoparticle albumin-bound paclitaxel with or without trastuzumab in metastatic breast cancer. Clinical breast cancer. 2011;11(2):121-8.

115. Kunjachan S, Błauż A, Möckel D, Theek B, Kiessling F, Etrych T, et al. Overcoming cellular multidrug resistance using classical nanomedicine formulations. European Journal of Pharmaceutical Sciences. 2012;45(4):421-8.

116. López-Dávila V, Seifalian AM, Loizidou M. Organic nanocarriers for cancer drug delivery. Current Opinion in Pharmacology. 2012;12(4):414-9.

117. Govender P, Therrien B, Smith GS. Bio-metallodendrimers–emerging strategies in metal-based drug design. European Journal of Inorganic Chemistry. 2012;2012(17):2853-62.

118. Makhubela BC, Meyer M, Smith GS. Evaluation of trimetallic Ru (II)-and Os (II)-arene complexes as potential anticancer agents. Journal of Organometallic Chemistry. 2014;772:229-41.

119. Singh SK, Pandey DS. Multifaceted half-sandwich arene–ruthenium complexes: interactions with biomolecules, photoactivation, and multinuclearity approach. RSC Advances. 2014;4(4):1819-40.

120. Wang K, Gao E. Recent advances in multinuclear complexes as potential anticancer and DNA binding agents. Anti-Cancer Agents in Medicinal Chemistry. 2014;14(1):147-69.

121. Burgoyne AR, Makhubela BC, Meyer M, Smith GS. Trinuclear half-sandwich Ru^{II}, Rh^{III} and Ir^{III} polyester organometallic complexes: synthesis and in vitro evaluation as antitumor agents. European Journal of Inorganic Chemistry. 2015;2015(8):1433-44.

122. Govender P, Sudding LC, Clavel CM, Dyson PJ, Therrien B, Smith GS. The influence of RAPTA moieties on the antiproliferative activity of peripheral-functionalised poly (salicylaldiminato) metallodendrimers. Dalton Transactions. 2013;42(4):1267-77.

123. Payne R, Govender P, Therrien B, Clavel CM, Dyson PJ, Smith GS. Neutral and cationic multinuclear half-sandwich rhodium and iridium complexes coordinated to poly

(propyleneimine) dendritic scaffolds: synthesis and cytotoxicity. Journal of Organometallic Chemistry. 2013;729:20-7.

124. Govender P, Edafe F, Makhubela BC, Dyson PJ, Therrien B, Smith GS. Neutral and cationic osmium (II)-arene metallodendrimers: synthesis, characterisation and anticancer activity. Inorganica Chimica Acta. 2014;409:112-20.

125. Sudding LC, Payne R, Govender P, Edafe F, Clavel CM, Dyson PJ, et al. Evaluation of the in vitro anticancer activity of cyclometalated half-sandwich rhodium and iridium complexes coordinated to naphthaldimine-based poly (propyleneimine) dendritic scaffolds. Journal of Organometallic Chemistry. 2014;774:79-85.

126. Govender P, Riedel T, Dyson PJ, Smith GS. Regulating the anticancer properties of organometallic dendrimers using pyridylferrocene entities: synthesis, cytotoxicity and DNA binding studies. Dalton Transactions. 2016;45(23):9529-39.

127. Buhleier E, Wehner W, Vögtle F. Cascade and nonskid-chain-like syntheses of molecular cavities topologies. Synthesis. 1978;1978(2):155-8.

128. Tomalia D, Baker H, Dewald J, Hall M, Kallos G, Martin S, et al. A new class of polymers: starburst-dendritic. Polymer Journal. 1985;17(1):117-32.

129. Boas U, Christensen JB, Heegaard PM. Dendrimers: design, synthesis and chemical properties. Journal of Materials Chemistry. 2006;16(38):3785-98.

130. Kesharwani P, Jain K, Jain NK. Dendrimer as nanocarrier for drug delivery. Progress in Polymer Science. 2014;39(2):268-307.

131. Percec V, Cho W-D, Mosier P, Ungar G, Yeardley D. Structural analysis of cylindrical and spherical supramolecular dendrimers quantifies the concept of monodendron shape control by generation number. Journal of the American Chemical Society. 1998;120(43):11061-70.

132. Esfand R, Tomalia DA. Poly (amidoamine) (PAMAM) dendrimers: from biomimicry to drug delivery and biomedical applications. Drug Discovery Today. 2001;6(8):427-36.

133. Kesharwani P, Iyer AK. Recent advances in dendrimer-based nanovectors for tumor-targeted drug and gene delivery. Drug Discovery Today. 2015;20(5):536-47.

134. Watkins DM, Sayed-Sweet Y, Klimash JW, Turro NJ, Tomalia DA. Dendrimers with hydrophobic cores and the formation of supramolecular dendrimer − surfactant assemblies. Langmuir. 1997;13(12):3136-41.

135. Hawker CJ, Frechet JM. Preparation of polymers with controlled molecular architecture. A new convergent approach to dendritic macromolecules. Journal of the American Chemical Society. 1990;112(21):7638-47.

136. Carlmark A, Hawker C, Hult A, Malkoch M. New methodologies in the construction of dendritic materials. Chemical Society Reviews. 2009;38(2):352-62.

137. Rodrigues J, Jardim MG, Figueira J, Gouveia M, Tomas H, Rissanen K. Poly(alkylidenamines) dendrimers as scaffolds for the preparation of low-generation ruthenium based metallodendrimers. New Journal of Chemistry. 2011;35(10):1938-43.

138. Svenson S. Dendrimers as versatile platform in drug delivery applications. European Journal of Pharmaceutics and Biopharmaceutics. 2009;71(3):445-62.

139. Mignani S, El Kazzouli S, Bousmina M, Majoral J-P. Expand classical drug administration ways by emerging routes using dendrimer drug delivery systems: a concise overview. Advanced Drug Delivery Reviews. 2013;65(10):1316-30.

140. Govender P, Antonels NC, Mattsson J, Renfrew AK, Dyson PJ, Moss JR, et al. Anticancer activity of multinuclear arene ruthenium complexes coordinated to dendritic polypyridyl scaffolds. Journal of Organometallic Chemistry. 2009;694(21):3470-6.

141. Zhao X, Loo SCJ, Lee PP-F, Tan TTY, Chu CK. Synthesis and cytotoxic activities of chloropyridylimineplatinum (II) and chloropyridyliminecopper (II) surface-functionalized poly (amidoamine) dendrimers. Journal of inorganic biochemistry. 2010;104(2):105-10.

142. Pisani MJ, Wheate NJ, Keene FR, Aldrich-Wright JR, Collins JG. Anionic PAMAM dendrimers as drug delivery vehicles for transition metal-based anticancer drugs. Journal of Inorganic Biochemistry. 2009;103(3):373-80.

143. Greish K. Enhanced permeability and retention effect for selective targeting of anticancer nanomedicine: are we there yet? Drug Discovery Today: Technologies. 2012;9(2):e161-e6.

144. Dawidczyk CM, Kim C, Park JH, Russell LM, Lee KH, Pomper MG, et al. State-of-the-art in design rules for drug delivery platforms: lessons learned from FDA-approved nanomedicines. Journal of Controlled Release. 2014;187:133-44.

145. Valetti S, Mura S, Stella B, Couvreur P. Rational design for multifunctional non-liposomal lipid-based nanocarriers for cancer management: theory to practice. Journal of Nanobiotechnology. 2013;11(1):S6.

146. Medina SH, El-Sayed ME. Dendrimers as carriers for delivery of chemotherapeutic agents. Chemical Reviews. 2009;109(7):3141-57.

147. Labieniec M, Watala C. PAMAM dendrimers - diverse biomedical applications. Facts and unresolved questions. Central European Journal of Biology. 2009;4(4):434-51.

148. Wrobel D, Appelhans D, Signorelli M, Wiesner B, Fessas D, Scheler U, et al. Interaction study between maltose-modified PPI dendrimers and lipidic model membranes. Biochimica et Biophysica Acta-Biomembranes. 2015;1848(7):1490-501.

149. Nanjwade BK, Bechra HM, Derkar GK, Manvi F, Nanjwade VK. Dendrimers: emerging polymers for drug-delivery systems. European Journal of Pharmaceutical Sciences. 2009;38(3):185-96.

150. Schilrreff P, Mundiña-Weilenmann C, Romero EL, Morilla MJ. Selective cytotoxicity of PAMAM G5 core–PAMAM G2.5 shell tecto-dendrimers on melanoma cells. International Journal of Nanomedicine. 2012;7:4121-33.

151. Ghorai S, Bhattacharyya D, Bhattacharjya A. The first examples of anthracene capped chiral carbohydrate derived dendrimers: synthesis, fluorescence and chiroptical properties. Tetrahedron letters. 2004;45(32):6191-4.

152. Darbre T, Reymond J-L. Peptide dendrimers as artificial enzymes, receptors, and drug-delivery agents. Accounts of Chemical Research. 2006;39(12):925-34.

153. Pushechnikov A, Jalisatgi SS, Hawthorne MF. Dendritic closomers: novel spherical hybrid dendrimers. Chemical Communications. 2013;49(34):3579-81.

154. Xiao Q, Zhang S, Wang Z, Sherman SE, Moussodia R-O, Peterca M, et al. Onion-like glycodendrimersomes from sequence-defined Janus glycodendrimers and influence of

architecture on reactivity to a lectin. Proceedings of the National Academy of Sciences. 2016;113(5):1162-7.

155. Kazzouli SE, Brahmi NE, Mignani S, Bousmina M, Zablocka M, Majoral JP. From metallodrugs to metallodendrimers for nanotherapy in oncology: a concise overview. Current Medicinal Chemistry. 2012;19(29):4995-5010.

156. Mintzer MA, Merkel OM, Kissel T, Simanek EE. Polycationic triazine-based dendrimers: effect of peripheral groups on transfection efficiency. New Journal of Chemistry. 2009;33(9):1918-25.

157. Van der Ende A, Croce T, Hamilton S, Sathiyakumar V, Harth E. Tailored polyester nanoparticles: post-modification with dendritic transporter and targeting units via reductive amination and thiol-ene chemistry. Soft Matter. 2009;5(7):1417-25.

158. Zhang X, Achazi K, Steinhilber D, Kratz F, Dernedde J, Haag R. A facile approach for dual-responsive prodrug nanogels based on dendritic polyglycerols with minimal leaching. Journal of Controlled Release. 2014;174:209-16.

159. Caminade AM, Maraval V, Laurent R, Majoral JP. Organometallic derivatives of phosphorus-containing dendrimers. Synthesis, Properties and Applications in Catalysis. Current Organic Chemistry. 2002;6(8):739-74.

160. Gissibl A, Padié C, Hager M, Jaroschik F, Rasappan R, Cuevas-Yañez E, et al. Synthesis and application of phosphorus dendrimer immobilized azabis (oxazolines). Organic Letters. 2007;9(15):2895-8.

161. Hayder M, Poupot M, Baron M, Nigon D, Turrin CO, Caminade AM, et al. A phosphorus-based dendrimer targets inflammation and osteoclastogenesis in experimental arthritis. Science Translational Medicine. 2011;3(81):81ra35.

162. Malik N, Evagorou EG, Duncan R. Dendrimer-platinate: a novel approach to cancer chemotherapy. Anti-cancer Drugs. 1999;10(8):767-76.

163. Haririan I, Alavidjeh MS, Khorramizadeh MR, Ardestani MS, Ghane ZZ, Namazi H. Anionic linear-globular dendrimer-cis-platinum (II) conjugates promote cytotoxicity in vitro against different cancer cell lines. International Journal of Nanomedicine. 2010;5:63-75.

164. Ahamad T, Mapolie S, Alshehri SM. Synthesis and characterization of polyamide metallodendrimers and their anti-bacterial and anti-tumor activities. Medicinal Chemistry Research. 2012;21(8):2023-31.

165. Robilotto TJ, Deligonul N, Updegraff III JB, Gray TG. Azido, triazolyl, and alkynyl complexes of gold (I): syntheses, structures, and ligand effects. Inorganic Chemistry. 2013;52(16):9659-68.

166. Mylerová V, Martínková L. Synthetic applications of nitrile-converting enzymes. Current Organic Chemistry. 2003;7(13):1279-95.

167. Gong JS, Lu ZM, Li H, Shi JS, Zhou ZM, Xu ZH. Nitrilases in nitrile biocatalysis: recent progress and forthcoming research. Microbial Cell Factories. 2012;11(1):142.

168. Bertani R, Mozzon M, Sgarbossa P, Tamburini S, Casarin M, Mangione G, et al. Pt (II) nitrile complexes: new insights on old complexes from a combined experimental and theoretical study. Inorganica Chimica Acta. 2017;455:489-504.

169. Ornelas C, Gandum C, Mesquita J, Rodrigues J, Garcia MH, Lopes N, et al. Synthesis, characterization and crystal structure of the bimetallic cyano-bridged $[(\eta^5\text{-}C_5H_5)(PPh_3)_2Ru(\mu\text{-}CN)Ru(PPh_3)_2(\eta^5\text{-}C_5H_5)][PF_6]$. Inorganica Chimica Acta. 2005;358(8):2482-8.

170. Garcia MH, Rodrigues JC, Dias AR, Piedade MFM, Duarte MT, Robalo MP, et al. Second harmonic generation of η^5-monocyclopentadienyl ruthenium p-benzonitrile derivatives by Kurtz powder technique. Crystal and molecular structure determinations of $[Ru(\eta^5\text{-}C_5H_5)((+)\text{-}DIOP)(p\text{-}NCC_6H_4NO_2)][X]$, $X=PF_6^-$, $CF_3SO_3^-$ and $[Ru(\eta^5\text{-}C_5H_5)((+)\text{-}DIOP)(NCCH_3)][PF_6]$. Journal of Organometallic Chemistry. 2001;632(1):133-44.

171. Savena A, Rao VL, Ninan KN. Synthesis and properties of polyether nitrile copolymers with pendant methyl groups. European Polymer Journal. 2003; 39(1):57-61.

172. Lee Y-G, Koyama Y, Yonekawa M, Takata T. New click chemistry polymerization based on 1,3-dipolar cycloaddition of a homo ditopic nitrile and *N*-oxide and transformation of the resulting polymers into reactive polymers. Macromolecules. 2009; 40(20):7709-17.

173. Fillaut JL, Dua NN, Geneste F, Toupet L, Sinbandhit S. Nitrile ligands for controlled synthesis of alkynyl-ruthenium based homo and hetero bimetallic systems. Journal of Organometallic chemistry. 2006;691(26):5610-8.

174. Benmansour S, Atmani C, Setifi F, Triki S, Marchivie M, Gómez-García CJ. Polynitrile anions as ligands: From magnetic polymeric architectures to spin crossover materials. Coordination Chemistry Reviews. 2010;254(13):1468-78.

175. Wenseleers W, Gerbrandij AW, Goovaerts E, Garcia MH, Robalo MP, Mendes PJ, et al. Hyper-Rayleigh scattering study of η^5-monocyclopentadienyl metal complexes for second order non-linear optical materials. Journal of Materials Chemistry. 1998;8(4):925-30.

176. Garcia MH, Robalo MP, Dias AR, Duarte MT, Wenseleers W, Aerts G, et al. Synthesis and nonlinear optical properties of η^5-monocyclopentadienyl iron (II) acetylide derivatives. X-ray crystal structures of $[Fe(\eta^5\text{-}C_5H_5)(DPPE)(p\text{-}C{\equiv}CC_6H_4NO_2)]$ and $[Fe(\eta^5\text{-}C_5H_5)(DPPE)((E)\text{-}p\text{-}C{\equiv}CC_6H_4C(H){=}C(H)C_6H_4NO_2)]$. Organometallics. 2002;21(10):2107-18.

177. Fairlie DP, Jackson WG, Skelton BW, Wen H, White AH, Wickramasinghe WA, et al. Models for arginine − metal binding. Synthesis of guanidine and urea ligands through amination and hydration of a cyanamide ligand bound to platinum (II), osmium (III), and cobalt (III). Inorganic Chemistry. 1997;36(6):1020-8.

178. Michelin RA, Mozzon M, Bertani R. Reactions of transition metal-coordinated nitriles. Coordination Chemistry Reviews. 1996;147:299-338.

179. Kukushkin VY, Pombeiro AJ. Additions to metal-activated organonitriles. Chemical Reviews. 2002;102(5):1771-802.

180. Kuznetsov ML. Theoretical studies of transition metal complexes with nitriles and isocyanides. Russian Chemical Reviews. 2002;71(4):265.

181. Govender P, Renfrew AK, Clavel CM, Dyson PJ, Therrien B, Smith GS. Antiproliferative activity of chelating N, O- and N, N-ruthenium (II) arene functionalised poly (propyleneimine) dendrimer scaffolds. Dalton Transactions. 2011;40(5):1158-67.

182. Aderibigbe B. Polymeric prodrugs containing metal-based anticancer drugs. Journal of Inorganic and Organometallic Polymers and Materials. 2015;25(3):339-53.

183. Ornelas C, Vertlib V, Rodrigues J, Rissanen K. Ruthenium metallodendrimers based on nitrile-functionalized poly(alkylideneimine)s. European Journal of Inorganic Chemistry. 2006;2006(1):47-50.

184. Jardim MG, Rissanen K, Rodrigues J. Preparation and characterization of novel Poly(alkylidenamine) nitrile ruthenium metallodendrimers. European Journal of Inorganic Chemistry. 2010;2010(11):1729-35.

185. Ornelas C, Ruiz J, Blais JC, Rodrigues J, Astruc D. Organometallic syntheses of hexa- and nonanitrile ligands and their ruthenium complexes. Organometallics. 2004;23(18):4271-6.

186. Shriver DF, Drezdzon MA. The manipulation of air-sensitive compounds: John Wiley & Sons, New York; 1986.

187. Errington RJ. Advanced practical inorganic and metalorganic chemistry: Blackie Academic & Professional, London; 1997.

188. Bruce M, Windsor N. Cyclopentadienyl-ruthenium and -osmium chemistry. IV. Convenient high-yield synthesis of some cyclopentadienyl ruthenium or osmium tertiary phosphine halide complexes. Australian Journal of Chemistry. 1977;30(7):1601-4.

189. Dias AR, Garcia MH, Rodrigues JC, Green MLH, Kuebler SM. Synthesis and characterization of η^5-monocyclopentadienyl(*p*-nitrobenzonitrile)ruthenium(II) salts: second harmonic generation powder efficiencies. Journal of Organometallic Chemistry. 1994;475(1):241-5.

190. Caminade AM, Laurent R, Majoral JP. Characterization of dendrimers. Advanced Drug Delivery Reviews. 2005;57(15):2130-46.

191. Riegel SD, Leskowitz GM. Benchtop NMR spectrometers in academic teaching. Trends in Analytical Chemistry. 2016;83, Part A:27-38.

192. Crews P, Rodriquez J, Jaspars M. Organic structure analysis: Oxford University Press, Oxford; 2010.

193. Fulmer GR, Miller AJM, Sherden NH, Gottlieb HE, Nudelman A, Stoltz BM, et al. NMR chemical shifts of trace impurities: common laboratory solvents, organics, and gases in deuterated solvents relevant to the organometallic chemist. Organometallics. 2010;29(9):2176-9.

194. Hung WI, Hung CB, Chang YH, Dai JK, Li Y, He H, et al. Synthesis and electroactive properties of poly(amidoamine) dendrimers with an aniline pentamer shell. Journal of Materials Chemistry. 2011;21(12):4581-7.

195. Davis AP, Ma G, Allen HC. Surface vibrational sum frequency and Raman studies of PAMAM G0, G1 and acylated PAMAM G0 dendrimers. Analytica Chimica Acta. 2003;496(1–2):117-31.

196. Vahedi H, Massoudi A, Hoseini S. Cyclization of PAMAM G0 and G1 dendrimer using DMAD and 2-benzylidenemalononitrile. International Journal of ChemTech Research. 2012;4(4):1654-7.

197. Lambert JB, Shurvell HF, Lightner DA, Cooks RG. Organic structural spectroscopy. Nuclear Magnetic Resonance spectroscopy. The chemical shift: Prentice Hall, New Jersey; 1998.

198. Ilaiyaraja P, Deb AKS, Ponraju D. Removal of uranium and thorium from aqueous solution by ultrafiltration (UF) and PAMAM dendrimer assisted ultrafiltration (DAUF). Journal of Radioanalytical and Nuclear Chemistry. 2015;303(1):441-50.

199. Mather BD, Viswanathan K, Miller KM, Long TE. Michael addition reactions in macromolecular design for emerging technologies. Progress in Polymer Science. 2006;31(5):487-531.

200. Wabnitz TC, Spencer JB. A general, brønsted acid-catalyzed hetero-michael addition of nitrogen, oxygen, and sulfur nucleophiles. Organic Letters. 2003;5(12):2141-4.

201. Rajasekaran A, Thampi PP, Murugesan S. Cyanoethylation: a vital reaction in the synthesis of biologically active heterocycles. Asian Journal of Chemistry. 2004;16(1):1-8.

202. Gonera A. Aminofunctional starch derivatives: Synthesis, analysis, and application: Cuvillier Verlag, Göttingen; 2004.

203. Wu D, Liu Y, He C, Chung T, Goh S. Effects of chemistries of trifunctional amines on mechanisms of michael addition polymerizations with diacrylates. Macromolecules. 2004;37(18):6763-70.

204. Maynard GD, Le TB. Substituted 4-(1H-benzimidazol-2-yl)[1,4]diazepanes useful for the treatment of allergic diseases. US patent 6,423,704, 2002.

205. Evans V, Mahon MF, Webster RL. A mild, copper-catalysed amide deprotection strategy: use of tert-butyl as a protecting group. Tetrahedron. 2014;70(41):7593-7.

206. Reddy DR, Iqbal MA, Hudkins RL, Messina-McLaughlin PA, Mallamo JP. A simple synthetic protocol for the protection of amides, lactams, ureas, and carbamates. Tetrahedron Letters. 2002;43(45):8063-6.

207. Cai Z, Shen B, Xin Z, Liu W, Ling H. Gas-phase cracking dicyclopentadiene using hydrogen as a carrier gas. Energy Sources, Part A: Recovery, Utilization, and Environmental Effects. 2011;33(7):594-603.

208. Cai Z, Shen B, Liu W, Xin Z, Ling H. Liquid-Phase Cracking of dicyclopentadiene by reactive distillation. Energy & Fuels. 2009;23(8):4077-81.

209. Hart MM, Adamson RH. Antitumor activity and toxicity of salts of inorganic group IIIa metals: aluminum, gallium, indium, and thallium. Proceedings of the National Academy of Sciences of the United States of America. 1971;68(7):1623-6.

210. Zuccaccia D, Clot E, Macchioni A. Aggregation in solution of neutral half-sandwich Ru(II) precatalysts for transfer hydrogenation. New Journal of Chemistry. 2005;29(3):430-3.

211. Zuccaccia D, Sabatini S, Bellachioma G, Cardaci G, Clot E, Macchioni A. PGSE and NOE NMR evidence for higher order aggregation in some cationic ruthenium complexes in both protic and aprotic solvents. Inorganic Chemistry. 2003;42(18):5465-7.

212. Griffith WP, Reddy B, Shoair AG, Suriaatmaja M, White AJ, Williams DJ. Ruthenate (VI)-catalysed dehydrogenation of primary amines to nitriles, and crystal structures of *cis*-[Ru $(bipy)_2(NH_2CH_2Ph)_2][PF_6]_2 \cdot 0.5MeOH$ and *cis*-$[Ru(bipy)_2(NCPh)_2][PF_6]_2 \cdot CH_2Cl_2$. Journal of the Chemical Society, Dalton Transactions. 1998(17):2819-26.

213. Hermansson K. Blue-shifting hydrogen bonds. The Journal of Physical Chemistry A. 2002;106(18):4695-702.

214. Csontos J, Murphy RF, Lovas S. The role of weakly polar and H-bonding interactions in the stabilization of the conformers of FGG, WGG and YGG: an aqueous phase computational study. Biopolymers. 2008;89(11):1002-11.

215. Meyer EA, Castellano RK, Diederich F. Interactions with aromatic rings in chemical and biological recognition. Angewandte Chemie International Edition. 2003;42(11):1210-50.

216. Tarazona-Vasquez F, Balbuena PB. Ab initio study of the lowest energy conformers and IR spectra of poly (amidoamine)-G0 dendrimers. The Journal of Physical Chemistry B. 2004;108(41):15982-91.

217. Cockroft SL, Hunter CA. Chemical double-mutant cycles: dissecting non-covalent interactions. Chemical Society Reviews. 2007;36(2):172-88.

218. Rodrigues JMC. Síntese de novos materiais organometálicos com propriedades de não linearidade óptica. Universidade de Lisboa, Faculdade de Ciências.1999. PhD Thesis.

219. Farona MF, Bremer NJ. Succinonitrile derivatives of halogenopentacarbonylmanganese (I)[1]. Journal of the American Chemical Society. 1966;88(16):3735-7.

220. Maiti PK, Çağın T, Lin S-T, Goddard WA. Effect of solvent and pH on the structure of PAMAM dendrimers. Macromolecules. 2005;38(3):979-91.

221. McMurry JE. Fundamentals of organic chemistry: Cengage Learning, USA; 2010.

222. Patrick G. Organic chemistry instant notes series. Chemistry Series: Taylor & Francis Routledge, London; 2004.

9. ATTACHMENT

9.1. Characterization spectra

9.1.1. G0/G1-PAMAM

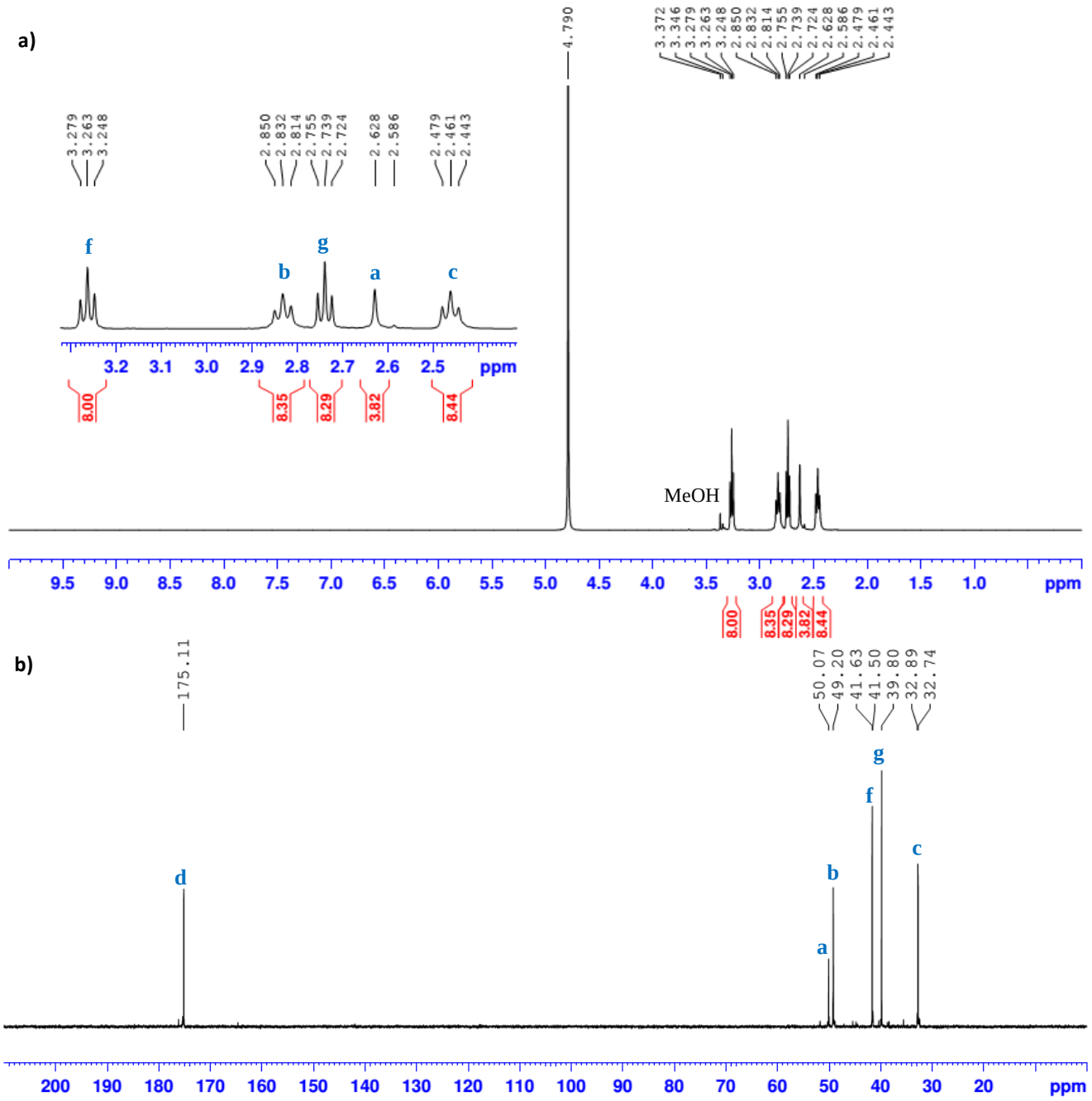

Figure 1A - a) ^{1}H-NMR and b) ^{13}C-NMR spectra of G0-PAMAM, in D_2O. Each signal is marked with the different group of carbons and protons that are represented with a unique letter – see scheme 1).

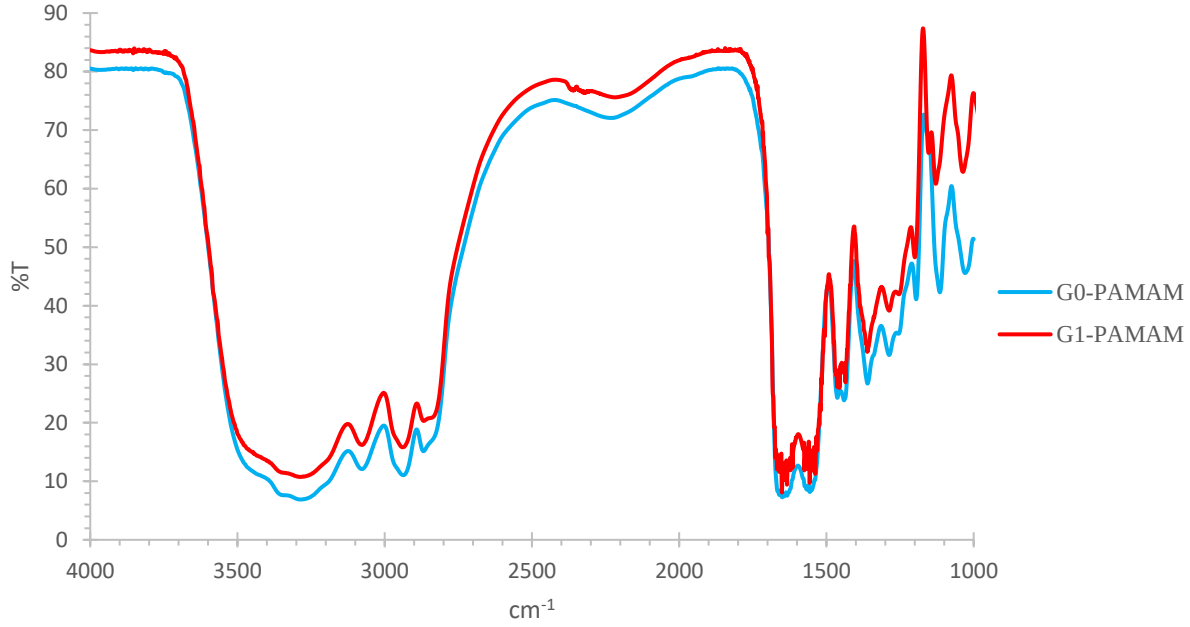

Figure 2A - FTIR spectra of G0/G1-PAMAM performed in KBr cells.

9.1.2. G0/G1-CN

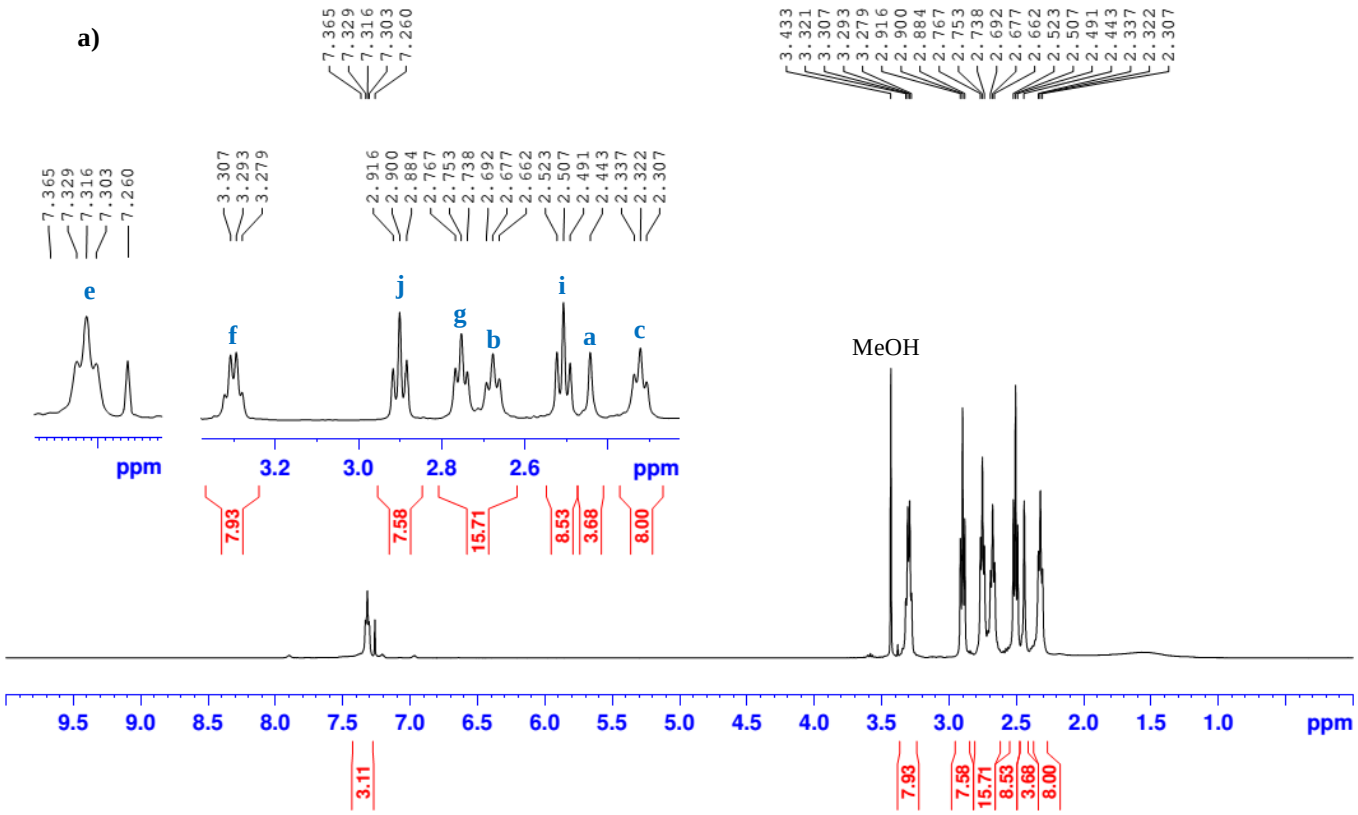

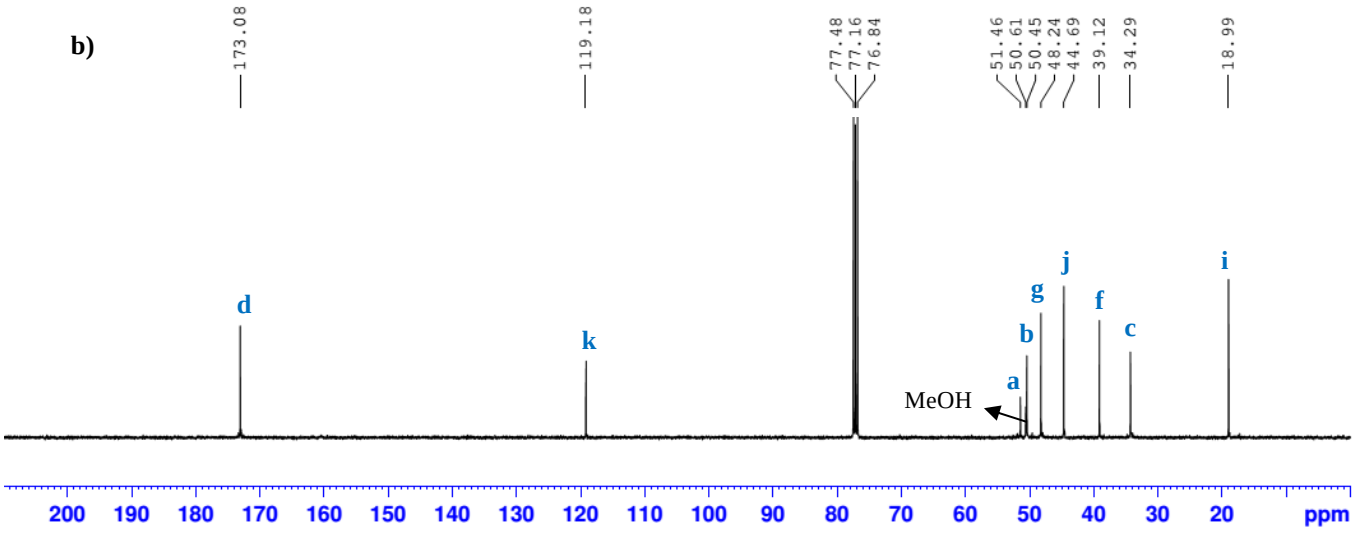

Figure 3A - a) ^{1}H-NMR and b) ^{13}C-NMR spectra of crude G0-(CN)$_4$, in $CDCl_3$. Each signal is marked with the different type of carbons and protons that are represented with a unique letter – see scheme 1).

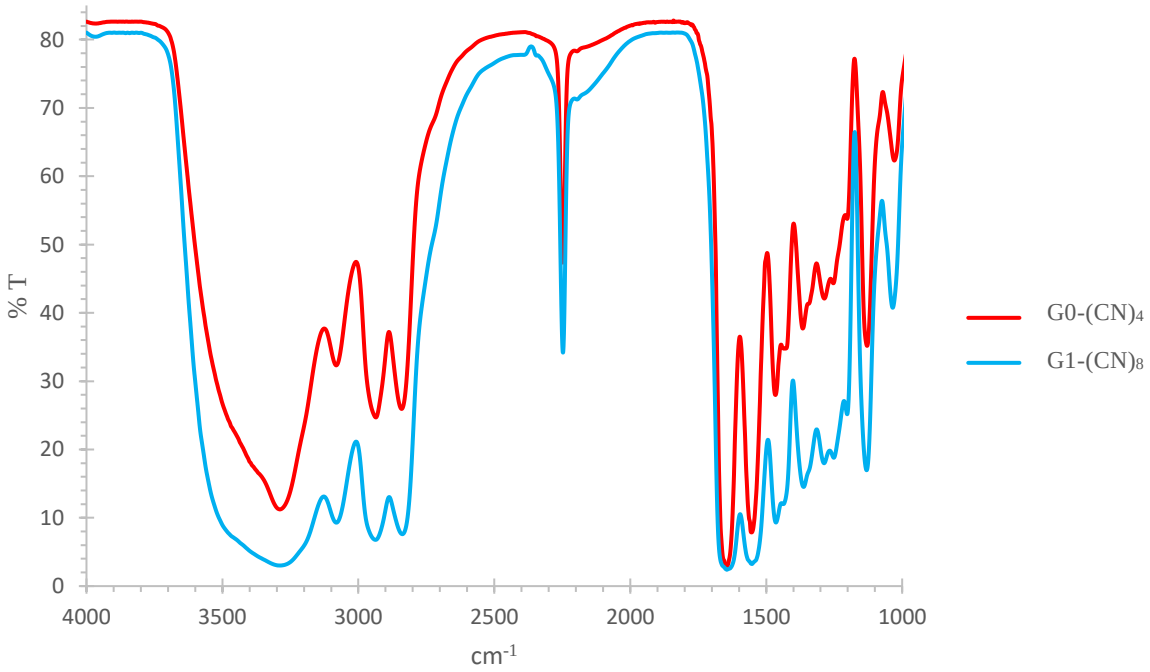

Figure 4A - FTIR spectra of purified G0/G1-CN performed in NaCl cells.

9.1.3. G0/G1-$(CNRuCp(PPh_3)_2)_x(CF_3SO_3)_x$

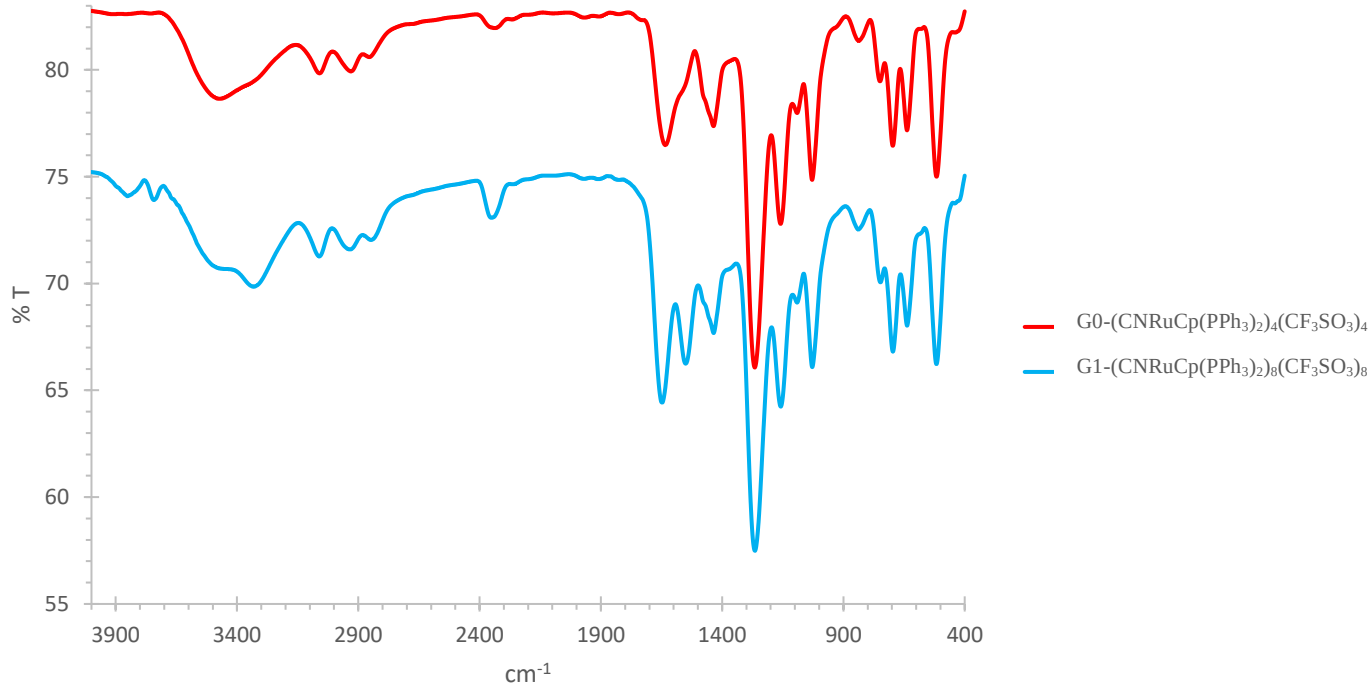

Figure 5A - FTIR spectra of purified G0/G1-$(CNRuCp(PPh_3)_2)_x(CF_3SO_3)_x$ performed in a KBr pellet.

9.1.4. G0/G1-$CO_2{}^t$Bu

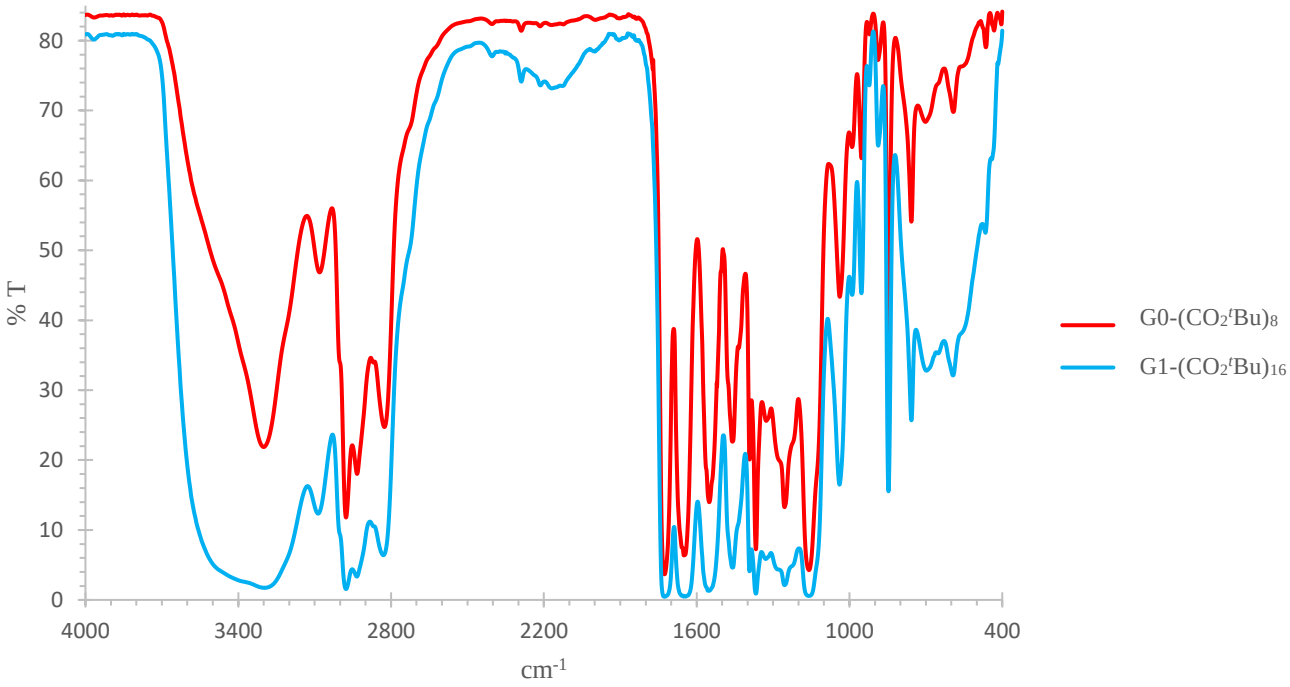

Figure 6A - FTIR spectra of purified G0/G1-$CO_2{}^t$Bu performed in KBr cells.

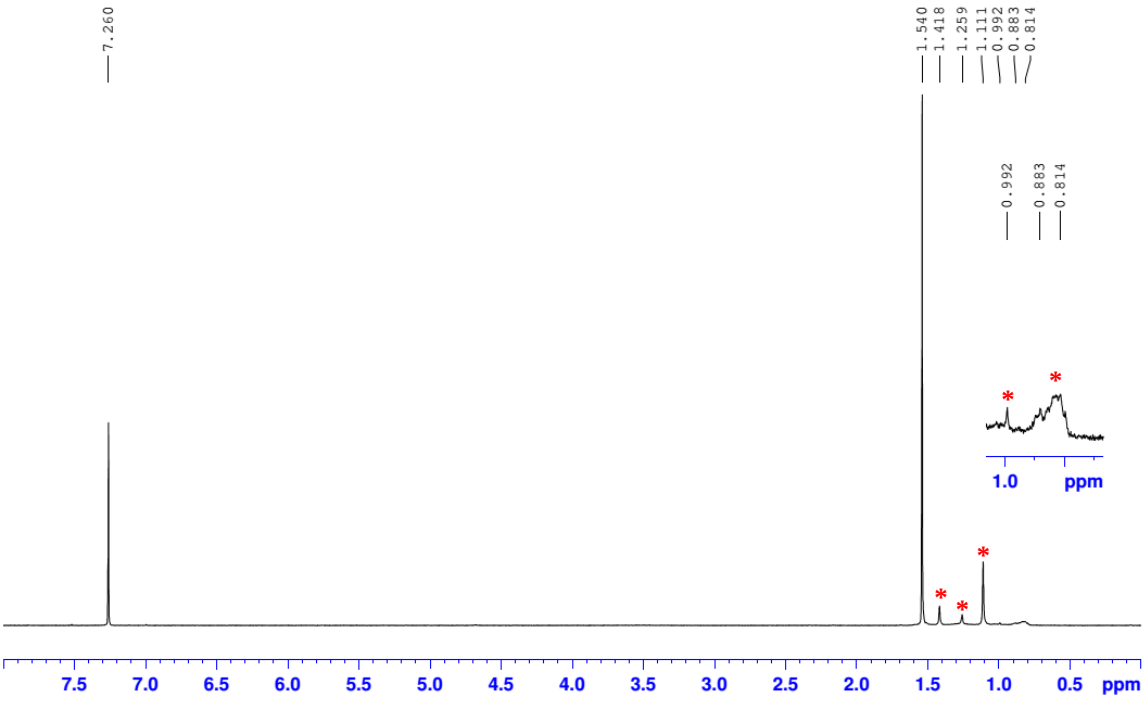

Figure 7A - ^{1}H-NMR spectra of $CDCl_3$ contaminated. The red stars represent the impurities of the sample.

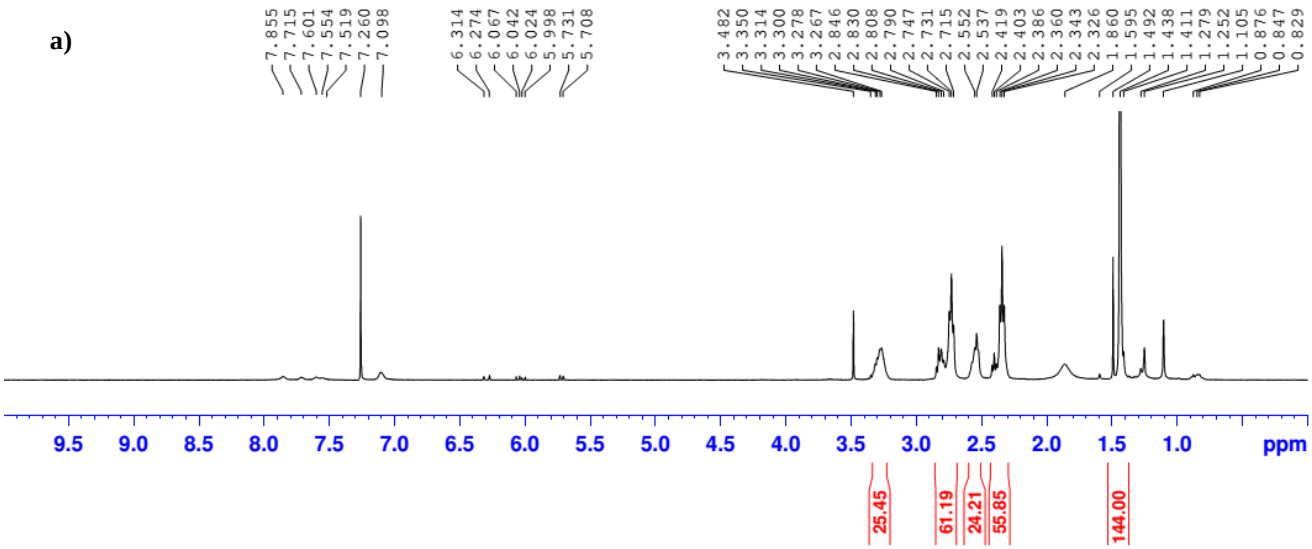

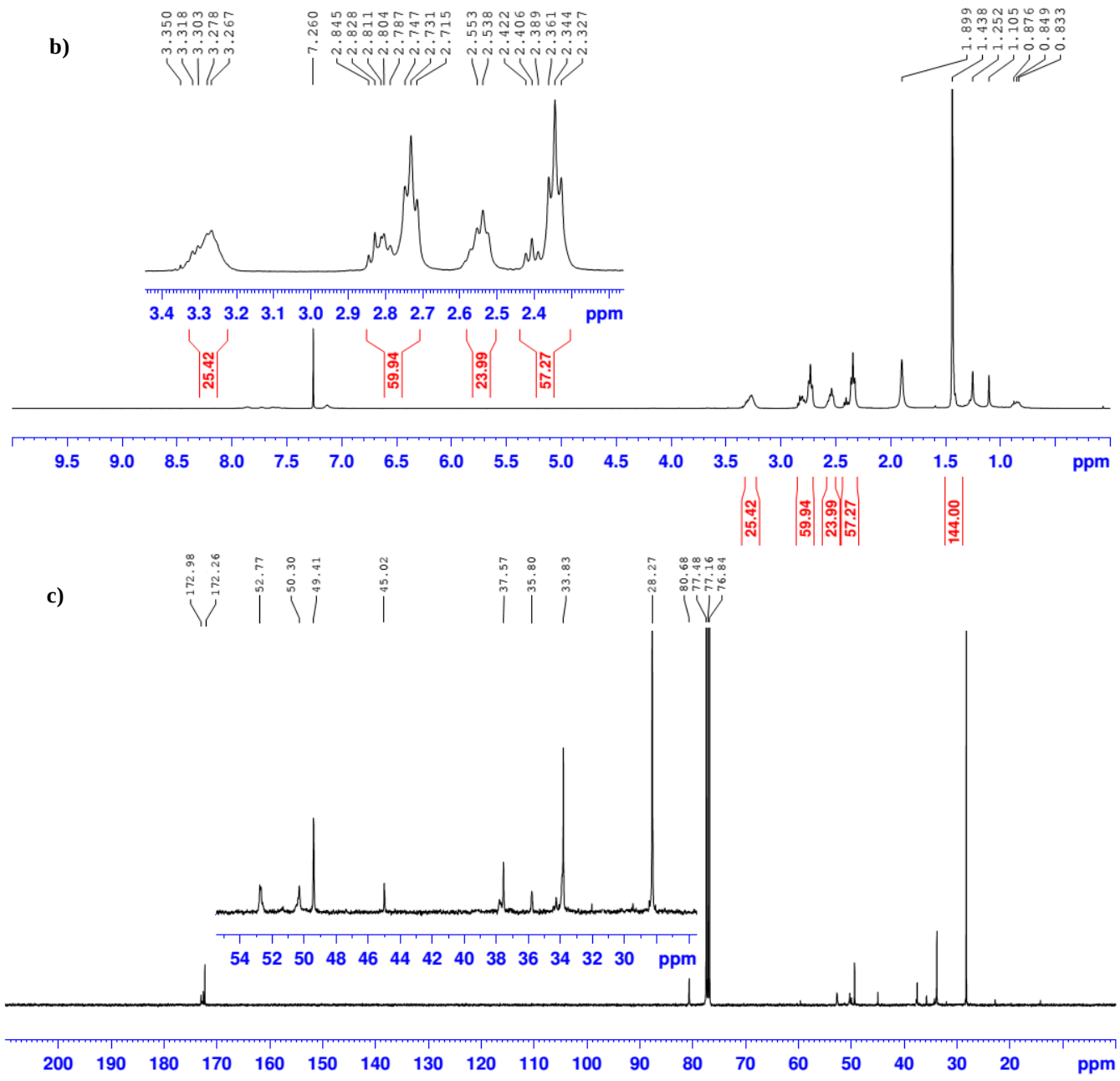

Figure 8A - NMR characterization of G1-$(CO_2{}^tBu)_{16}$: ^{1}H-NMR spectra of the a) crude and b) purified product; c) ^{13}C-NMR spectrum of the purified, in $CDCl_3$.

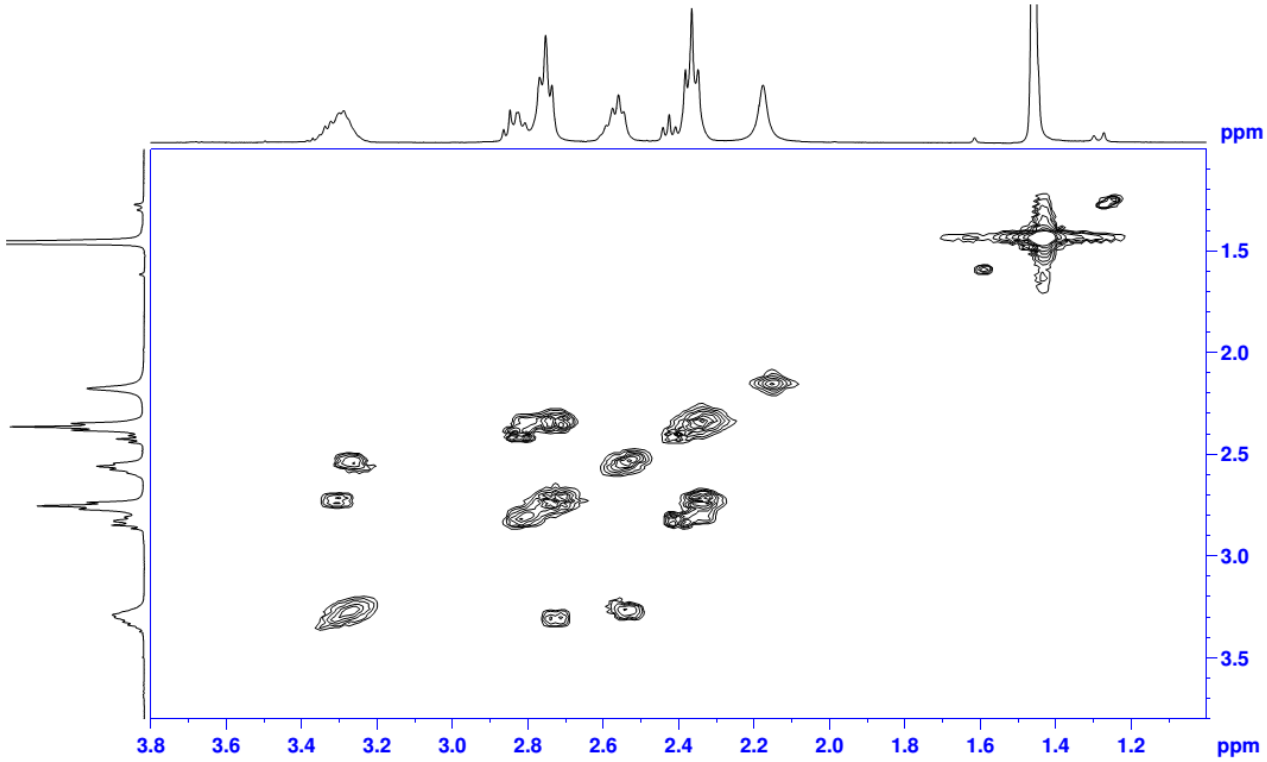

Figure 9A - COSY spectrum of purified G1-$(CO_2{}^tBu)_8$, in D_2O.

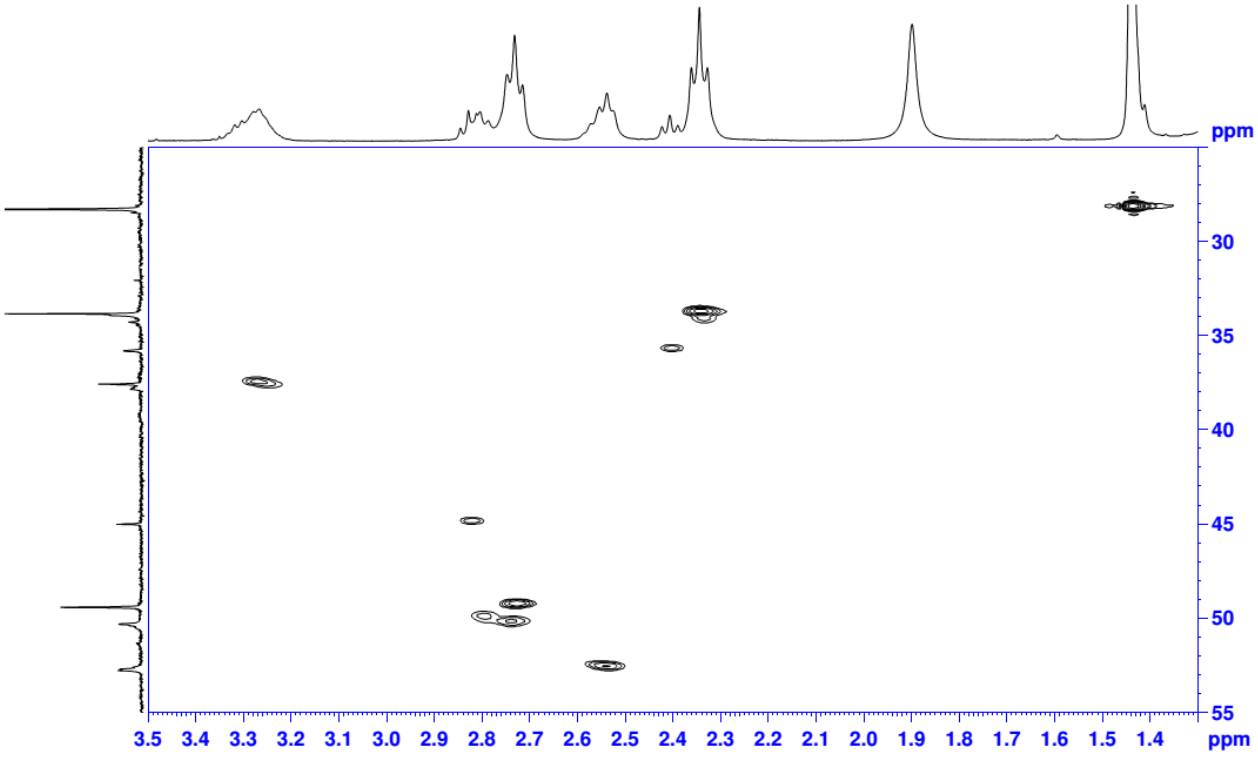

Figure 10A - HSQC spectrum of purified G1-$(CO_2{}^tBu)_8$, in D_2O.

9.1.5. G0/G1-OH

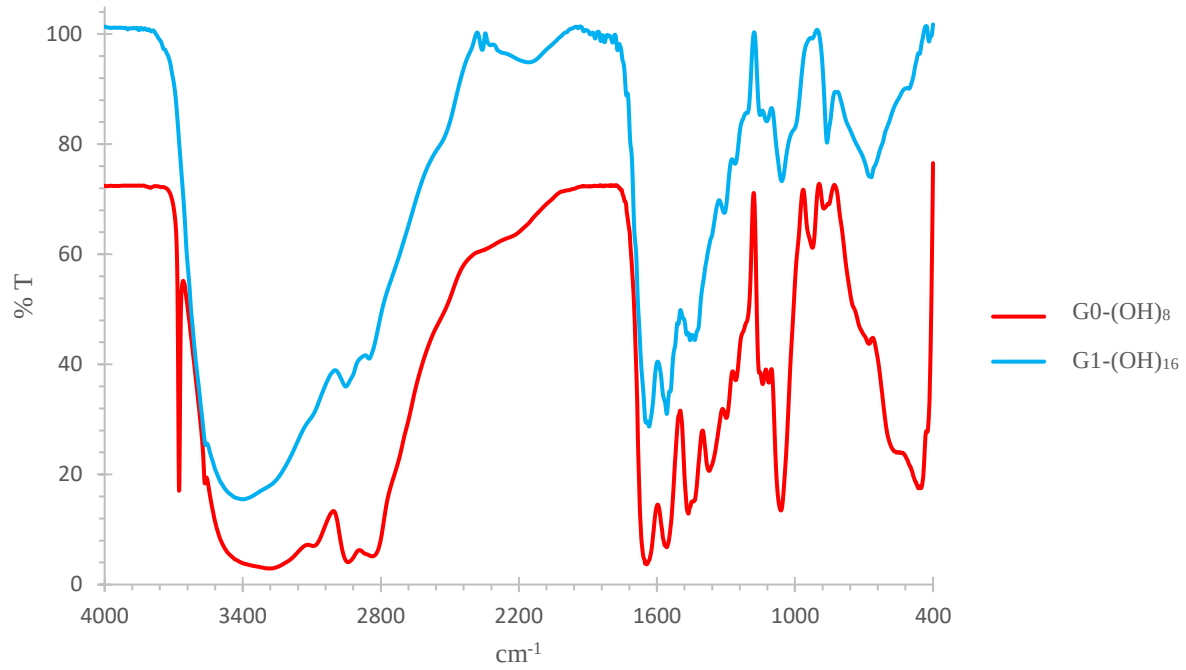

Figure 11A - FTIR spectra of G0/G1-OH performed in KBr cells.

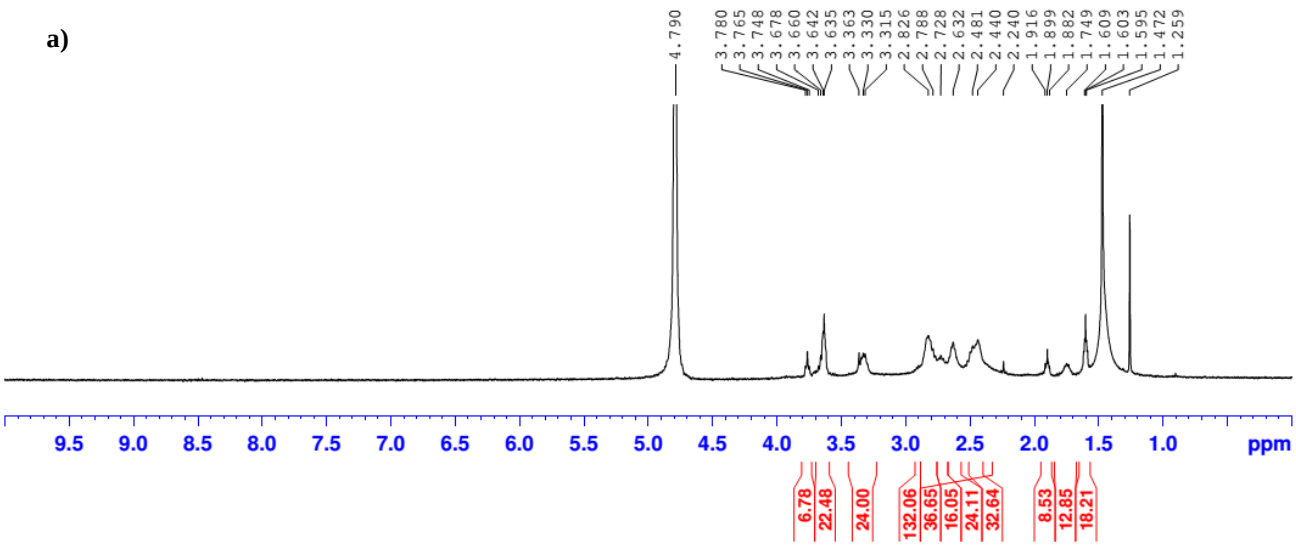

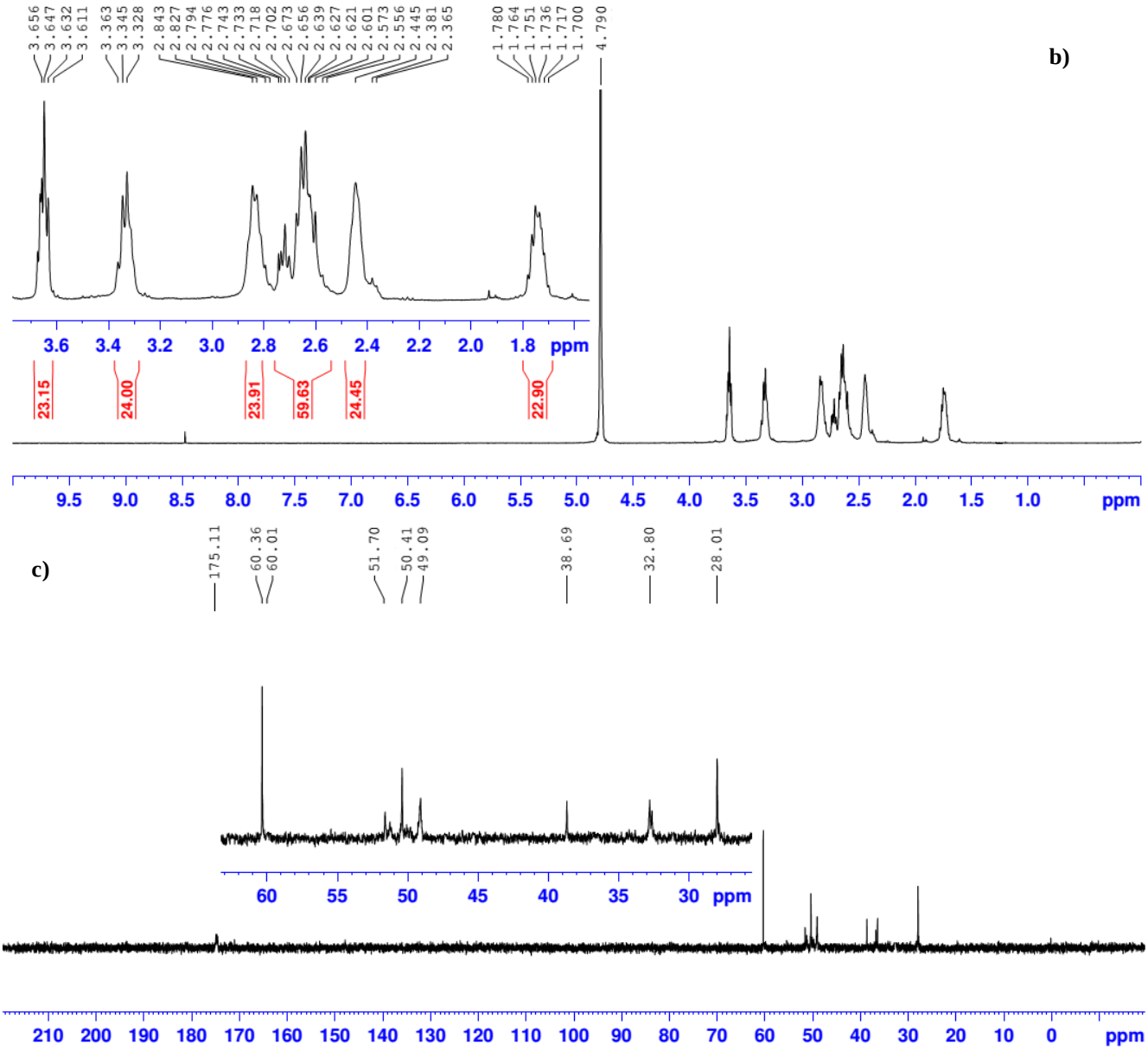

Figure 12A - NMR characterization of G1-$(OH)_{16}$: ^{1}H-NMR spectra of the a) impure and b) "pure" fraction; c) ^{13}C-NMR spectrum of the "pure" fraction, in D_2O.

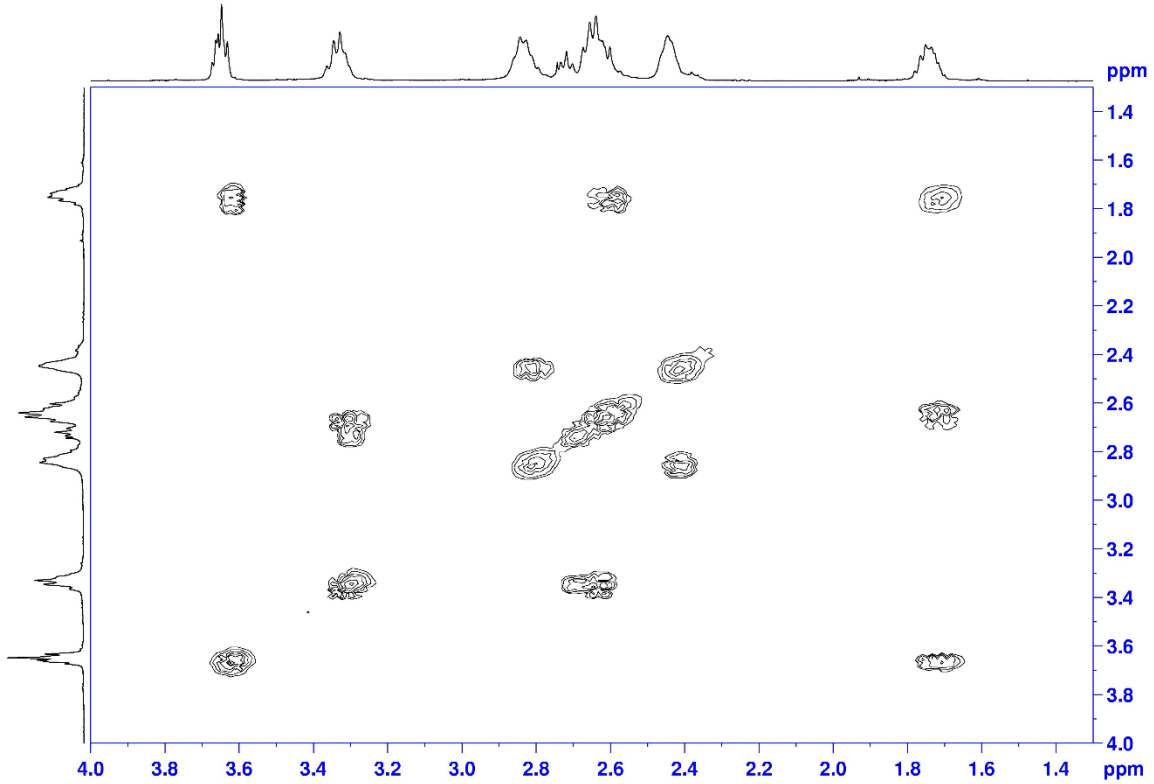

Figure 13A - COSY spectrum of the pure fraction of G1-$(OH)_{16}$, in D_2O.

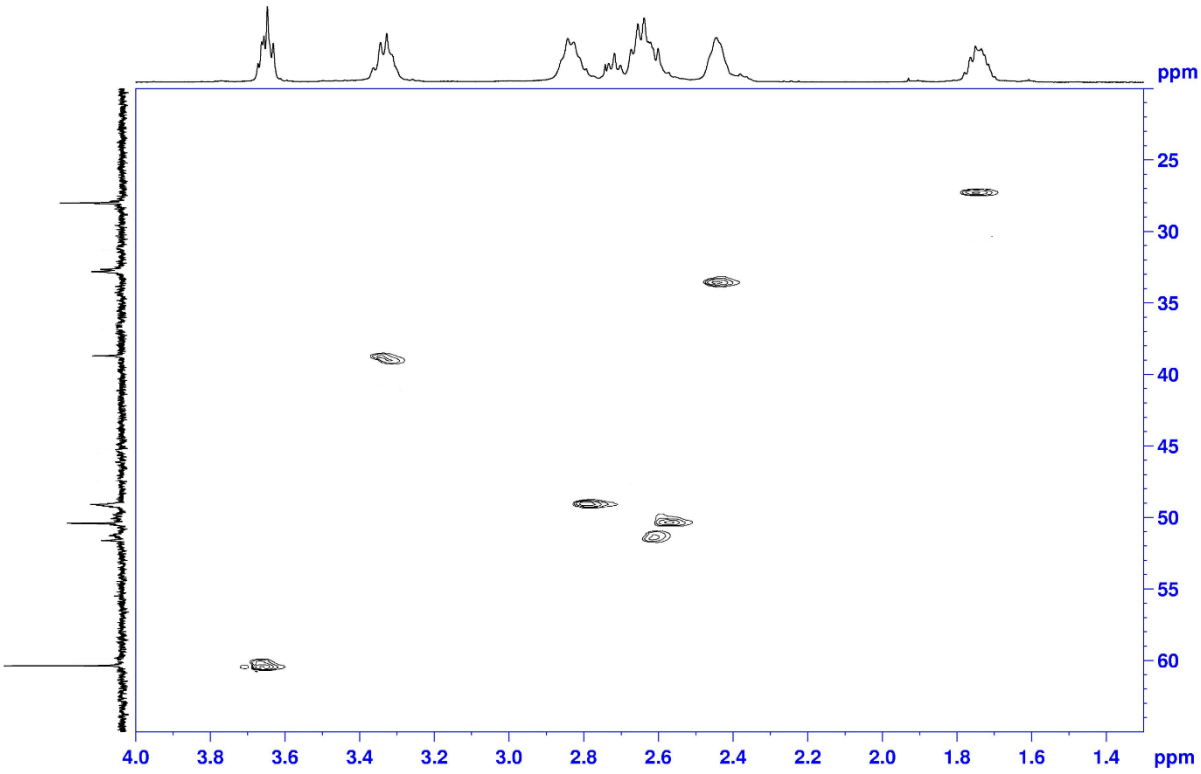

Figure 14A: HSQC spectrum of pure fraction of G1-$(OH)_{16}$, in D_2O.

FCT Fundação para a Ciência e a Tecnologia
MINISTÉRIO DA CIÊNCIA, TECNOLOGIA E ENSINO SUPERIOR

PEst-OE/QUI/UI0674/2013

M1420-01-0145-FEDER-000005

Centro de Química da Madeira – CQM+ (Madeira 14-20)

Cofinanciado por: